AD_____

Award Number: W81XWH-10-1-1017

TITLE: Chemically Modified Bacteriophage as a Streamlined Approach to Noninvasive Breast Cancer Imaging

PRINCIPAL INVESTIGATOR: Michelle E. Farkas, Ph.D.

CONTRACTING ORGANIZATION: University of California, Berkeley; Berkeley, CA 94720

REPORT DATE: December 2013

TYPE OF REPORT: Annual Summary

PREPARED FOR: U.S. Army Medical Research and Materiel Command
Fort Detrick, Maryland 21702-5012

REPORT DOCUMENTATION PAGE

Form Approved
OMB No. 0704-0188

1. REPORT DATE	2. REPORT TYPE	3. DATES COVERED
December-2013	Annual Summary	28 September 2010-27 September 2013

4. TITLE AND SUBTITLE

Chemically Modified Bacteriophage as a Streamlined Approach to Noninvasive Breast Cancer Imaging

5a. CONTRACT NUMBER

5b. GRANT NUMBER
W81XWH-10-1-1017

5c. PROGRAM ELEMENT NUMBER

6. AUTHOR(S)

Michelle E. Farkas, Ph.D.

E-Mail: farkas@chem.umass.edu

5d. PROJECT NUMBER

5e. TASK NUMBER

5f. WORK UNIT NUMBER

7. PERFORMING ORGANIZATION NAME(S) AND ADDRESS(ES)

University of California, Berkeley; Berkeley, CA 94720

8. PERFORMING ORGANIZATION REPORT NUMBER

9. SPONSORING / MONITORING AGENCY NAME(S) AND ADDRESS(ES)
U.S. Army Medical Research and Materiel Command
Fort Detrick, Maryland 21702-5012

10. SPONSOR/MONITOR'S ACRONYM(S)

11. SPONSOR/MONITOR'S REPORT NUMBER(S)

12. DISTRIBUTION / AVAILABILITY STATEMENT
Approved for Public Release; Distribution Unlimited

13. SUPPLEMENTARY NOTES

14. ABSTRACT

I have been able to convert cell surface marker-specific phage identified from library screens into imaging agents that can target and differentiate breast cancer cell types. This is accomplished by using efficient synthetic protocols to conjugate small molecules to phage coat proteins. In the current work, I have examined the use of phage targeting HER2, EGFR, HER3, CD44, and CD73 as immunofluorescence agents in order to visualize these cell surface receptors in cell button models of cancer tissues. Furthermore, I have initiated work whereby the targeting moieties (single chain antibody fragments, or scFv's) displayed by the filamentous phage are displayed on significantly smaller phage types (nanophage), which can be modified similarly and may possess improved biodistribution characteristics compared with the full length fd. I have also initiated the study of chemically modified icosahedral bacteriophage MS2 in order to target specific breast cancer-associated cell surface receptors in cell culture and mouse models of cancer. The work described in this final report ended on July 30, 2013, because I accepted an independent academic position in the chemistry department at the University of Massachusetts, Amherst.

15. SUBJECT TERMS
Bacteriophage, Cancer Imaging, Bio-distribution, Cellular Targeting

16. SECURITY CLASSIFICATION OF:			17. LIMITATION OF ABSTRACT	18. NUMBER OF PAGES	19a. NAME OF RESPONSIBLE PERSON
a. REPORT	b. ABSTRACT	c. THIS PAGE			USAMRMC
U	U	U	UU		19b. TELEPHONE NUMBER *(include area code)*

Table of Contents

Page

INTRODUCTION: Diagnostic imaging methods play a key role in the detection, treatment, and study of breast cancer. Although techniques such as positron emission tomography (PET) enable disease visualization, current imaging methods and agents used yield little information with regard to the type of cancer present. Invasive biopsy follow-ups are typically required to determine patient prognoses and recommended treatment regimens. As a non-invasive alternative, my research involves the chemical modification and subsequent use of bacteriophage targeting specific breast cancer markers in order to visualize and study these cells and tumors in culture, immunohistology, and *in vivo*. The generation of imaging agents relies on the attachment of functional groups that can be detected (i.e. radioactive or fluorescent labels) to a molecule that shows some specificity for a marker of interest on the cell surface. The binding moieties are selected through the use of phage display techniques, where members of a library of diversified phage are isolated based on their ability to associate with a particular target. I have previously demonstrated that I can selectively modify significant quantities of the pVIII coat proteins lining the sides of the phage in order to incorporate fluorescent labels and other small molecules. Following generation and modification of the targeted agents, their selectivities are evaluated. By directly converting phage recovered from library screens into imaging agents, this research has the potential to significantly stream-line the process of targeted imaging agent generation. Building upon the work performed and results obtained in the previous periods of this fellowship, I have diversified the platforms to be used and involved other members of the Francis group so that this line of research may be continued within the laboratory following my departure from the University of California, Berkeley in July 2013.

BODY: My research involves the use of chemically modified filamentous (fd) bacteriophage in the targeting and differentiation of breast cancer tissues bearing specific surface markers, directly converting library-identified phage into imaging agents. In the first year of the fellowship, I generated and modified HER2 and EGFR-targeting phage to display small molecules, and performed *in vitro* evaluations of the phage's abilities to bind breast cancer and other cell lines that express the targeted markers of interest at varying levels. Xenograft models of breast cancer have been prepared in order to perform preliminary optical imaging experiments to evaluate phage tumor targeting capabilities. In the second year of the fellowship, I expanded the repertoire of cell surface markers targeted to include CD44, HER3, and CD73. Using methods established earlier in this project, phage targeting these markers were modified and evaluated *in vitro* and *in vivo*. In the current work, panels of phage were incorporated in histology experiments as immunofluorescence agents, optimizing protocols for their use with 'cell buttons' derived from cell lines of interest as tumor surrogates. Based on our previous lack of positive findings using *in vivo* optical imaging, further efforts are currently being invested in the radiolabeling of these agents (since fluorophore quenching may play a significant role here). Additional efforts during the course of this project period were given to *in vitro* and *in vivo* bio-distribution evaluations of the icosahedral MS2 bacteriophage scaffold described below. We also initiated studies of 'nanophage,'which can be modified to display the same targeting groups as fd using the same methods, but may have improved potential in biological systems resulting from their diminished size (50 nm versus 1000 nm).

Task 1. Generation and *in-vitro* evaluation of PET imaging agents based on filamentous phage

Other research groups have previously demonstrated the *in vivo* targeting of phage to the prostate and prostate carcinoma[1,2] and other tissues of interest,[3,4] based on moieties displayed on their terminal pIII capsid proteins. In my research, I have used filamentous bacteriophage (fd) that display marker-specific single-chain variable fragment (scFv) molecules identified by collaborators in the laboratory of James D. Marks, M.D., Ph.D. (UCSF) using molecular evolution techniques. In studies described in the previous annual reports, I used fd that are selective for the epidermal growth factor receptor (EGFR)[5], and human epidermal growth factor Receptor 2 (HER2 or ERBB-2),[6] while phage targeting botulinum toxin serotype A (BoNT/A)[7] were used as a

control. In subsequent work, phage targeting HER3, CD44, and CD73 were also generated, and modified for evaluation *in vitro* and *in vivo*. The overexpression of HER3 has been shown to be a marker of reduced patient breast cancer-specific survival,[8] CD44 is a cell adhesion molecule involved in tumor metastasis, and a marker used to identify human cancer stem cells,[9,10] while CD73 is a cell surface protein overexpressed in many solid tumors that may promote tumor progression.[11,12]

Escherichia coli (*E. coli)* infected with anti-EGFR, HER2, BoNT/A, HER3, -CD44, and -CD73 phage had been generated by the Marks group, and given to the Francis lab in order further propagate fd of interest for our studies, along with fundamental methodology to do so.[13] I had previously optimized a number of the steps required for phage production, but found that recovery continued to be dependent upon phage type, time since re-plating of *E. coli* colonies, and other miscellaneous factors. Phage targeting EGFR, HER2, HER3, CD44, and CD73 were each produced numerous times for further modification and experiments. The optimized procedure for phage production has been previously described in the *methods* section of the annual report from 2012, and may also be found here in ***Appendix 1***: Reprint of ACS Nano Journal Article (including Supporting Information).[14] An overview of the two-step chemical modification strategy used for subsequent modification of isolated phage with small molecules is shown in **Figure 1**. The conditions used for the transamination and appendage of small molecules via oxime formation following the production of phage proteins are also described in ***Appendix 1***.

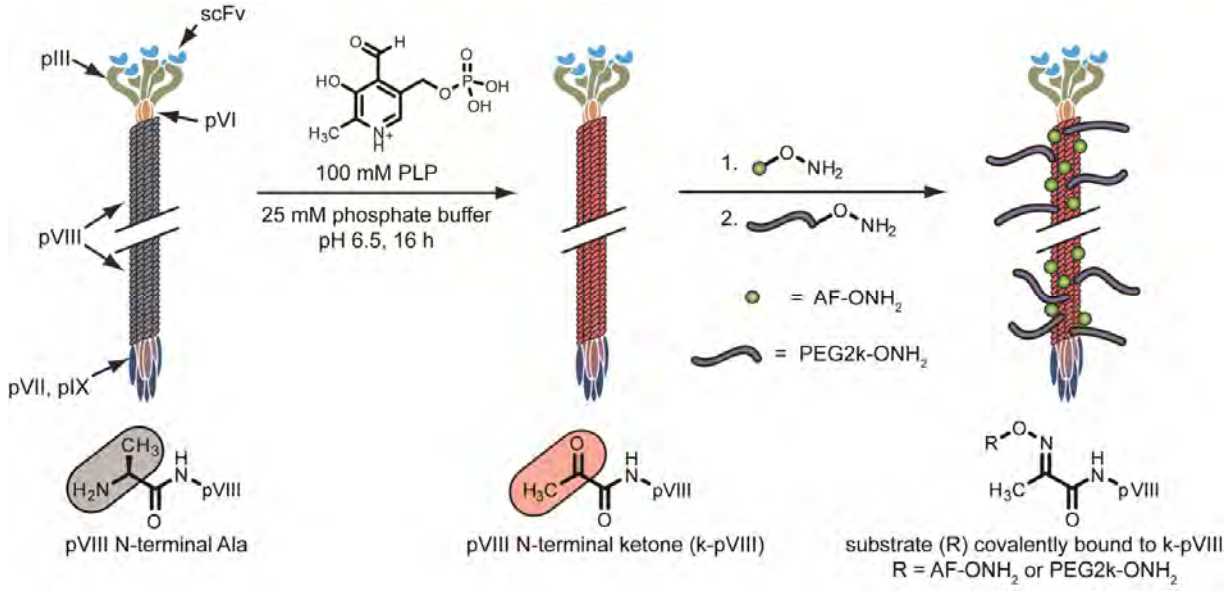

Figure 1. Chemical modification of filamentous (fd) phage. N-terminal alanines (Ala) of the pVIII coat proteins lining the filamentous phage are converted to ketone groups, which can be subsequently modified with small molecule alkoxyamines including dyes (AF-ONH_2) and polyethylene glycol chains (PEG2k-ONH_2).

As these agents are intended for imaging use *in vivo*, I sought to enhance the characteristics of the phage by appending polyethylene glycol (PEG) chains, which via shielding and other effects have been shown to increase the plasma circulation times of proteins, liposomes, and other nanoparticles.[15-17] Our previous work demonstrated that various numbers of PEG chains (molecular weight 2,000 Da, PEG2k) could be introduced per phage, ranging from 20-70% modification of coat proteins or 900-3150 copies per phage, as determined by reverse-phase HPLC, while zeta potential measurements showed that increased numbers of 5 kDa PEG chains shield surface charge.[14] In the first annual report, PEG-AF-647-anti-EGFR phage were generated with varying

levels of PEG (10%, 25%, 50%, and 75%), and evaluated with regard to cell binding and *in vivo*. More recently, this modification has been similarly applied to other phage types, yielding nearly identical results.

For the application of the phage toward clinically-relevant imaging modalities, our initial strategies included the labeling of fd with ^{18}F via the oxidative coupling of ^{18}F-fluoroaniline to small molecule alkoxyamines containing aminophenol groups. However, the reaction times required to generate the desired radio-labeled phage products proved to be incompatible with the short-lived isotope ^{18}F, whose half-life is 109 minutes, and labeling of PEGylated phage was minimal. Concurrently, in order to thoroughly evaluate the circulation, stability, and clearance properties of these agents, a longer-lived radionuclide was deemed to be required. For these reasons, we have initiated use of ^{64}Cu, whose half-life is 12.7 hours. The copper radionuclide is incorporated with the phage via chelation to 1,4,7,10-tetraazacyclododecane-1,4,7,10-tetraacetic acid (DOTA) or 1,4,7-triazacyclononane-N,N',N''-triacetic acid (NOTA), either of which are be appended to the phage beforehand by using chemistry similar to that previously described (and shown in **Figure 1**). The ^{64}Cu is typically allowed to react with the phage-chelator complex for two hours at room temperature. Due to the increased time window afforded by the longer half-life of the isotope, we elected to develop a size-exclusion chromatography (SEC)-based HPLC method to ensure that all copper in the sample was associated with the phage via the chelator (that there was no 'non-specific sticking') following purification. This analysis allowed us to track the removal of free copper and optimize our washing procedures, maintaining that all of our experimental samples were free of un-incorporated ^{64}Cu. However, it was also found that where polyethylene glycol (PEG) chains were appended to the phage (see above), a significant amount of 'non-specific sticking' of the copper occurred, and radiochemical yields of the agent with free copper purified away were quite low. Optimization of this labeling strategy for PEGylated phage is still on-going. Faster chemical methodologies for the modification and pre-injection characterization of phage with ^{18}F are still being sought.

The biomarker binding site at the phage terminus is presumed to be located a few nanometers from the bulk of the chemical modifications, thereby minimizing interference with scFv binding (**Figure 1**). In previous work testing the potential for interference, PEG-modified phage samples were evaluated for their ability to bind MDA-MB-231 cells (EGFR-positive), and compared to control phage (anti-BoNT/A), which do not bind EGFR. Excellent binding selectivity was observed at all levels of PEG modification, although increased levels of PEG resulted in slightly diminished binding. Neither anti-EGFR nor anti-BoNT/A phage bound to SUM-52PE cells, which lack EGFR.[14] Following reactions yielding increased levels of AF-488 modification, anti-EGFR, -HER2, -CD44, -HER3, -CD73 , and -BoNT/A phage binding were evaluated via flow cytometry in a panel of receptor positive and negative cell lines, including both basal and luminal sub-type immortalized breast cancer cells of a variety of origins. These data have been described in the previous annual reports, along with the procedures used. Methods information may also be found in ***Appendix 1***.

Experiments to detect non-specific phage binding in serum (rat, rabbit, or mouse), as described in the statement of work and mentioned in previous annual reports have not yet been conducted. Although we have now successfully developed HPLC methods in order to be able to quantify phage stability in blood/serum and radiochemical purity following labeling, because the PEGylated phage samples were of the greatest interest for the *in vivo* studies, these analyses were postponed until we were able to reliably radiolabel all samples. Upon development of successful labeling conditions, we plan to concurrently evaluate phage stability and non-specific binding in a series of experiments.

In previously described work, live-cell confocal microscopy protocols were devised in order to visualize phage cell binding and uptake.[14] Experiments were performed using the breast cancer cell lines HCC1954

(basal, carcinoma), MDA-MB-231 (basal, adenocarcinoma), MCF-7 clone 18 (a HER2-overexpressing variant of the luminal, adenocarcinoma cell line MCF-7), and MDA-MB-468 cells (basal, adenocarcinoma, which possess no detectable levels of HER2).[18] Cells were both treated with individual phage types and mixtures of various phage differentially labeled. Co-cultures of MDA-MB-231 and MCF-7 clone 18 cells were also generated and studied in imaging experiments. These data and methods used are described in previous annual reports and in ***Appendix 1***. Following prolonged phage exposure to cells (>1h), uptake was observed in many instances. Further microscopy experiments to evaluate the mechanism by which it occurs have since been conducted, demonstrating that receptor-mediated endocytosis and trafficking via clathrin-coated vesicles are involved. It was also confirmed that phage remain intact following internalization. Data obtained and protocols used in the assays are described in the previous annual report.

A significant area of need in breast cancer diagnostics remains the generation of new tools for the molecular characterization of biopsied tissues. Because our agents combine marker-specific binders with detectable functionalities, they were deemed inherently well-suited for this application. In order to test and optimize our use of these reagents, we used cell buttons, which are paraffin-embedded sections that can be mounted on slides for visualization using microscopy, as models. They are treated in the same manner as tissue sections, and at the same time can be generated by using well-characterized cell lines identical to those used in xenograft tumor models or *in vitro* studies. Different phage types can be modified with different fluorescent labels and up to three phage types can be studied in a single section/slide (and is limited only by the quantity of dyes available). A clear benefit of this method is the ability to multiplex: since the fluorophores are directly bound to the phage, secondary elements for detection are not required (as opposed to the use of antibodies, where each type must originate from a different species in order to avoid 'cross-talk' between them). Another benefit of using phage in immunofluorescence staining, also related to the coupling of fluorophore and targeting groups, is that a second incubation (as with a secondary antibody) is not required, resulting in a significantly shorter time for processing.

Using combinations of anti-EGFR, -HER2, -CD44, and -HER3 phage, imaging experiments were performed using cell buttons generated from AU565, HCC1954, MCF-7, MCF-7cl18, MDA-MB-231, and MDA-MB-468 cell lines (**Figure 2**). Although some cell line and phage combinations consistently gave appropriate results (with signal arising from phage targeting markers that were over-expressed in a given cell line), some cell lines and/or phage types resulted in high levels of background or no binding depending on how the protocols were adjusted. All phage-based agents were validated by comparison with antibodies, and various methods of antigen retrieval were used. The CD73-targeted phage was extremely unreliable in these assays (with both non-specific and lack of binding) and was omitted from these studies pending further modifications/analyses. Needless to say, not all of the parameters could be optimized within the allotted time, however, significant progress was made and the preliminary data obtained are very promising. The final version of the protocol as it had been revised is included in the *Methods* section of this report.

(on following page) Figure 2. Evaluation of phage as agents in immunofluorescence studies. Anti-HER2 (green), -CD44 (orange), -EGFR (not shown), and –HER3 (not shown) phage binding to cell button models of tumor sections were studied. Each row reflects the staining of a single slide, with columns representing different versions of the same image. Protocols used were described in the *Methods* section. Nuclei are stained with Hoechst (blue).

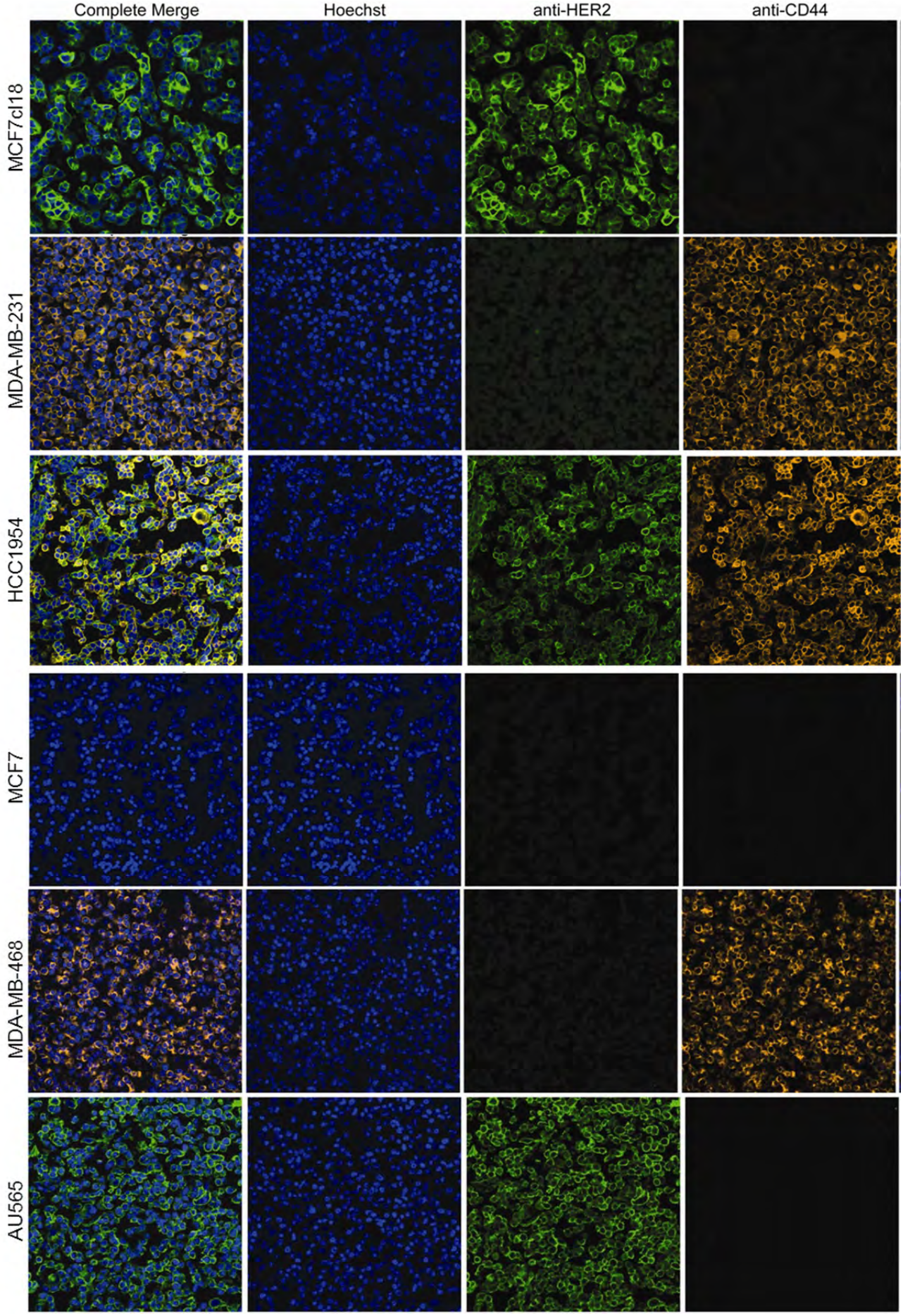
Complete Merge
Hoechst
anti-HER2
anti-CD44
MCF7cl18
MDA-MB-231
HCC1954
MCF7
MDA-MB-468
AU565

As an alternative strategy to the use of fd, preliminary studies with MS2 icosahedral bacteriophage were initiated. Other members of the Francis group have previously generated MS2 constructs bearing targeting peptides,[19] aptamers,[20] and DARPins[21] (Designed Ankyrin Repeat Proteins) on the exterior surfaces. Two of these targeted agents, one aptamer (targeting PTK7) and one DARPin (targeting HER2) were used in assessing the binding abilities of these constructs to a small panel of breast cancer cell lines, including MDA-MB-453, MDA-MB-231, MCF-7cl18, and HCC1954 by using flow cytometry (**Figure 3**). Scrambled, non-targeted aptamers and DARPins conjugated to MS2 were used as controls.

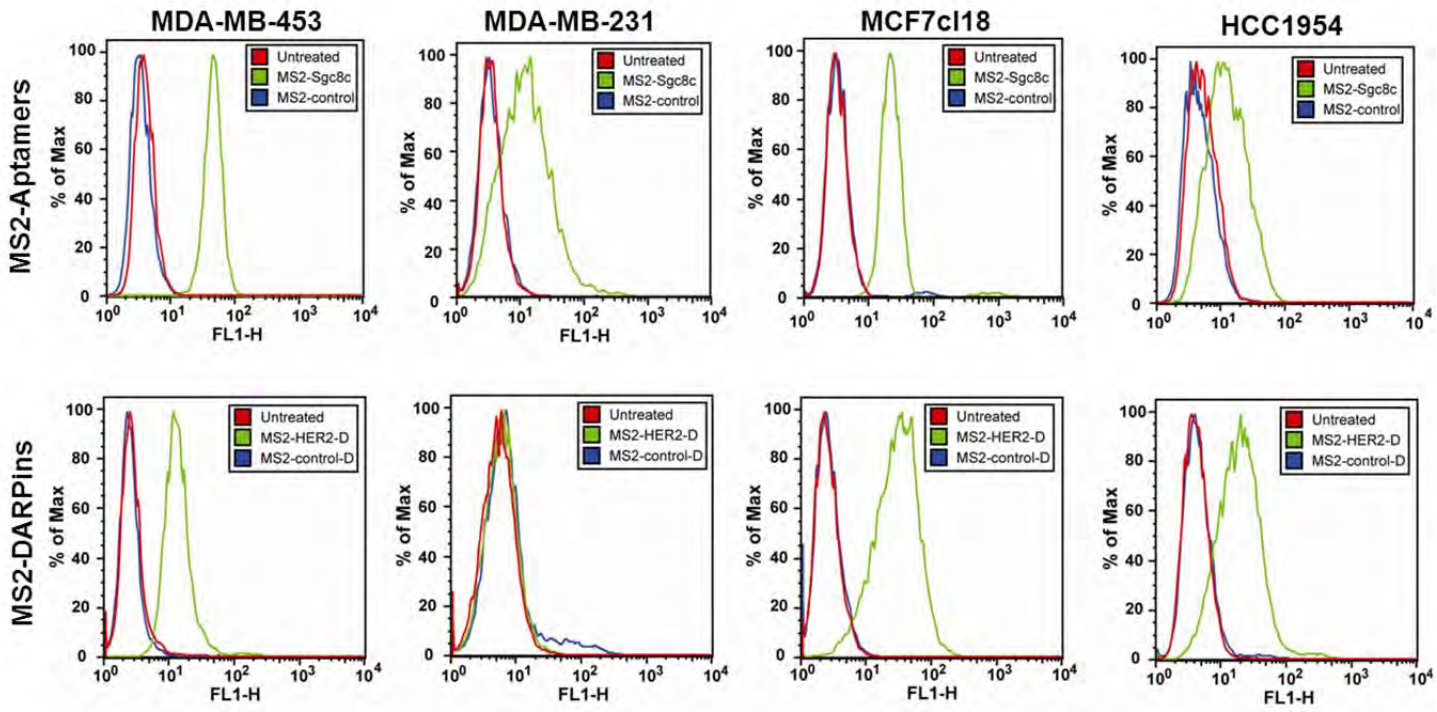

Figure 3. Evaluation of MS2-phage agents *in vitro*. Targeted aptamer MS2-Sgc8c (top row, green), and HER2 DARPin-MS2 (MS2-HER2-D, bottom row, green) treated cells, were compared against control aptamer-treated (MS2-control) and control DARPin-treated (MS2-control-D) (top and bottom rows, respectively, blue) and untreated cells (top and bottom rows, red). MDA-MB-453, MDA-MB-231, MCF-7cl18, and HCC1954 breast cancer cell lines were used.

Having ascertained that these agents could also be used to specifically bind to breast cancer subtypes, conversion into radionuclide imaging agents and further evaluation were required. Using methodologies previously investigated in our group, I used two orthogonal strategies to modify the interior and exterior surfaces with chelators and PEG chains, respectively (**Figure 4**). Dual mutants of MS2 bearing internal cysteine and exterior para-amino-phenylalanine residues[22] enable capsid cargo-loading with maleimide-chelator functionalities and the use of an oxidative coupling reaction for appending PEG chains to the exterior, respectively.[23] The scaffolds can then be incubated with ^{64}Cu solution and purities and levels of radiochemical yields can be determined by using the SEC-HPLC method previously described for filamentous bacteriophage. Further details and information regarding the preparation and analyses (including stability) of the radio-labeled PEGylated and non-PEGylated MS2 capsids may be found in ***Appendix 2.***

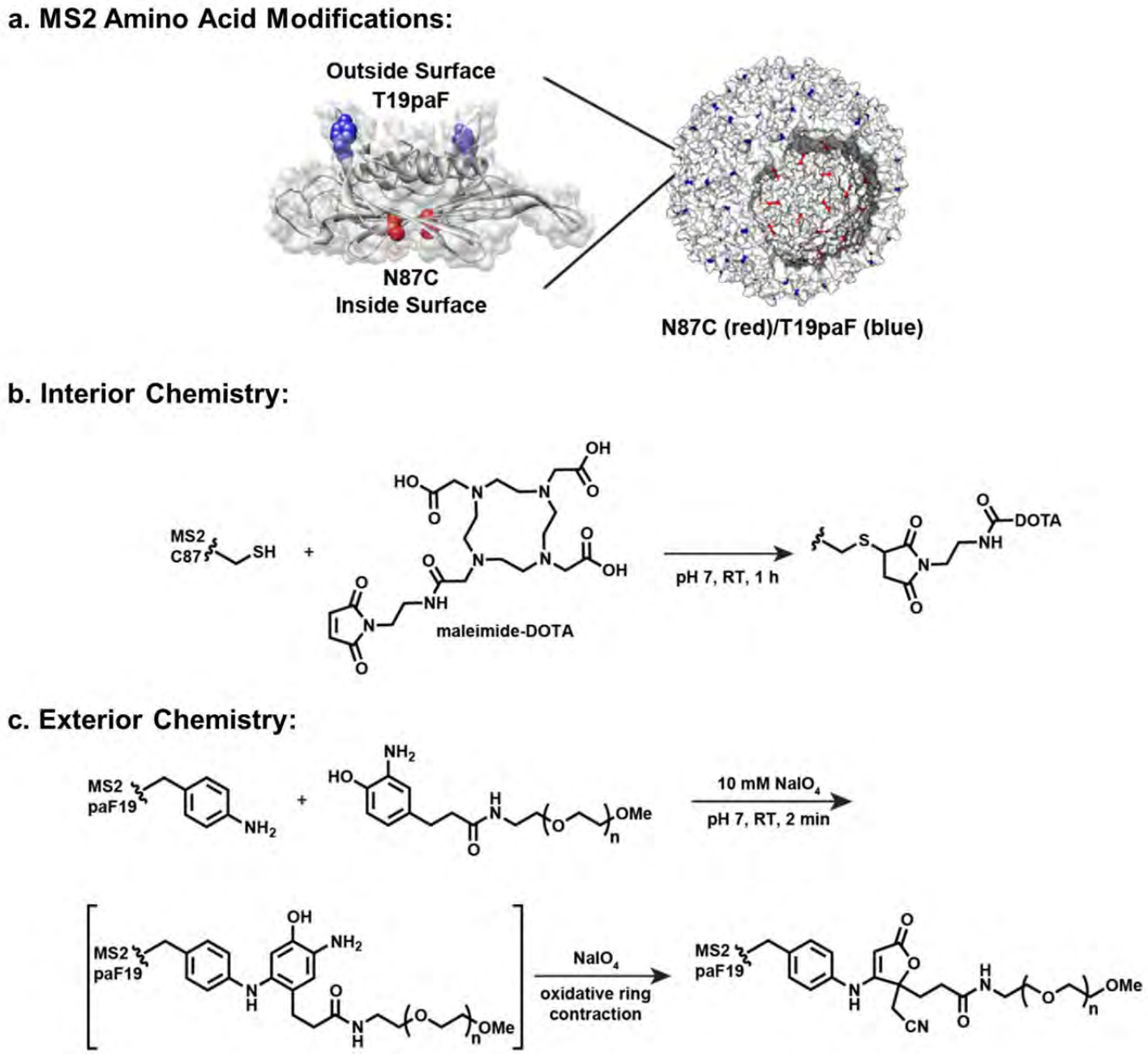

Figure 4. Overview of synthetic modifications to bacteriophage MS2. (a) Bacteriophage MS2 is composed of 180 monomeric subunits, each of which possesses an internal cysteine (red) and external *p*-aminophenylalanine (blue) mutant. At left, a dimer within the assembly is shown, highlighting these residues. **(b)** Because MS2 possesses 2 nm pores, interior modification of the assembled bacteriophage with small molecules is possible. Here, cysteine residues are reacted with maleimide functionalities of copper chelators (DOTA shown). **(c)** Functionalization of the exterior portion may be accomplished by sodium periodate mediated oxidative coupling reaction. In my case, this is used to modify the aminophenylalanine moieties with PEG chains for enhanced biodistribution.

Task 2. *In vivo* animal imaging with radiolabeled agents

In the first annual report prepared, the evaluation of phage bio-distribution in healthy animals had been postponed pending the completion of initial optical imaging experiments using tumor bearing mice and optimization of the chemistry to modify the agents with ^{18}F. As mentioned above, it was deemed that the short half-life of ^{18}F and the reaction conditions used for its incorporation were not complementary. It was for this reason that I initiated the use of ^{64}Cu and its chelation using DOTA and/or NOTA. In combination with the aforementioned HPLC method development for determination of radiochemical purity, I anticipate that this system will provide a comprehensive assessment of phage circulation and fate.

In vivo biodistribution experiments had been carried out using anti-EGFR, -HER2, -CD44, -HER3, and -CD73 fluorophore (AF647) labeled phage imaged with a fluorescence molecular tomography optical imaging system. I had initially chosen to use optical imaging because results from *in vitro* cell culture binding experiments could be directly correlated with *in vivo* targeting, since identical agents are used for both assays. Several experiments were performed using different types of xenografts; some were orthotopic in their placement and others placed in the hind flank. Different cell lines were used: MDA-MB-231, MCF-7cl18, and HCC1954. One experimental platform used dual MDA-MB-231/MCF-7cl18 tumors, implanted in opposing mammary fat pads, however the synchronization of tumor size posed to be difficult. MCF-7cl18-derived cells grew faster in some cases, while in others MDA-MB-231 tumors did. In general, there were instances where tumors had either over-grown (sometimes appearing necrotic), while in others the tumors failed to grow. In most studies the agents did not appear to be taken up by the tumor(s), and possessed similar localization profiles independent of targeting group. Major sites where the phage accumulated included the liver and kidneys, followed by the bladder. In many cases, phage also appeared to localize in the area of the tumor/inguinal lymph nodes, and the majority of the agents were found to clear after 48-72 h. Additional sites of accumulation determined from *ex-vivo* biodistribution included the spleen, pancreas, and lungs, and small amounts could be found in the tumors. Further experimental details can be found in the *Methods* section of the previous annual report submitted.

In an effort to improve agent circulation time and biodistribution, fluorescently labeled anti-EGFR phage with 25% and 75% of the pVIII coat proteins modified with PEG chains were also used for imaging. It was observed that the addition of PEG chains resulted in an extension of circulation time, as evidenced by the amount of time taken for maximum amount of signal to reach the liver (1 h for 0% PEG, 3 h for 25% PEG). Increasing the level of PEG modification to 75% did not appear to result in a significant additional change, however, as both PEGylated phage types were only used in a single pilot experiment each, I do not believe these results to be conclusive. Because it was at this time that fluorescence quenching (and liberation) was deemed to be a significant issue with the agents, these experiments were not repeated. Instead, it was planned that they would be conducted with the same phage type and PEG levels but labeled with radionuclides. However, due to difficulties with the radiolabeling of these agents, those experiments have not yet been conducted.

Since a feasible synthetic strategy was already accessible for bacteriophage MS2, versions with and without exterior PEG modifications were labeled with ^{64}Cu. Its biodistribution and tumor uptake were assessed *in vivo* using mice bearing orthotopic tumors consisting of MCF-7cl18 cells. Neither capsid type possessed targeting groups, so the ~8% ID/g (injected dose per gram) was likely the result of the enhanced permeation and retention (epr) effect. It was also significant to note that there was an appreciable difference between the PEGylated and non-PEGylated capsids in the spleen, which was likely the result of the shielding effect of the

PEG chains. The data and experimental details for this experiment may be found in ***Appendix 2***.

Methods:

Please note that only methods new to this annual report and not present in either ***Appendix 1*** or ***Appendix 2*** are described here. Please refer to prior annual reports for historical methods.

Phage immunofluorescence staining: Cell buttons and slides were prepared by the Pathology Core at the University of California, San Francisco. Slides were baked at 37 °C, followed by 60 °C for 30 minutes each, and then allowed to cool. Slides were deparaffinized and rehydrated by washing three times in xylene for five minutes each, 100% ethanol twice for 5 minutes each, 95% ethanol twice for 2 minutes each, 70% ethanol for 2 minutes each, and distilled water for 5 minutes. Slides were pressure cooked (Dako, US) in 10 mM citrate buffer according to manufacturer's instructions. After cooling, slides were washed in distilled water for 5 minutes, then 0.025% PBST for 5 minutes. To prevent non-specific binding interactions, slides were incubated with 1% BSA for 30 min at room temperature and blotted to remove. Phage were added at a 1 nM concentration in 85 μL of 1% BSA, covered with a coverslip, and allowed to incubate with slides for 1h at room temperature (in the dark). The coverslip was then washed off in 0.025% PBST for 8 min, and washed 3 more times in 0.025% PBST 5 min each, wiping off after each time. Counterstaining with Hoescht was performed for 15 min, followed by three 10 min washes in PBS, and treatment with Prolong Gold anti-fade reagent, which was allowed to cure overnight in the dark. Slides were stored at 4 °C for short- or -20 °C for long-term.

KEY RESEARCH ACCOMPLISHMENTS:

1. Successful generation of fd phage targeting different markers bearing various levels of PEG modifications.
2. Radiolabeling of fd phage with ^{64}Cu and assessment of purity and radiochemical yield with size exclusion chromatography (SEC) HPLC.
3. Utilization of multiple fluorophore-labeled phage as immunofluorescence (IMF) agents to simultaneously detect markers in cell button sections, as models of cancer tissue.
4. Evaluation of targeted aptamer and DARPin-MS2 agent binding in breast cancer cell lines.
5. Generation and evaluation of ^{64}Cu labeled PEGylated and non-PEGylated MS2 *in vitro* and *in vivo.*

REPORTABLE OUTCOMES: Provide a list of reportable outcomes that have resulted from this research to include:

Employment gained:

As a result of the training and research supported by this award, I have successfully obtained a principal investigator position. Since Aug. 1, 2013 I have been employed by the University of Massachusetts, Amherst in the department of chemistry at the rank of Assistant Professor.

Peer-reviewed journal articles:

1. Farkas, M. E., Aanei, I. L., Behrens, C. R., Tong, G. F., Murphy, S., O'Neil, J. P., Francis, M. B. "PET Imaging and Biodistribution of Chemically Modified Bacteriophage MS2." *Mol. Pharm.* **2013,** *10*, 69-76.

2. Carrico, Z. M.*, Farkas, M. E.*, Yu, Z., Hsiao, S. C., Marks, J. D., Chokhawala, H., Clark, D. S., Francis, M. B. "N-Terminal Labeling of Filamentous Phage to Create Cancer Marker Imaging Agents." *ACS Nano.* **2012**. *6,* 6675-6680.

*Joint first-authors

Oral presentations:

1. Farkas, M. E., Aanei, I. L., O'Neil, J. P., Francis, M. B. "Chemical Modification and Biodistribution of Bacteriophage MS2 in Mouse Models of Cancer." **2013 American Chemical Society Northeast Regional Meeting**, New Haven, CT, October, 2013.

2. Farkas, M. E., Gray, J. M., Francis, M. B. "Chemically Modified Bacteriophage as a Streamlined Approach Toward Non-Invasive Breast Cancer Imaging." **245th National Meeting of the American Chemical Society**, Philadelphia, PA, August 2012.

Poster presentations:

1. Farkas. M. E.; Carrico, Z. M.; Tong, G. J.; Wu, W.; Behrens, C. R.; Gray, J. M.; Francis, M. B. "Chemically Modified Bacteriophage as a Streamlined Approach Toward Non-Invasive Breast Cancer Imaging" **Gordon Conference in Mammary Gland Biology**, Newport, RI, June 2011

2. Farkas. M. E.; Carrico, Z. M.; Tong, G. J.; Wu, W.; Behrens, C. R.; Gray, J. M.; Francis, M. B. "Chemically Modified Bacteriophage as a Streamlined Approach Toward Non-Invasive Breast Cancer Imaging" **Department of Defense Breast Cancer Research Program 6th Era of Hope Conference**, Orlando, FL, August 2011

CONCLUSION: During the course of this research program, I have successfully generated and selectively modified filamentous bacteriophage targeting cancer-associated cell surface receptors HER2, EGFR, HER3, CD44, and CD73, effectively converting library-isolated entities into imaging agents. These agents have been demonstrated to retain their marker-binding specificities via flow cytometry and confocal microscopy assays. Although *in vivo* imaging with these agents has remained inconclusive, with the development of protocols for radionuclide installation, PET evaluation should be fairly straight-forward and forthcoming. The potential use of phage in immunofluorescence staining applications for multiplexed visualization of tumor markers has also been demonstrated. The icosahedral bacteriophage MS2, which can be differentially modified on the interior and exterior surfaces has also shown promise as a targeted imaging and/or drug delivery agent based on initial evaluations.

REFERENCES:

1. Arap, W.; Haedicke, W.; Bernasconi, M.; Kain, R.; Rajotte, D.; Krajewski, S.; Ellerby, H. M.; Bredesen, D. E.; Pasqualini, R.; Ruoslahti, E. Targeting the prostate for destruction through a vascular address. *Proc. Natl. Acad. Sci. U. S. A.* **2002**. *99,* 1527-1531.
2. Newton-Northup, J. R.; Figueroa, S. D.; Quinn, T. P.; Deutscher, S. L. Bifunctional phage-based pretargeted imaging of human prostate carcinoma. *Nucl. Med. Biol.* **2009**. *36,* 789-800.
3. Kelly, K. A.; Waterman, P.; Weissleder, R. In vivo imaging of molecularly targeted phage. *Neoplasia.* **2006**. *8,* 1011-1018.
4. Yacoby, I.; Benhar, I. Targeted filamentous bacteriophages as therapeutic agents. *Expert Opin. Drug Deliv.* **2008**. *5,* 321-329.

5. Heitner, T.; Moor, A.; Garrison, J. L.; Marks, C.; Hasan, T.; Marks, J. D. Selection of cell binding and internalizing epidermal growth factor receptor antibodies from a phage display library. *J. Immunol. Methods.* **2001**. *248*, 17-30.
6. Poul, M. A.; Becerril, B.; Nielsen, U. B.; Morisson, P.; Marks, J. D. Selection of tumor-specific internalizing human antibodies from phage libraries. *J. Mol. Biol.* **2000**. *301*, 1149-1161.
7. Amersdorfer, P.; Marks, J. D. Phage libraries for generation of Anti-Botulinum scFv antibodies. *Methods Mol. Biol.* **2000**. *145*, 219-240.
8. Chiu, C. G.; Masoudi, H.; Leung, S.; Voduc, D. K.; Gilks, B.; Huntsman, D. G.; Wiseman, S.M. HER-3 Overexpression is prognostic of reduced breast cancer survival: a study of 4046 patients. *Ann. Surg.* **2010**. *251*, 1107-1116.
9. Lopez, J. I.; Camenisch, T. D.; Stevens, M. V.; Sands, B. J.; McDonald, J.; Schroeder, J. A.; CD44 attenuates metastatic invasion during breast cancer progression. *Cancer Res.* **2005.** *65*, 6755-6763.
10. Fillmore, C.; Kuperwasser, C. Human breast cancer stem cell markers CD44 and CD24: enriching for cells with functional properties in mice or in man? *Breast Cancer Res.* **2007.** *9*, 303.
11. Zhi, X.; Wang, Y.; Zhou, X.; Yu, J.; Jian, R.; Tang, S.; Yin, L.; Zhou, P. RNAi-mediated CD73 suppression induces apoptosis and cell-cycle arrest in human breast cancer cells. *Cancer Sci.* **2010,** *101*, 2561-2569.
12. Stagg, J.; Divisekera, U.; McLaughlin, N.; Sharkey, J.; Pommey, S.; Denoyer, D.; Dwyer, K. M.; Smyth, M. J. Anti-CD73 antibody therapy inhibits breast tumor growth and metastasis. *Proc. Natl. Acad. Sci. U.S.A.*, **2010,** *107*, 1547-1552.
13. Zhou, Y.; Marks, J. D. Identification of target and function specific antibodies for effective drug delivery. *Therapeutic Antibodies: Methods and Protocols.* **2009**. *525*, 145-160.
14. Carrico, Z. M.; Farkas, M. E.; Yu, Z., Hsiao, S. C.; Marks, J. D.; Chokhawala, H.; Clark, D. S.; Francis, M. B. N-Terminal Labeling of Filamentous Phage to Create Cancer Marker Imaging Agents. *ACS Nano.* **2012.** *6*, 6675-6680.
15. O'Riordan, C.R.; Lachapelle, A.; Delgado, C.; Parkes, V.; Wadsworth, S.C.; Smith, A.E.; Francis, G.E. PEGylation of Adenovirus with Retention of Infectivity and Protection from Neutralizing Antibody In Vitro and In Vivo. *Hum. Gene. Ther.*, **1999**, *10*, 1349-1358.
16. Caliceti, P.; Veronese, F.M. Pharmacokinetic and Biodistribution Properties of Poly(Ethylene Glycol)-Protein Conjugates. *Adv. Drug Deliv. Rev.*, **2003**, *55*, 1261-1277.
17. Owens, D.E.; Peppas, N.A. Opsonization, Biodistribution, and Pharmacokinetics of Polymeric Nanoparticles. *Int. J. Pharm.*, **2006,** *307*, 93-102.
18. Belsches-Jablonski, A. P.; Biscardi, J. S.; Peavy, D. R.; Tice, D. A.; Romney, D. A.; Parsons, S. J. Src Family Kinases and HER2 Interactions in Human Breast Cancer Cell Growth and Survival. *Oncogene*, **2001**, *20*, 1465-1475.
19. Carrico, Z. M., Romanini, D. W., Mehl, R. A., Francis, M. B. Oxidative Coupling of Peptides to a Virus Capsid Containing Unnatural Amino Acids. *Chem. Commun.*, **2008**, *10*, 1205-1207.
20. Tong, G. F., Hsiao, H. C., Carrico, Z. M., Francis, M. B. Viral Capsid DNA Aptamer Conjugates as Multivalent Cell-Targeting Vehicles. *J. Am. Chem. Soc.*, **2009**, *131*, 11174-11178
21. Wu, W., Francis, M. B. *Unpublished Results*, **2012.**
22. Stephanopoulos, N., Tong, G. J., Hsiao, S. C., Francis, M. B. Dual-Surface Modified Virus Capsids for Targeted Delivery of Photodynamic Agents to Cancer Cells. *ACS Nano*. **2009**, *131*, 11174-11178
23. Behrens, C. R., Hooker, J. M., Obermeyer, A. C., Romanini, D. W., Katz, E. M., Francis, M. B. Rapid Chemoselective Bioconjugation Through the Oxidative Coupling of Anilines and Aminophenols. *J. Am. Chem. Soc.* **2011**, *133*, 16398-16401.

Supporting information:

The following two manuscripts (and their supporting information sections) are provided as ***Appendix 1*** and ***Appendix 2***, respectively.

1. Carrico, Z. M.*, Farkas, M. E.*, Yu, Z., Hsiao, S. C., Marks, J. D., Chokhawala, H., Clark, D. S., Francis, M. B. "N-Terminal Labeling of Filamentous Phage to Create Cancer Marker Imaging Agents." *ACS Nano.* **2012**. *6*, 6675-6680.

2. Farkas, M. E., Aanei, I. L., Behrens, C. R., Tong, G. F., Murphy, S., O'Neil, J. P., Francis, M. B. "PET Imaging and Biodistribution of Chemically Modified Bacteriophage MS2." *Mol. Pharm.* **2013,** *10*, 69-76.

N-Terminal Labeling of Filamentous Phage To Create Cancer Marker Imaging Agents

Zachary M. Carrico,[†,⊥] Michelle E. Farkas,[†,⊥] Yu Zhou,[‡] Sonny C. Hsiao,[†] James D. Marks,[‡] Harshal Chokhawala,[§] Douglas S. Clark,[§] and Matthew B. Francis[†,*]

[†]Department of Chemistry, University of California, Berkeley, California 94720, United States, [‡]Department of Anesthesia and Pharmaceutical Chemistry, University of California, San Francisco, California 94143, United States, and [§]Department of Chemical Engineering, University of California, Berkeley, California 94720, United States. [⊥]These authors contributed equally to this work.

ABSTRACT

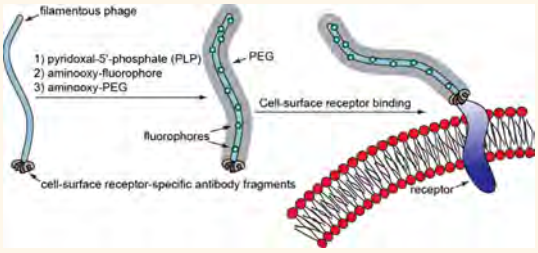

We report a convenient new technique for the labeling of filamentous phage capsid proteins. Previous reports have shown that phage coat protein residues can be modified, but the lack of chemically distinct amino acids in the coat protein sequences makes it difficult to attach high levels of synthetic molecules without altering the binding capabilities of the phage. To modify the phage with polymer chains, imaging groups, and other molecules, we have developed chemistry to convert the N-terminal amines of the ~4200 coat proteins into ketone groups. These sites can then serve as chemospecific handles for the attachment of alkoxyamine groups through oxime formation. Specifically, we demonstrate the attachment of fluorophores and up to 3000 molecules of 2 kDa poly(ethylene glycol) (PEG2k) to each of the phage capsids without significantly affecting the binding of phage-displayed antibody fragments to EGFR and HER2 (two important epidermal growth factor receptors). We also demonstrate the utility of the modified phage for the characterization of breast cancer cells using multicolor fluorescence microscopy. Due to the widespread use of filamentous phage as display platforms for peptide and protein evolution, we envision that the ability to attach large numbers of synthetic functional groups to their coat proteins will be of significant value to the biological and materials communities.

KEYWORDS: phage display · bioorthogonal · bioconjugation · materials science · cancer imaging

Through the use of molecular diversity techniques, filamentous phage can be evolved to bind proteins, polymers, small molecules, and metal ions with high affinity and selectivity.[1] The success of this platform is due to the ability of filamentous phage to express a wide variety of peptides and proteins as extensions of the p3 and p8 coat proteins that comprise the capsid (Figure 1). This method has provided useful binders for a variety of research efforts in molecular biology, biotechnology, biomedicine, and materials science.[2] In addition, the body of the phage has also proven useful as a robust scaffold for nanoparticle nucleation,[3] electrode templating,[4] light collection,[5] cell growth and differentiation,[6] and drug delivery.[7] To enhance these capabilities, we describe herein a convenient N-terminal-selective modification method that can introduce synthetic functionality on the phage coat proteins without interfering with their binding abilities. We demonstrate the utility of this technique by directly converting evolved phage into targeted imaging agents for *in vitro* cell targeting experiments. Furthermore, we use this method to attach up to 3000 polymer chains to these structures without compromising their ability to recognize specific receptors on live cells—a useful capability for reducing background binding and a likely requirement for developing future phage-based agents for *in vivo* applications.

Filamentous phage, such as M13 and fd, have approximately five copies of each of their minor coat proteins (p3, p6, p7, and p9, Figure 1). In addition, fd and M13 phage have 4200 and 2700 copies of the major coat protein (p8), respectively.[2] The p3 sites serve as the principal locations for molecular evolution, especially for large protein inserts such as single-chain antibody variable fragments (scFvs) and enzymes. This leaves the p8 sites as abundant locations for the attachment of additional molecules. To introduce synthetic components into these assemblies, the covalent modification of filamentous phage has typically been accomplished through the

* Address correspondence to mbfrancis@berkeley.edu.

Received for review March 14, 2012 and accepted July 25, 2012.

Published online July 25, 2012
10.1021/nn301134z

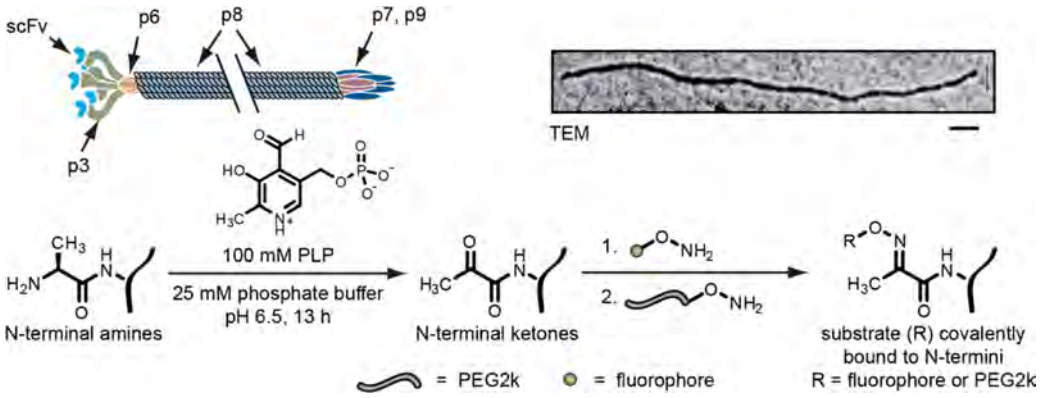

Figure 1. Cartoon (above) and chemical scheme (below) for the transamination of filamentous phage and the attachment of synthetic molecules. The N-termini are transaminated to yield ketone-bearing proteins, which are then reacted with aminooxy-functionalized fluorophores (green circles), followed by aminooxy-functionalized PEG2k (gray strands). The double slash indicates that the phage is much longer than shown when scaled to the minor coat proteins. The TEM image was stained with uranyl acetate (top right, scale bar represents 100 nm).

nonspecific modification of amine groups on the capsid surfaces with NHS esters.[8,9] However, this approach also leads to extensive acylation of the many lysine residues on the p3 proteins and their associated protein fusions, adding considerable heterogeneity and possible binding interference at high modification levels. Tyrosine residues have also been targeted on the phage surface through the use of diazonium coupling reactions,[10] but this approach is also expected to lead to significant modification of critical residues in the evolved proteins. Methods requiring the genetic modification of phage DNA have been attempted to increase specificity. In one case, serine or threonine was genetically introduced at p3 N-termini and oxidized with sodium periodate to produce an aldehyde for chemical labeling.[11] This was not demonstrated for the major coat protein p8 and requires use of sodium periodate, which can undesirably oxidize cysteines. Enzymatic ligations offer another genetic approach, as demonstrated with biotin ligase[12] and sortase A.[13,14] These techniques offer more specificity than prior chemical-labeling approaches, but they also require genetic engineering of phage DNA, which may be undesired or unfeasible in certain contexts. Our goal was to develop a simple yet reliable chemical strategy that did not require prior genetic engineering.

To provide a facile, controlled method for modifying filamentous phage with hundreds or even thousands of new functional groups, we have applied a two-step transamination/oxime formation technique.[15−18] This reaction sequence has been shown to be highly selective for N-terminal groups and does not lead to the transamination of lysine ε-amines. Using high-throughput solid phase screening methods, we have previously determined that this reaction proceeds most readily when N-terminal alanine residues are present and that it can be accelerated by proximal lysine side chains.[19] The phage p8 monomers possess a solvent-exposed N-terminal alanine and a lysine at the i+7 position, making this an especially promising substrate for this reaction.

This modification strategy was developed using filamentous fd phage that display single-chain antibody fragments (scFvs) on their p3 minor coat proteins. These scFvs recognize either epidermal growth factor receptor (EGFR) or human epidermal growth factor receptor 2 (HER2) and were identified using phage display.[20−22] The overexpression of these receptors is associated with many different breast cancer serotypes, thus providing a motivation for the installation of imageable groups[23,24] on these phage for use in diagnostic applications.[25] In parallel, we also used fd phage bearing an scFv targeting botulinum toxin serotype A (anti-BoNT) as a negative control.[22]

RESULTS AND DISCUSSION

To introduce ketones into the coat proteins, phage were transaminated using a 100 mM solution of pyridoxal 5′-phosphate (PLP) at pH 6.5 for 13 h. The excess PLP was then removed by precipitating the phage, after which they were exposed to various alkoxyamine compounds in pH 6.5 buffer for up to 24 h. Aniline catalysis was used to accelerate oxime formation, as has been previously reported by Dawson and coworkers.[26] The specific reaction times and alkoxyamine concentrations were selected based on the levels of modification sought. To estimate the overall extent of p8 modification, a sample of ketone-labeled fd phage was reacted with 2-(aminooxy)acetic acid. Analysis of the coat proteins was achieved using MALDI-TOF mass spectrometry, revealing that the vast majority of the p8 proteins formed the oxime product (Figure 2a and Supporting Information Figure S1), indicating that each fd phage can be loaded with thousands of molecules. Only one addition per p8 was observed, indicating N-terminal specificity even in the presence of five p8 lysines. The overall protein recovery for the transamination and oxime formation steps ranged

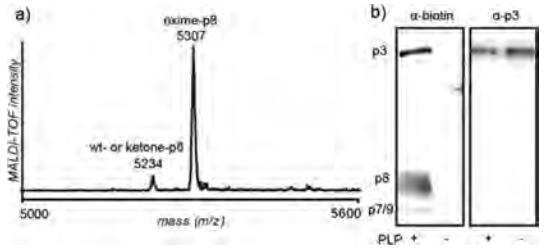

Figure 2. Analysis of filamentous phage modified with small molecules. (a) Matrix-assisted laser desorption/ionization time-of-flight (MALDI-TOF) spectrum showing p8 oxime formation following reaction with 2-(aminooxy)acetic acid (expected mass increase: 73 *m/z*, observed: 73 *m/z*). Non-transaminated fd proteins exposed to the same alkoxyamine resulted in no oxime product formation (see Supporting Information Figure S1). (b) Western blot of M13KE coat protein labeling with biotin followed by blotting with neutravidin-HRP or α-p3 antibodies. Coat protein molecular weights are as follows: p3, 46.5 kDa; p6, 12.4 kDa; p7, 3.6 kDa; p8, 5.2 kDa; p9, 3.7 kDa. Labeling of p7 and p9 cannot be distinguished due to their similar molecular weights (3.6 and 3.7 kDa, respectively). The p6 is not observed, congruent with an N-terminus inaccessible for modification.

from 55 to 95%, with 80% being a typical value. Unfortunately, despite many attempts, protein digest experiments failed to give any cleaved species for the p8 protein, presumably due to its very low solubility and propensity for aggregation once removed from the assembled structure.

The only byproduct was a small amount of a covalent adduct of the protein with the PLP, which presumably formed through an aldol addition of the N-terminal pyruvamide to the pyridoxal aldehyde group. This PLP adduct was not visible following reaction of phage with aminooxy-derivatized molecules *via* MALDI-TOF mass spectrometry analysis, possibly due to its poor ionization or insufficient quantity. It was, however, identified by mass spectrometry after disassembling the phage using RP-HPLC to isolate the PLP adduct-p8 from wt- and ketone-p8 species (Supporting Information Figures S2 and S3). The negative charge of the phosphate group resulted in the earlier elution *via* RP-HPLC. This species has been observed in transamination reactions previously, and since it possesses a ketone group, it can still participate in oxime formation.[16] This, in addition to its very low abundance, renders it insignificant for most applications.

The small p3-to-p8 ratio for fd phage prevented p3 detection by mass spectrometry and Western blotting. Instead, we turned to the use of M13KE phage, which are fd analogues with smaller genomes. They require a smaller number of p8 proteins to tile the length of the phage and therefore have a higher ratio of p3 to p8 proteins. The M13KE and wt-fd coat proteins are identical, except for a single D12N point mutation in p8.[27,28] To detect the modifications with improved sensitivity, transaminated M13KE was exposed to biotin-ONH_2 and analyzed *via* Western blotting with neutravidin-HRP (Figure 2b). All of the coat proteins with accessible N-termini, including p3, showed labeling. The α-p3 blot in Figure 2b shows that both lanes contain approximately the same concentration of phage, while the neutravidin-HRP (α-biotin) blot shows that only PLP-reacted phage are biotin-labeled.

To verify the ability of the modified phage to bind their targets, samples of transaminated anti-EGFR, anti-HER2, and anti-BoNT fd phage were reacted with Alexa Fluor 488 or 647 C5-aminooxyacetamide (AF488/647-ONH_2) dyes. For the cell microscopy experiments described below, approximately 6−8% of the p8 proteins (~300 copies/phage, as determined using UV/vis) were labeled with the fluorophores. Up to 80% of the p8 proteins could be labeled using 100 mM aniline as a catalyst,[26] albeit with decreased solubility. The modified phage bound to their appropriate cell surface receptors with excellent specificity, as revealed using flow cytometry (Figure 3a and Supporting Information Figures S4−S7). The negative control anti-BoNT phage showed no binding. In terms of cell viability, these data also indicated that only 0.25 to 3.0% of the cells had died during the exposure to the phage-based imaging agents, which was in line with untreated cell samples.

The selective binding capabilities of the EGFR and HER2 targeted phage were also confirmed in microscopy experiments. A panel of breast cancer cells was treated with the phage and visualized using live cell confocal microscopy. These images (Figure 3b and Supporting Information Figures S8−S12) demonstrated the retention of excellent specificities and binding capabilities of fd for their targeted receptors following chemical modification. Upon increased incubation times (>2 h), phage targeting overexpressed markers were observed to be internalized by the respective cells. Preliminary results indicate that this occurs *via* receptor-mediated endocytosis; however, further experiments to clarify this behavior are in progress.

The ability of these fd to image receptor overexpression *in vitro*, even when different cell types are mixed, portends well for their use *in vivo*. In anticipation of future *in vivo* applications, we investigated the attachment of poly(etheylene glycol) (PEG) polymers to the phage capsids. PEG has been shown to reduce nonspecific binding, decrease immunogenicity, and increase the solubility of attached molecules.[29] Ketone-labeled fd were reacted with 2 kDa *O*-(methoxypoly(ethylene glycol))-hydroxylamine (PEG2k-ONH_2),[30] and the percentage of p8 proteins that were modified was quantified using RP-HPLC (Supporting Information Figure S13). By varying the reaction times, samples with differing levels of PEG2k-labeled p8s were prepared. Presumably higher concentrations of the PEG2k-ONH_2 could achieve shorter modification times,

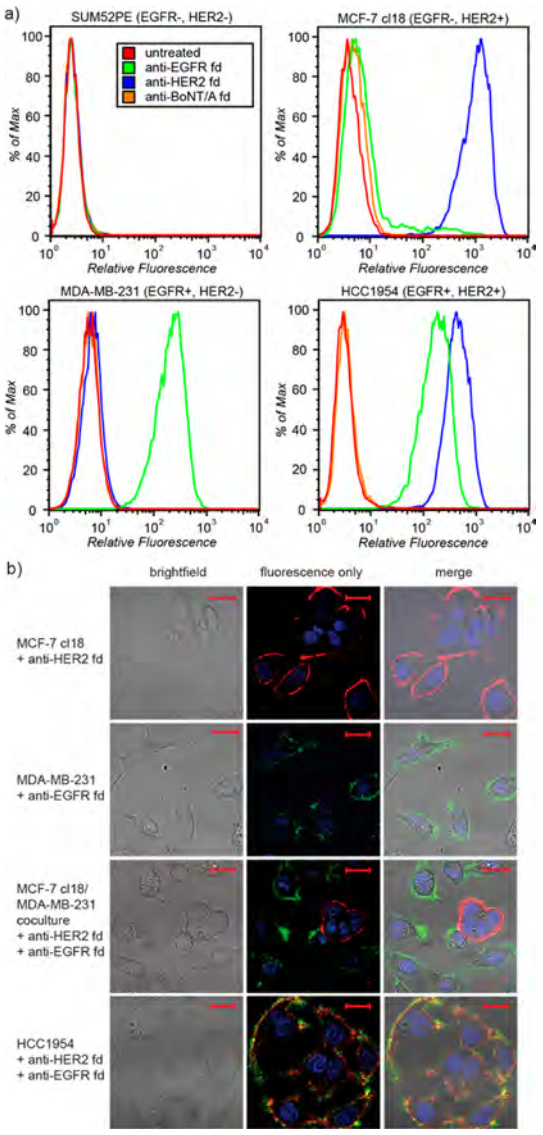

Figure 3. Fluorophore-modified fd phage cell binding results. (a) Flow cytometry with AF488-labeled phage (applied at 0.8 nM) indicated selective recognition of EGFR and HER2 epitopes. The legend for all histograms is shown in SUM52PE inset. Gating data are shown in Supporting Information Figures S4–S7. (b) Live cell confocal microscopy images of fluorescently labeled anti-HER2 and anti-EGFR fd showed marker-specific binding to breast cancer cell lines. Fluorescence is as follows: DAPI (blue), anti-HER2 fd (red), anti-EGFR fd (green). Scale bars represent 20 μm. Control and larger images with all fluorescence channels are shown in Supporting Information Figures S8–S12.

but we avoided using them to prevent precipitation of the phage. For phage labeled with fluorophores, there were no observed changes in the absorption or emission properties of the dyes upon addition of the chains. The added PEG chains also caused no morphological changes that could be observed by TEM (Supporting Information Figure S14).

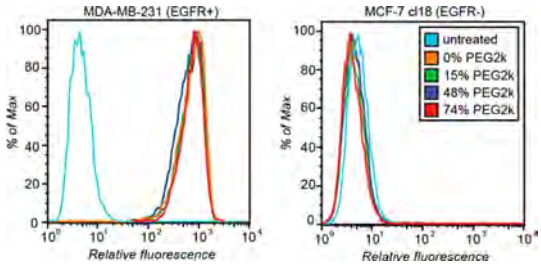

Figure 4. Flow cytometry analysis of AF488-labeled anti-EGFR fd possessing various levels of PEG modifications. The target cells were MDA-MB-231 ($EGFR^+$, left), and the control cells were MCF-7 cl18 ($EGFR^-$, right). Phage concentrations were 0.8 nM. Gating data are shown in Supporting Information Figure S16. As a negative control, anti-BoNT fd labeled with nearly identical levels of PEG showed no binding (see Supporting Information Figures S17 and S18).

Zeta-potential measurements were obtained in order to determine the ability of the PEG polymers to shield fd charge (Supporting Information Figure S15). An increase in negative charge was noted following PLP modification, presumably due to the loss of the cationic N-terminal amino groups on the p8 monomers. As anticipated, the negative charge decreased with increasing levels of PEG modification. At 67% p8 labeling, the zeta-potential was -5.5 ± 7.3 mV, nearly an order of magnitude less than that of ketone-labeled fd. The binding abilities of PEG-labeled fd were also evaluated by flow cytometry (Figure 4 and Supporting Information Figures S16–S18). The PEG-labeled anti-EGFR fd continued to bind MDA-MB-231 (EGFR positive) cells, while none bound the MCF-7 cl18 cells (EGFR negative).

SUMMARY

The chemical modifications to fd phage described herein were used to produce highly selective fluorescent imaging agents that can be readily adapted for use with MRI, PET, and other detection modalities. Furthermore, the binding molecule, phage length, and labeling molecule type can be adjusted for a variety of *in vitro* and *in vivo* applications.[31] By combining the ability of phage display to obtain genetically encodable binding molecules with the N-terminal transamination/oximation method for appending chemical functionality, a much wider variety of well-defined multifunctional materials can now be accessed.

METHODS

Unless otherwise noted, all chemical reagents were purchased from Aldrich. Alexa Fluor 488 and 647 C5-aminooxyacetamide, bis(triethylammonium) salt, *N*-(aminooxyacetyl)-*N*′-(D-biotinoyl) hydrazine, trifluoroacetic acid salt, and neutravidin-HRP were purchased from Invitrogen. Anti-M13 p3 was purchased from New England Biolabs. *O*-(Methoxypoly(ethylene glycol))-hydroxylamine (PEG2k-ONH_2) was prepared as previously described.[30] Cells were maintained according to

ATCC recommended guidelines. For specific instrumentation and detailed experimental information, see the Supporting Information.

Fd Production. Fd displaying anti-EGFR, -HER2, and -BoNT scFvs used in these experiments have been reported previously[20−22] and were generated using standard techniques.[32]

Transamination. Fd (75−128 nM) were transaminated using 100 mM PLP in 25 mM phosphate buffer at pH 6.5 for 13 h at room temperature. Excess PLP was removed *via* a series of precipitations with 20% PEG8k/2.5 M NaCl, supernatant removal, and resuspension in PBS.

Reaction with Biotin and Western Blotting. The final reaction concentrations were 296 nM M13KE, 10 mM phosphate buffer (pH 6.2), 10 mM aniline, and 16 mM biotin-ONH_2. After 15 h at room temperature, the reaction was quenched by adding D,L-glyceraldehyde to a final concentration of 33.3 μM, followed by SDS-PAGE. A 1:10 000 dilution of anti-p3 and a 1:2000 dilution of Neutravidin-HRP were used for blotting experiments. A Genscript 1 h western kit was used for detection.

Reaction with 2-(Aminooxy)acetic Acid. Twenty-four nanomolar fd was reacted with 5 mM 2-(aminooxy)acetic acid in 100 mM anilinium acetate, pH 4.7, for 21 h at room temperature. Reaction conditions were different from those used for other labeling reactions because the objective of this experiment was to estimate the percentage of transaminated p8s. For this reason, low pH and high aniline concentrations were used to maximize p8 labeling. Other experiments used higher pH values and lower aniline concentrations to better control the percent of p8s modified.

Reaction with Fluorophores. The final reaction concentrations were 185 nM fd, 20 mM phosphate buffer (pH 6.2), 10 mM (for AF488) or 100 mM aniline (for AF647), and 1 mM AF488/647-ONH_2. Exposure to these conditions for 45 min at room temperature resulted in 2% p8 modification (for phage to be reacted with PEG subsequently). Otherwise, reactions continued for 16−18 h at room temperature, resulting in 6−8% levels of dye modification. After the reaction, the excess fluorophore was removed using the purification described above.

Flow Cytometry. Five hundred thousand cells in 100 μL of 1% FBS/DPBS were mixed with 100 μL of 0.8 nM fd and incubated at 4 °C. After 1 h, each sample was diluted to 1 mL with 1% FBS/DPBS, and the cells were washed before resuspending in 200 μL of 1% FBS/DPBS.

Cell Microscopy. Two milliliters of 25 000 cells/mL in 35 mm glass bottom dishes (Mattek) was grown at 37 °C with 5% CO_2 for 72−96 h. The cells were washed with PBS, and 150 μL of 0.8 nM fd in 1% FBS/DPBS was added before incubating at 37 °C with 5% CO_2 for 1 h. The cells were washed three times with PBS followed by addition of 1 mL of phenol-red-free media with 10% FBS. DAPI was added to 1 μM prior to imaging.

Reaction with PEG2k. Thirty-seven nanomolar fd, 20 mM PEG2k-ONH_2, 20 mM phosphate buffer (pH 6.2), and 10 mM aniline were combined. Following the appropriate reaction times, samples were washed over an Illustra Nap-5 gel filtration column, eluting with PBS.

Conflict of Interest: The authors declare no competing financial interest.

Acknowledgment. These studies were generously supported by the DOD Breast Cancer Research Program (BC061995) and the NCI SPORE in Breast Cancer (P50-CA58207). Z.M.C. was supported by the Berkeley Chemical Biology Graduate Program (NRSA Training Grant 1 T32 GMO66698). M.E.F. is supported by a DOD BCRP postdoctoral fellowship (BC100159). H.C. was supported by the Dow Foundation Sustainable Products and Solutions Program.

Supporting Information Available: Full characterization of conjugates, chromatograms, and additional flow cytometry data are provided. This material is available free of charge *via* the Internet at http://pubs.acs.org.

REFERENCES AND NOTES

1. Smith, G. P.; Petrenko, V. A. Phage Display. *Chem. Rev.* **1997**, *97*, 391–410.
2. Kehoe, J. W.; Kay, B. K. Filamentous Phage Display in the New Millennium. *Chem. Rev.* **2005**, *105*, 4056–4072.
3. Mao, C. B.; Solis, D. J.; Reiss, B. D.; Kottmann, S. T.; Sweeney, R. Y.; Hayhurst, A.; Georgiou, G.; Iverson, B.; Belcher, A. M. Virus-Based Toolkit for the Directed Synthesis of Magnetic and Semiconducting Nanowires. *Science* **2004**, *303*, 213–217.
4. Lee, Y. J.; Yi, H.; Kim, W. J.; Kang, K.; Yun, D. S.; Strano, M. S.; Ceder, G.; Belcher, A. M. Fabricating Genetically Engineered High-Power Lithium-Ion Batteries Using Multiple Virus Genes. *Science* **2009**, *324*, 1051–1055.
5. Nam, Y. S.; Shin, T.; Park, H.; Magyar, A. P.; Choi, K.; Fantner, G.; Nelson, K. A.; Belcher, A. M. Virus-Templated Assembly of Porphyrins into Light-Harvesting Nanoantennae. *J. Am. Chem. Soc.* **2010**, *132*, 1462–1463.
6. Merzlyak, A.; Indrakanti, S.; Lee, S.-W. Genetically Engineered Nanofiber-like Viruses for Tissue Regenerating Materials. *Nano Lett.* **2009**, *9*, 846–852.
7. Arap, W.; Pasqualini, R.; Ruoslahti, E. Cancer Treatment by Targeted Drug Delivery to Tumor Vasculature in a Mouse Model. *Science* **1998**, *279*, 377–380.
8. Yacoby, I.; Benhar, I. Targeted Filamentous Bacteriophages as Therapeutic Agents. *Expert Opin. Drug Delivery* **2008**, *5*, 321–329.
9. Hilderbrand, S. A.; Kelly, K. A.; Niedre, M.; Weissleder, R. Near Infrared Fluorescence-Based Bacteriophage Particles for Ratiometric pH Imaging. *Bioconjugate Chem.* **2008**, *19*, 1635–1639.
10. Li, K.; Chen, Y.; Li, S.; Nguyen, H. G.; Niu, Z.; You, S.; Mello, C. M.; Lu, X.; Wang, Q. Chemical Modification of M13 Bacteriophage and Its Application in Cancer Cell Imaging. *Bioconjugate Chem.* **2010**, *21*, 1369–1377.
11. Ng, S.; Jafari, M. R.; Matochko, W. L.; Derda, R. Quantitative Synthesis of Genetically Encoded Glycopeptide Libraries Displayed on M13 Phage. *ACS Chem. Biol.* **2012**, 10.1021/cb300187t.
12. Chen, I.; Choi, Y.-A.; Ting, A. Y. Phage Display Evolution of a Peptide Substrate for Yeast Biotin Ligase and Application to Two-Color Quantum Dot Labeling of Cell Surface Proteins. *J. Am. Chem. Soc.* **2007**, *129*, 6619–6625.
13. Hess, G. T.; Cragnolini, J. J.; Popp, M. W.; Allen, M. A.; Dougan, S. K.; Spooner, E.; Ploegh, H. L.; Belcher, A. M.; Guimaraes, C. P. M13 Bacteriophage Display Framework That Allows Sortase-Mediated Modification of Surface-Accessible Phage Proteins. *Bioconjugate Chem.* **2012**, *23*, 1478–1487.
14. Popp, M. W.; Antos, J. M.; Grotenbreg, G. M.; Spooner, E.; Ploegh, H. L. Sortagging: A Versatile Method for Protein Labeling. *Nat. Chem. Biol.* **2007**, *3*, 707–708.
15. Gilmore, J. M.; Scheck, R. A.; Esser-Kahn, A. P.; Joshi, N. S.; Francis, M. B. N-Terminal Protein Modification through a Biomimetic Transamination Reaction. *Angew. Chem., Int. Ed.* **2006**, *45*, 5307–5311.
16. Scheck, R. A.; Dedeo, M. T.; Iavarone, A. T.; Francis, M. B. Optimization of a Biomimetic Transamination Reaction. *J. Am. Chem. Soc.* **2008**, *130*, 11762–11770.
17. Dixon, H. B. F. N-Terminal Modification of Proteins. *J. Protein Chem.* **1984**, *3*, 99–108.
18. Snell, E. E. The Vitamin B_6 Group. V. The Reversible Interconversion of Pyridoxal and Pyridoxamine by Transamination Reactions. *J. Am. Chem. Soc.* **1945**, *67*, 194–197.
19. Witus, L. S.; Moore, T.; Thuronyi, B. W.; Esser-Kahn, A. P.; Scheck, R. A.; Iavarone, A. T.; Francis, M. B. Identification of Highly Reactive Sequences for PLP-Mediated Bioconjugation Using a Combinatorial Peptide Library. *J. Am. Chem. Soc.* **2010**, *132*, 16812–16817.
20. Zhou, Y.; Drummond, D. C.; Zou, H.; Hayes, M. E.; Adams, G. P.; Kirpotin, D. B.; Marks, J. D. Impact of Single-Chain Fv Antibody Fragment Affinity on Nanoparticle Targeting of Epidermal Growth Factor Receptor-Expressing Tumor Cells. *J. Mol. Biol.* **2007**, *371*, 934–947.
21. O'Connell, D.; Becerril, B.; Roy-Burman, A.; Daws, M.; Marks, J. D. Phage *versus* Phagemid Libraries for Generation of Human Monoclonal Antibodies. *J. Mol. Biol.* **2002**, *321*, 49–56.

22. Amersdorfer, P.; Wong, C.; Smith, T.; Chen, S.; Deshpande, S.; Sheridan, R.; Marks, J. D. Genetic and Immunological Comparison of Anti-Botulinum Type A Antibodies from Immune and Non-immune Human Phage Libraries. *Vaccine* **2002**, *20*, 1640–1648.
23. Hooker, J. M.; O'Neil, J. P.; Romanini, D. W.; Taylor, S. E.; Francis, M. B. Genome-Free Viral Capsids as Carriers for Positron Emission Tomography Radiolabels. *Mol. Imaging Biol.* **2008**, *10*, 182–191.
24. Datta, A.; Hooker, J. M.; Botta, M.; Francis, M. B.; Aime, S.; Raymond, K. N. High Relaxivity Gadolinium Hydroxypyridonate-Viral Capsid Conjugates: Nanosized MRI Contrast Agents. *J. Am. Chem. Soc.* **2008**, *130*, 2546–2552.
25. Milanezi, F.; Carvalho, S.; Schmitt, F. C. EGFR/HER2 in Breast Cancer: A Biological Approach for Molecular Diagnosis and Therapy. *Expert Rev. Mol. Diagn.* **2008**, *8*, 417–434.
26. Dirksen, A.; Hackeng, T. M.; Dawson, P. E. Nucleophilic Catalysis of Oxime Ligation. *Angew. Chem., Int. Ed.* **2006**, *45*, 7581–7584.
27. van Wezenbeek, P. M.; Hulsebos, T. J.; Schoenmakers, J. G. Nucleotide Sequence of the Filamentous Bacteriophage M13 DNA Genome: Comparison with Phage Fd. *Gene* **1980**, *11*, 129–148.
28. Noren, K. A.; Noren, C. J. Construction of High-Complexity Combinatorial Phage Display Peptide Libraries. *Methods* **2001**, *23*, 169–178.
29. Pasut, G.; Veronese, F. M. PEG Conjugates in Clinical Development or Use as Anticancer Agents: An Overview. *Adv. Drug Delivery Rev.* **2009**, *61*, 1177–1188.
30. Schlick, T. L.; Ding, Z.; Kovacs, E. W.; Francis, M. B. Dual-Surface Modification of the Tobacco Mosaic Virus. *J. Am. Chem. Soc.* **2005**, *127*, 3718–3723.
31. Specthrie, L.; Bullitt, E.; Horiuchi, K.; Model, P.; Russel, M.; Makowski, L. Construction of a Microphage Variant of Filamentous Bacteriophage. *J. Mol. Biol.* **1992**, *228*, 720–724.
32. Barbas, C. F.; Burton, D. R.; Scott, J. K.; Silverman, G. J. *Phage Display: A Laboratory Manual*; Cold Spring Harbor Laboratory Press: Cold Spring Harbor, NY, 2001.

N-terminal Labeling of Filamentous Phage to Create Cancer Marker Imaging Agents

Zachary M. Carrico,[a,‡] Michelle E. Farkas, [a,‡] Yu Zhou,[b] Sonny C. Hsiao,[a] James D. Marks,[b] Harshal Chokhawala,[c] Douglas S. Clark,[c] and Matthew B. Francis[a,*]

[a]Department of Chemistry, University of California, Berkeley, CA 94720, [b]Department of Anesthesia and Pharmaceutical Chemistry, University of California, San Francisco, CA 94143, and [c]Department of Chemical Engineering, University of California, Berkeley, CA 94720. [‡]These authors contributed equally to this work.
[*]To whom correspondence should be addressed: mbfrancis@berkeley.edu

Supporting Information

Materials

Unless otherwise noted, all chemical reagents were purchased from Aldrich. Alexa Fluor® 488 C5-aminooxyacetamide, bis(triethylammonium) salt (AF488-ONH_2), Alexa Fluor® 647 C5-aminooxyacetamide, bis(triethylammonium) salt (AF647-ONH_2), *N*-(aminooxyacetyl)-*N*'-(D-biotinoyl) hydrazine, trifluoroacetic acid salt, and neutravidin-HRP were purchased from Invitrogen. M13KE and Anti-M13 p3 antibodies were purchased from New England Biolabs. *O*-(Methoxypoly(ethylene glycol))-hydroxylamine (PEG2k-ONH_2) was prepared as previously described.[1] Water used in biological procedures and chemical reactions was deionized using a NANOpure purification system (Barnstead, USA). All cell culture reagents were obtained from Gibco/Invitrogen Corp (Carlsbad, CA) unless otherwise noted.

Instrumentation

High performance liquid chromatography (HPLC). HPLC was performed on an Agilent 1100 Series HPLC System (Agilent Technologies, USA). Sample analysis for all HPLC experiments was achieved with an inline diode array detector (DAD) and an Agilent Zorbax 300 SB-CN column. 0.1% TFA/water (A) and 0.1% TFA/acetonitrile (B) were used as HPLC solvents. The following method was used: 35% B for the first 4 min, ramping to 70% B over 15 min, then to 95% B over the next 30 s, and a 5.5 min wash with 95% B.

Matrix assisted laser desorption-ionization time-of-flight mass spectrometry (MALDI-TOF MS). MALDI-TOF MS was performed on a Voyager-DETM system (PerSeptiveBiosystems, USA) in the QB3/Chemistry Mass Spectrometry Facility. Sinipinic acid was used as the matrix.

Transmission electron microscopy (TEM). TEM images were obtained at the UC Berkeley Electron Microscope Lab (www.em-lab.berkeley.edu) using an FEI Tecnai 12 transmission electron microscope with a 100 kV accelerating voltage. Samples were prepared for TEM analysis by pipetting 8 µL of 0.1 nM fd solutions onto grids and allowing them to equilibrate for 3 min. The samples were wicked dry with filter paper, and the grids exposed to 8 µL of 10 mg/mL aqueous uranyl acetate solution for 90 s as a negative stain. The excess stain was removed by wicking, and the grid was allowed to dry in air.

Flow cytometry. A FACSCalibur flow cytometer (BD Biosciences, USA) equipped with 488 and 633 nm lasers were used for all flow cytometry measurements, usage courtesy of Prof. Carolyn Bertozzi (UC Berkeley).

Confocal microscopy. Images were acquired on a Zeiss 510 NLO Axiovert 200M Tsunami microscope equipped with 488 and 633 nm lasers, usage courtesy of Prof. Christopher Chang (UC Berkeley).

Zeta potential. Zeta potential measurements were obtained using a Malvern Instruments Zetasizer Nano ZS and DTS1060 cuvettes, usage courtesy of Prof. Jean M. J. Fréchet (UC Berkeley). Measurements were taken in water. Thirty measurements were taken per sample.

Calculation of phage concentration

phage/mL = ((absorbance at 269 nm – absorbance at 320 nm) / 6 x 10^6) / (number of single stranded DNA bases in the phage genome)[2]

Detailed Experimental Procedures

fd and M13KE phage growth and purification. fd phage displaying anti-EGFR, -HER2, and -BoNT scFvs were propagated in and reacted under identical conditions.[3–5] A tetracycline resistance gene was previously introduced into the fd phage genome to allow measurement of *E. coli* infectivity in colony forming units (cfu) using LB-agar plates containing 20 μg/mL tetracycline. A colony of *E. coli* TG1 cells infected with fd were inoculated into 2 mL of LB growth media containing 20 μg/mL tetracycline, incubated at 37 °C with 250 rpm shaking. After approximately 6 h, 1 mL culture was added to 1 L of 2xYT media containing 20 μg/mL tetracycline. The culture was incubated at 30 °C for approximately 13 h with 250 rpm shaking. Cells were removed via centrifugation at 6,000 rpm for 10-30 min at 4 °C. The supernatant was collected and the fd were precipitated for 1 h at 4 °C after thorough mixing with 0.15 volumes of 20% PEG8k/2.5M NaCl solution. The resulting suspension was centrifuged at 8,000 rpm for 20 min at 4 °C, and the recovered pellet was resuspended in 30 mL of 4 °C PBS. This solution of fd was centrifuged at 6,000 rpm for 10 min at 4 °C to remove additional cell debris. The supernatant was collected, and fd were precipitated for 40 min at 4 °C after thorough mixing with 0.15 volumes of a solution of 20% PEG8k and 2.5 M NaCl. The samples were then centrifuged at 9,000 rpm for 30 min to isolate the precipitated fd. The resulting pellet was resuspended in 5 mL of 4 °C PBS.

M13KE filamentous phage were used for western blotting experiments. Because M13KE lacks antibiotic resistance, it was grown from plaques rather than colonies. It was grown in media lacking antibiotics at 37 ºC and its purification was identical to that used for fd.

Transamination. fd and M13KE were transaminated using 100 mM pyridoxal-5'-phosphate (PLP) in 100 mM phosphate buffer, pH 6.5, for 13 h at rt. Concentrations of 75-128 nM fd were used in these experiments, typically at total volumes of 5-20 mL. Due to the large excess of PLP used, fd concentration was not found to be critical for successful transamination. As an example reaction: 4.7 mL of water was added to 3.3 mL of 128 nM anti-EGFR fd, followed by 1 mL of 250 mM phosphate buffer at pH 6.5, and 1 mL of 1 M PLP in 125 mM phosphate buffer, pH 6.5. The transamination was allowed to proceed for approximately 13 h, at which point the excess PLP was removed by a series of precipitations and resuspensions in PBS. After thorough mixing with 0.15 volumes of a 20% PEG8k/2.5 M NaCl solution, the fd were precipitated for 1 h at 4 °C. The fd were then isolated by centrifugation at 9,000 rpm for 30 min. The fd pellet was resuspended in 30 mL of PBS, and then the precipitation, centrifugation, and

resuspension cycle was repeated two additional times. The final pellet was resuspended in PBS to yield a final volume of approximately 2 mL. To prepare the PLP solution used in these reactions, a 2 M solution of PLP in 250 mM phosphate buffer (pH 6.5) was made. The pH was adjusted to 6.5 with 3 M NaOH, and the solution was diluted with 250 mM phosphate buffer, pH 6.5 to give a 1 M PLP solution. The PLP solution must be freshly made before use.

Reaction with 2-(aminooxy)acetic acid. 24 nM transaminated fd was reacted with 5 mM 2-(aminooxy)acetic acid in 100 mM anilinium acetate, pH 4.7, for 21 h at rt. For M13KE, 25 nM transaminated M13KE was reacted with 7 mM 2-(aminooxy)acetic acid in 100 mM phosphate buffer, pH 4 with 1 mM aniline for 21 h at rt. Both reactions conditions yield approximately equivalent percentages of oxime product (Supporting Information Figure S1 and S3).

M13KE reaction with biotin and western blotting. M13KE filamentous phage were used for biotin labeling as an fd surrogate because fd could not be sufficiently concentrated to observe all minor coat proteins by western blot. M13KE is a one amino acid variant of fd, and is shorter because its genome has not been enlarged by genetic engineering. This decrease in length enables higher minor coat protein concentrations to be obtained.[2] The final reaction concentrations were: 296 nM M13KE, 10 mM phosphate buffer (pH 6.2), 10 mM aniline, and 16 mM biotin-ONH_2. After 15 h at rt, the reaction was quenched by adding DL-glyceraldehyde to a final concentration of 33.3 μM, followed by SDS-PAGE. A 1:10,000 dilution of anti-p3 antibodies and a 1:2,000 dilution of Neutravidin-HRP were used for blotting. A Genscript 1-hour western kit was used for detection.

Conjugation of fluorophores to ketone-modified fd phage. A sample of ketone-labeled fd phage prepared as described above was exposed to the appropriate alkoxyamine and an aniline catalyst[6] in an Eppendorf tube. The final reaction concentrations were: 185 nM fd, 20 mM phosphate buffer pH 6.2, aniline (10 mM for AF-488 or 100 mM for AF-647, as a catalyst for the oxime formation), and 1 mM fluorophore. Total reaction volumes were typically <100 μL. The reaction was quenched by fd precipitation and solution removal after 45 min at rt, resulting in 2% p8 labeling with the fluorophore. For higher levels of modification, the reactions were allowed to proceed for up to 18 h. Levels of modification were calculated using the extinction coefficients of the fluorophores (AF488: 71,000 M^{-1} cm^{-1}, AF647: 237,000 M^{-1} cm^{-1} according to Molecular Probes/Invitrogen) to determine the fluorophore concentration. After the fluorophore contribution to the 269 and 320 nm absorbance has been subtracted from the total 269 and 320 nm absorbance, the fd concentration can be calculated. Excess fluorophore was removed in an analogous fashion to the removal of excess PLP.

Conjugation of PEG2k to ketone-modified fd phage. Fluorophore labeled fd were reacted with PEG2k-ONH_2 for varying lengths of time. The conditions for the PEG2k-ONH_2 reaction were: 37 nM phage, 20 mM PEG2k-ONH_2, 20 mM phosphate buffer pH 6.2, and 10 mM aniline. After 1.5, 4, and 22 h at rt, aliquots from the reaction mixture were washed over an Illustra Nap-5 gel filtration column (GE Healthcare). If desired, DL-glyceraldehyde can also be used to quench the reaction before passing it over an Illustra Nap-5 gel filtration column; however, this quench was not used for the samples described in this report. The extent of PEG2k labeling was quantified using reverse phase HPLC. The typical p8 coat protein elution time was 10-13 min.

Zeta potential measurement. Zeta potential measurements were performed using a Zetasizer Nano-DS and DTS1060 cuvettes. fd labeled with PEG2k, but not with fluorophore, were used. Following the PEG conjugation reaction, the fd were eluted from NAP-5 columns in water to improve the reproducibility of the zeta-potential measurements.

Cell culture. Immortalized human breast cancer cells were maintained according to ATCC guidelines. SUM52PE cells were from the Tissue Culture Facility, Department of Molecular & Cell Biology, UC Berkeley, and were grow in Ham's F-12 media supplemented with 5% FBS, 5 μg/mL insulin, 1 μg/mL hydrocortisone, and 10 mM HEPES (pH 7.4). MCF-7 clone 18 cells were from the Preclinical Therapeutics Core Facility, UCSF. All cells were grown at 37 °C in 5% CO_2.

Cell microscopy. Cells were washed with PBS, trypsinized, and trypsin was quenched with growth media. Cells were centrifuged at 125 rcf for 5 min, and resuspended in growth media. Following counting via hemocytometer, the cells were centrifuged again, and resuspended in normal growth media at a concentration of 25,000 cells/mL. 2 mL was added to each 35 mm glass bottom dish (MatTek Corp.). For MCF-7 clone 18/MDA-MB-231 co-cultures, 1 mL (25,000 cells/mL) of each cell line was added to a centrifuge tube and mixed by pipetting prior to plating in dishes together. Cells were allowed to grow at 37 °C with 5% CO_2 for 72-96 h. All media was removed from the dishes, and cells were washed once with 1 mL PBS. 150 μL of 0.8 nM fd in flow cytometry buffer (FCB, see below) was added to each well of the plate, and the dishes were incubated at 37 °C with 5% CO_2. After 1 h, 1 mL of PBS was added to wash the cells gently, and was then removed. Two more washes with 1 mL of PBS were performed, and then 1 mL of phenol red-free media with 10% FBS was added to the cells. DAPI was added to 1 μM prior to imaging.

Flow cytometry. Following the harvesting and counting of cells as above, cells were resuspended in flow cytometry buffer (FCB; 1% FBS in DPBS). The cells were aliquotted into Eppendorf tubes at 100 μL (500,000 cells) per tube and kept on ice. 100 μL of 0.8 nM fd in FCB was added and incubated at 4 ºC. After 1 h, each sample was diluted to 1 mL with FCB, and the tubes were centrifuged at 2,000 rpm for 5 min. The supernatant was removed, and the cells were resuspended in 1 mL of FCB, followed by centrifugation, and removal of the supernatant. The cells were finally resuspended in 200 μL of FCB. Data were analyzed using FlowJo analysis software (Tree Star Inc.). Gating was performed by applying the autogating tool in FlowJo onto the major population of cells in the FSC x SSC (forward versus side scatter plots) of untreated samples; additional (agent treated) samples were subject to the same gating as the untreated populations for that respective cell line.

Supporting Information References

[1] Schlick, T. L.; Ding, Z.; Kovacs, E. W.; Francis, M. B. Dual-Surface Modification of the Tobacco Mosaic Virus. *J. Am. Chem. Soc.* **2005**, *127*, 3718-3723.

[2] Barbas, C. F.; Burton, D. R.; Scott, J. K.; Silverman, G. J. *Phage Display: A Laboratory Manual*; Cold Spring Harbor Laboratory Press: Cold Spring Harbor, New York, **2001**.

[3] Zhou, Y.; Drummond, D. C.; Zou, H.; Hayes, M. E.; Adams, G. P.; Kirpotin, D. B.; Marks, J. D. Impact of Single-Chain Fv Antibody Fragment Affinity on Nanoparticle Targeting of Epidermal Growth Factor Receptor-Expressing Tumor Cells. *J. Mol. Biol.* **2007**, *371*, 934-947.

[4] Amersdorfer, P.; Wong, C.; Smith, T.; Chen, S.; Deshpande, S.; Sheridan, R.; Marks, J. D. Genetic and Immunological Comparison of Anti-Botulinum Type A Antibodies from Immune and Non-Immune Human Phage Libraries. *Vaccine* **2002**, *20*, 1640-1648.

[5] O'Connell, D.; Becerril, B.; Roy-Burman, A.; Daws, M.; Marks, J. D. Phage Versus Phagemid Libraries for Generation of Human Monoclonal Antibodies. *J. Mol. Biol.* **2002**, *321*, 49-56.
[6] Dirksen, A.; Hackeng, T. M.; Dawson, P. E. Nucleophilic Catalysis of Oxime Ligation. *Angew. Chem., Int. Ed.* **2006**, *45*, 7581-7584.

Figure S1

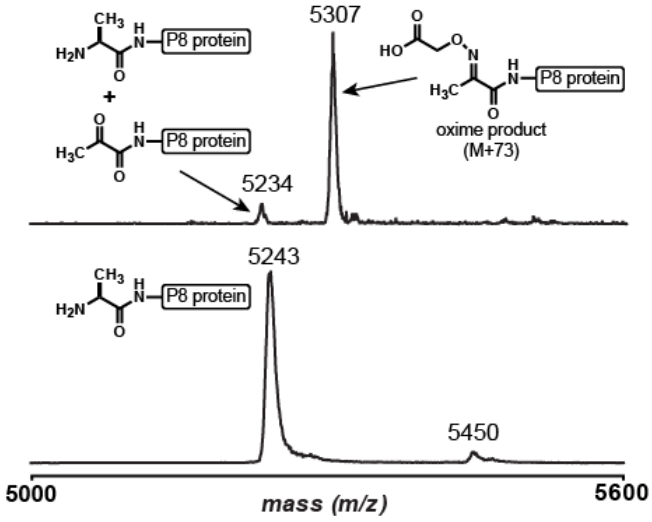

Figure S1. MALDI-TOF spectrum of transaminated fd (top) and non-transaminated fd (bottom) following reaction with 2-(aminooxy)acetic acid. The expected molecular weight of p8 is 5240 Da. The observed 5234 *m*/*z* peak (top) and the 5243 m/z peak (bottom) correspond to the transaminated and/or unmodified p8 proteins. The peak at 5307 m/z (top) corresponds to the oxime product (expected mass increase: 73 m/z, observed 73 *m*/z).

Figure S2

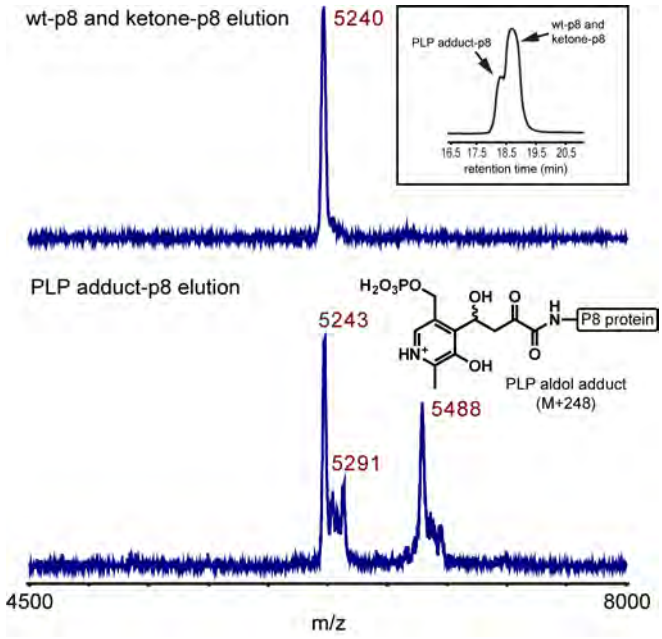

Figure S2. Characterization of modified M13KE phage p8 using MALDI-TOF MS after M13KE transamination and separation of p8 modifications via reversed phase HPLC**.** (Inset) HPLC chromatogram of modified M13KE. (Top) MALDI-TOF spectrum corresponding to the major peak of the p8 elution (see Figure S13, top spectrum for the analogous elution profile of fd). The expected molecular weight of wt-p8 is 5239 Da and overlaps with that of the expected ketone-p8 mass of 5238 Da. (Bottom) MALDI-TOF spectrum of the shoulder-peak, which elutes slightly before the main peak, corresponding to the PLP adduct-P8; some of the major elution peak bleeds into this peak, explaining the 5243 Da signature. The 5291 peak is of unknown origin. The observed mass difference between the two major MALDI peaks is 245 Da, which is presumably an aldol addition of the ketone group to the PLP aldehyde (expected change: 248 Da).

Figure S3

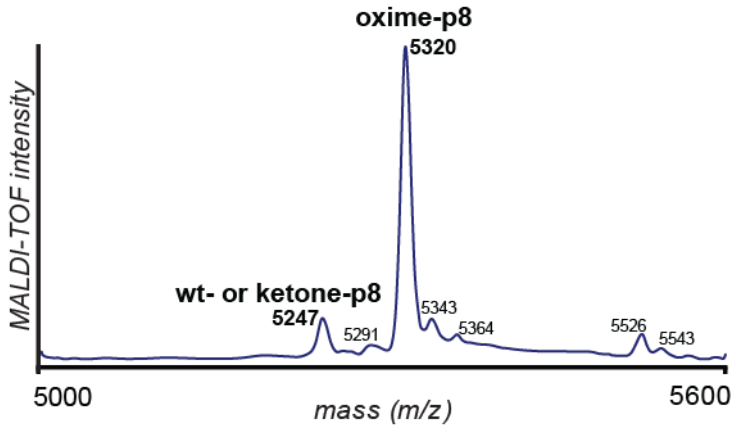

Figure S3. Characterization of modified M13KE phage using MALDI-TOF MS. The spectrum shows p8 oxime formation following reaction with 2-(aminooxy)acetic acid (expected mass increase: 73 m/z, observed: 73 m/z). The smaller peaks cannot be attributed to any coat protein and are of unknown origin.

Figure S4

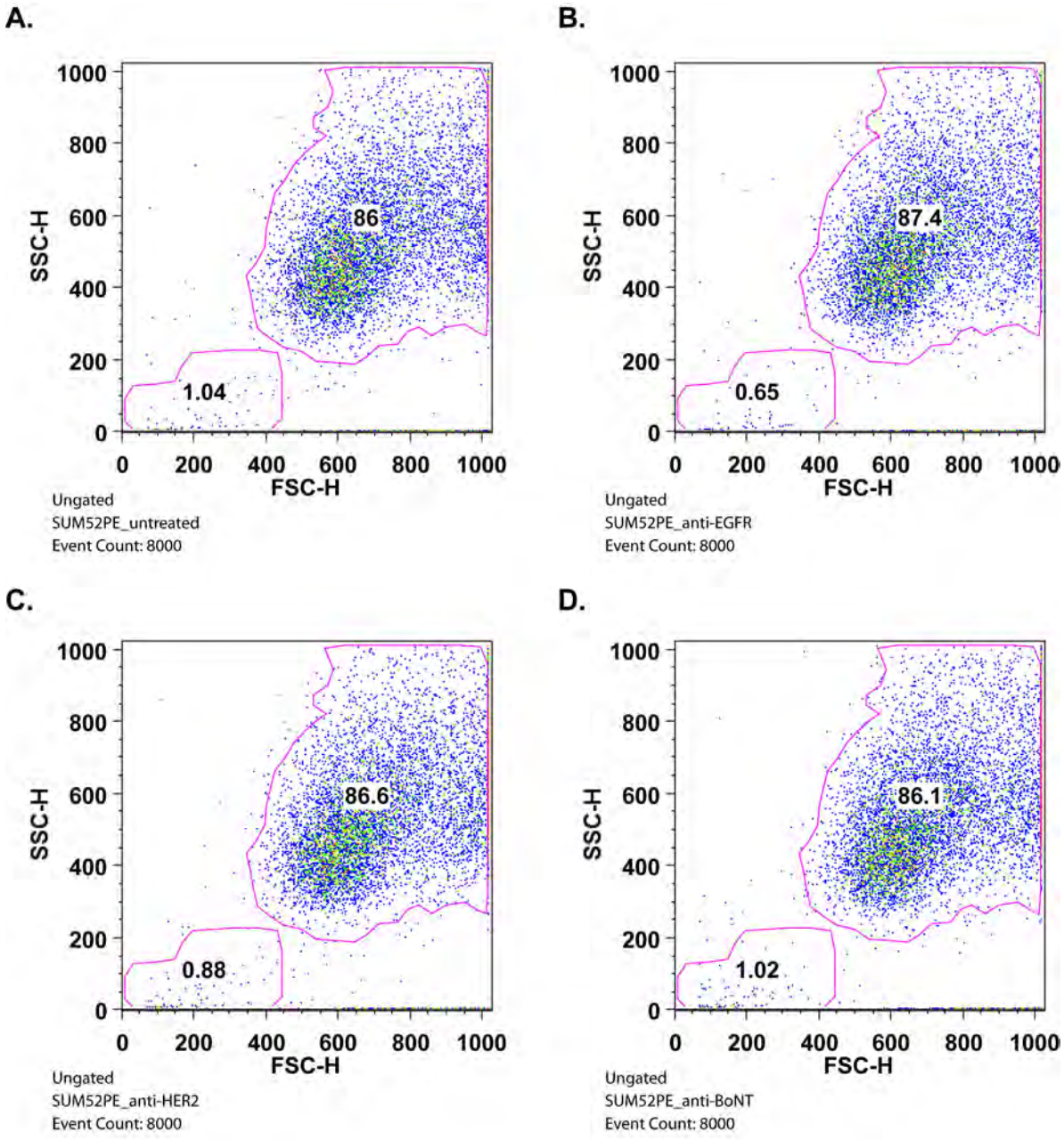

Figure S4. Forward and side scatter plots for flow cytometry with SUM52PE cells. Plots are shown for (**A**) untreated, (**B**) anti-EGFR phage treated, (**C**) anti-HER2 phage treated, and (**D**) anti-BoNT treated cells. The gating of the majority population was used for histogram generation (Figure 3a) as indicated by the pink outline; the gating of the minority population reflects dead or dying cells. Number inside of the plot reflects percentage of cells within each gate.

Figure S5

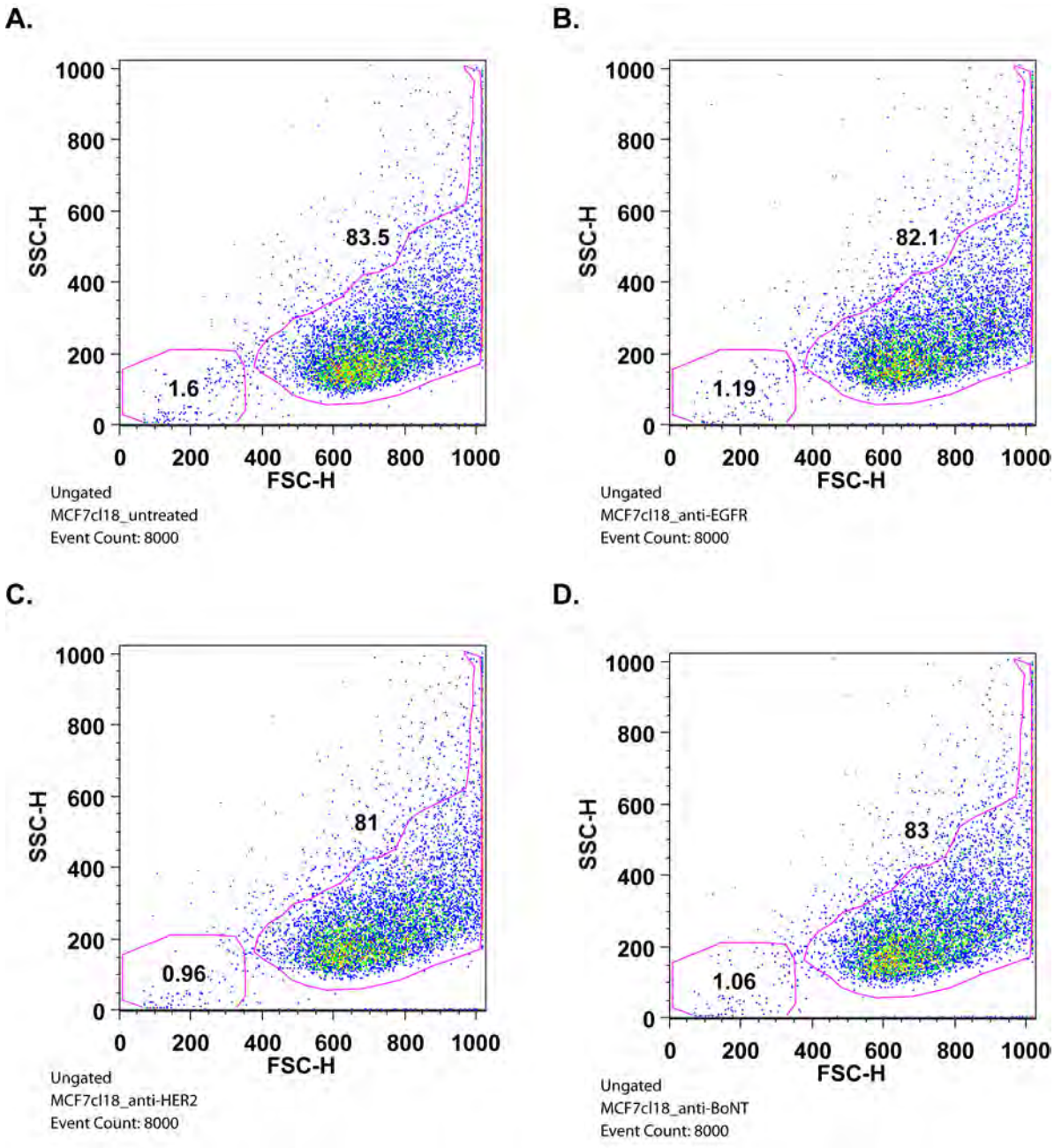

Figure S5. Forward and side scatter plots for flow cytometry with MCF-7 clone 18 cells. Plots are shown for (**A**) untreated, (**B**) anti-EGFR phage treated, (**C**) anti-HER2 phage treated, and (**D**) anti-BoNT treated cells. The gating of the majority population was used for histogram generation (Figure 3a) as indicated by the pink outline; the gating of the minority population reflects dead or dying cells. Number inside of the plot reflects percentage of cells within each gate.

Figure S6

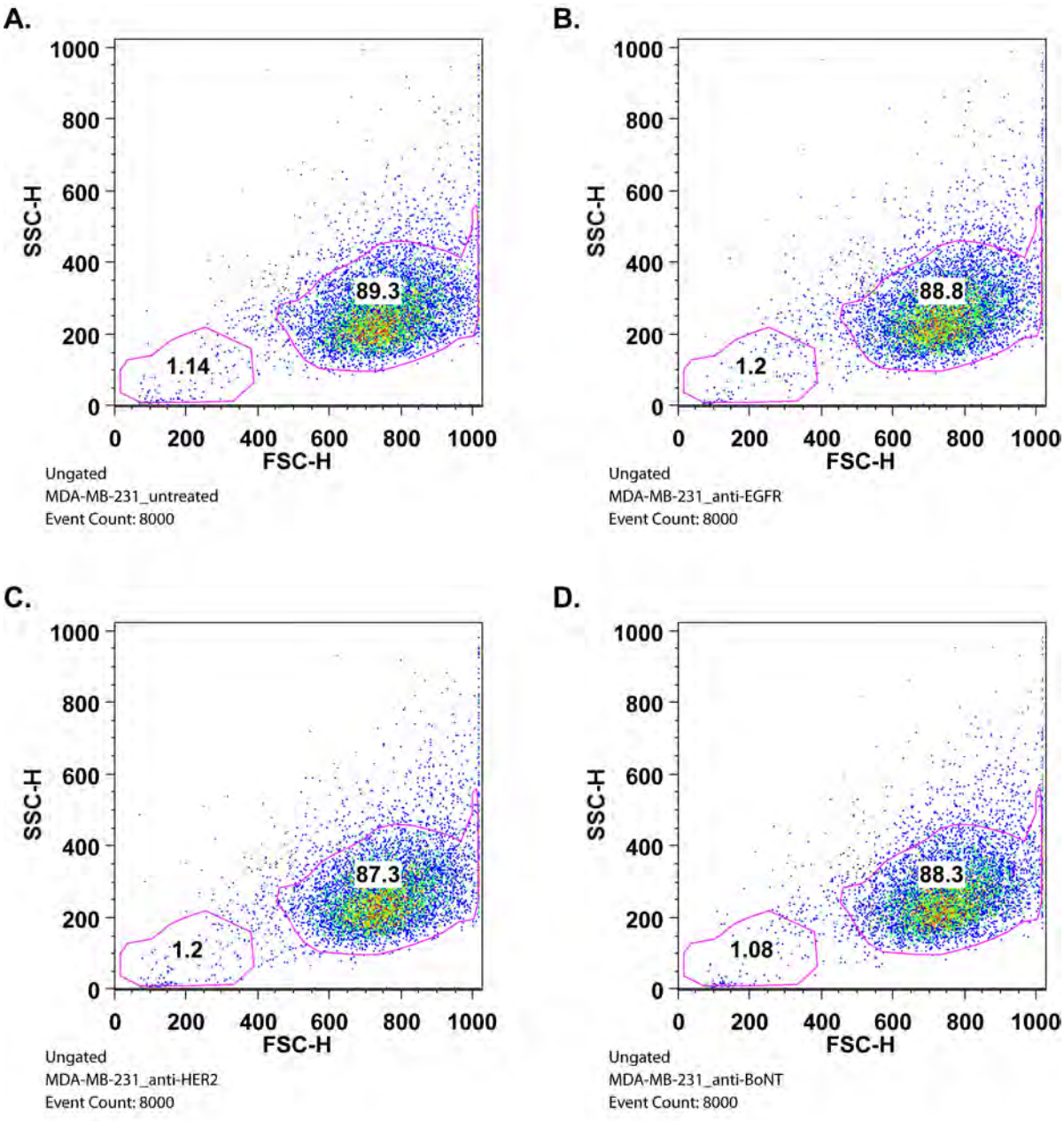

Figure S6. Forward and side scatter plots for flow cytometry with MDA-MB-231 cells. Plots are shown for (**A**) untreated, (**B**) anti-EGFR phage treated, (**C**) anti-HER2 phage treated, and (**D**) anti-BoNT treated cells. The gating of the majority population was used for histogram generation (Figure 3a) as indicated by the pink outline; the gating of the minority population reflects dead or dying cells. Number inside of the plot reflects percentage of cells within each gate.

Figure S7

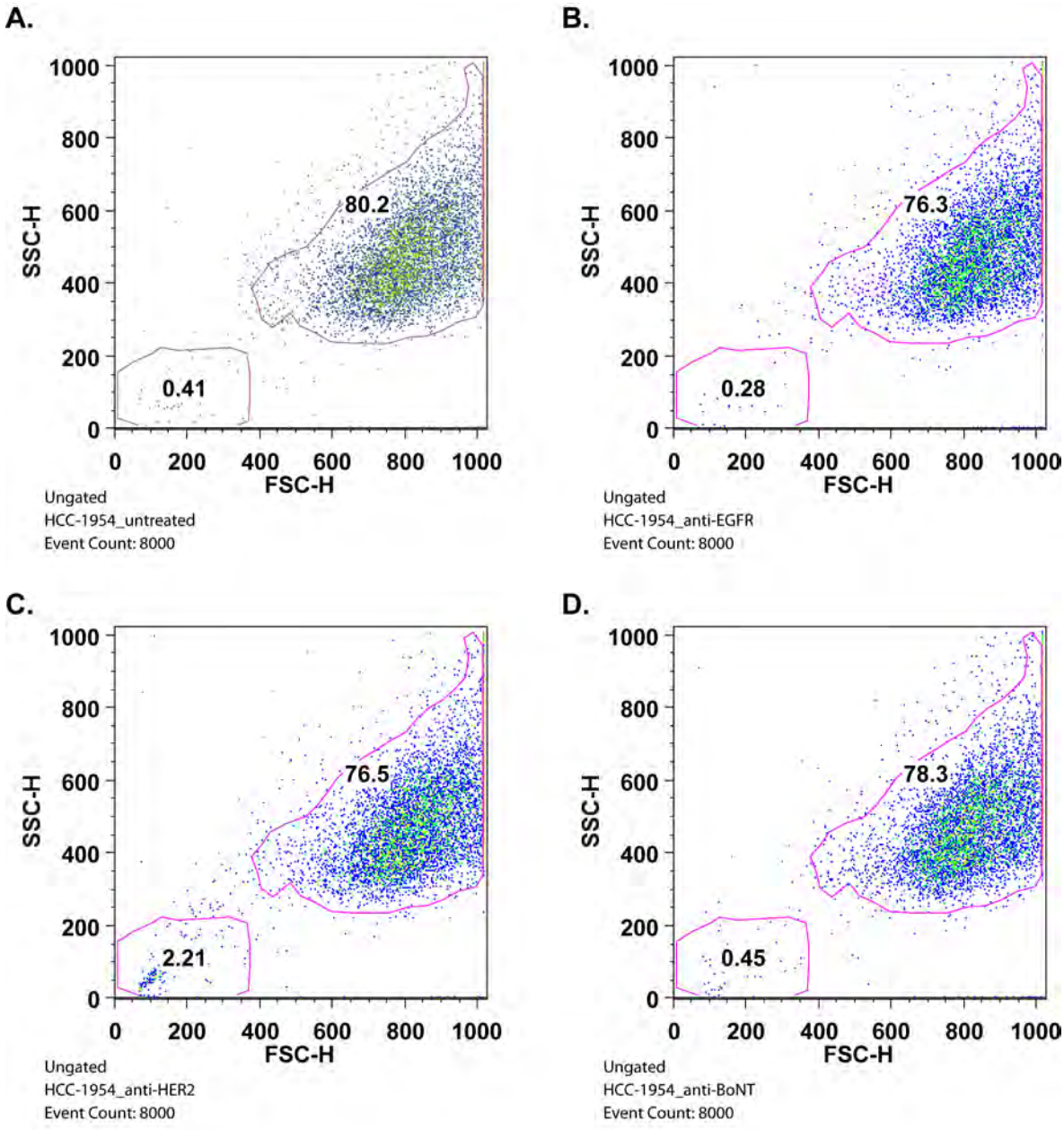

Figure S7. Forward and side scatter plots for flow cytometry with HCC1954 cells. Plots are shown for (**A**) untreated, (**B**) anti-EGFR phage treated, (**C**) anti-HER2 phage treated, and (**D**) anti-BoNT treated cells. The gating of the majority population was used for histogram generation (Figure 3a) as indicated by the pink outline; the gating of the minority population reflects dead or dying cells. Number inside of the plot reflects percentage of cells within each gate.

Figure S8

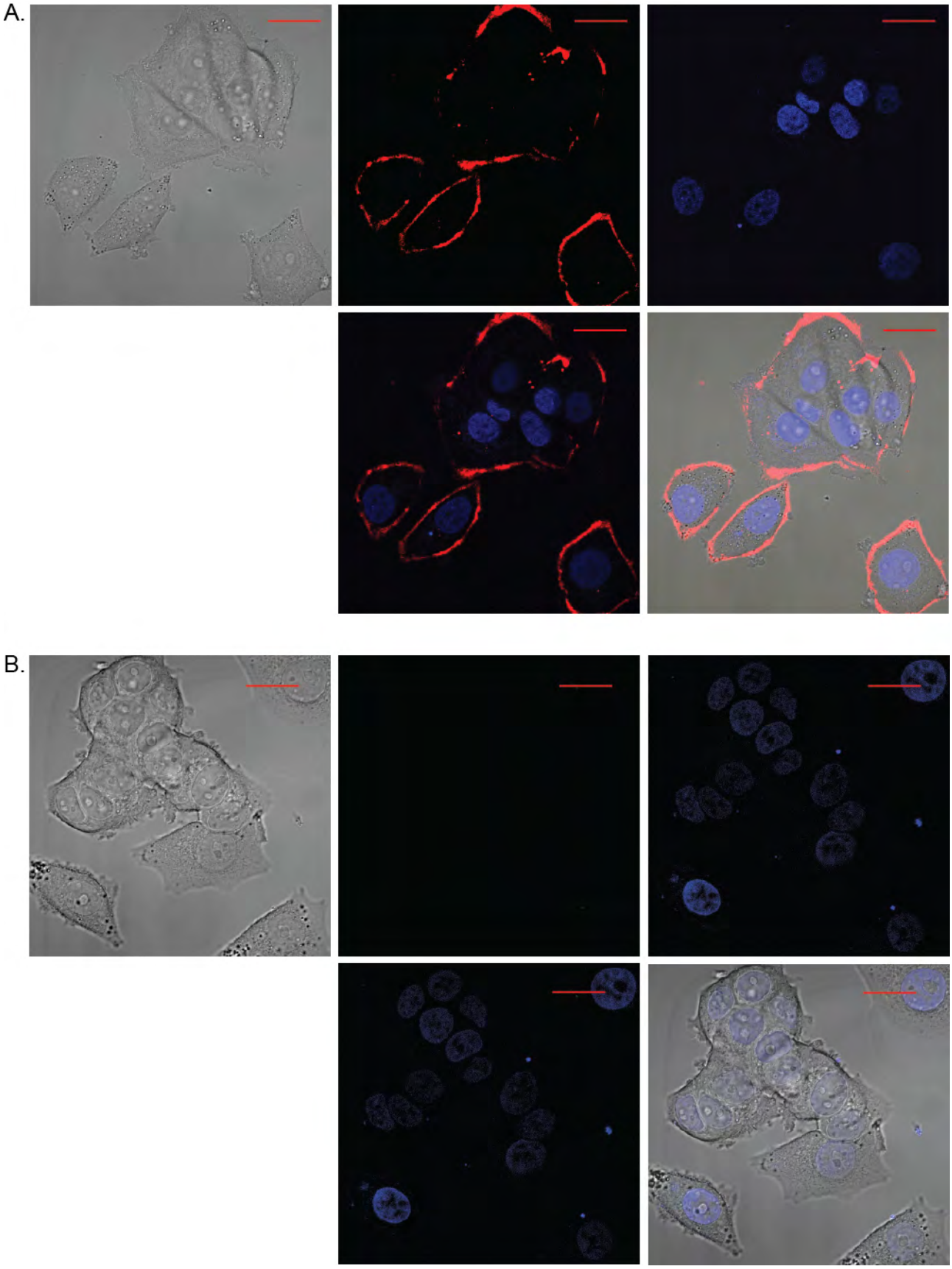

Figure S8. Live cell confocal microscopy images of MCF-7 clone 18 cells treated with anti-HER2 (**A**) and anti-EGFR (**B**) fd. Fd were added at 0.8 nM in 150 µL of PBS. Scale bars indicate 20 µm. Fluorescence is as follows: DAPI (blue), anti-HER2

(red), anti-EGFR (green). Top row (L to R): bright field image, red (**A**) or green (**B**) channel only, blue channel only; bottom row (L to R): all fluorescence channels, merge.

Figure S9

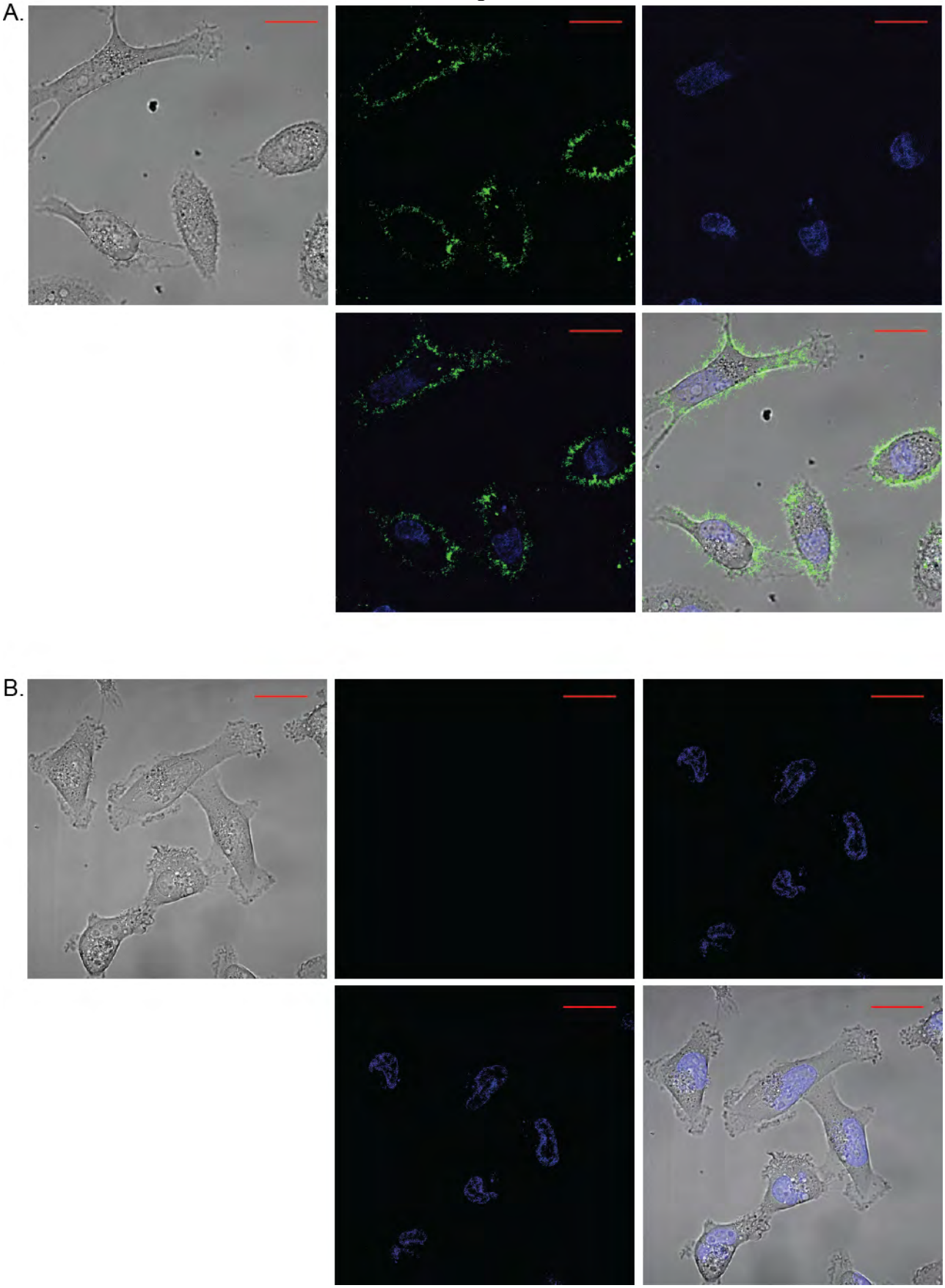

Figure S9. Live cell confocal microscopy images of MDA-MB-231 cells treated with anti-EGFR (**A**) and anti-HER2 (**B**) fd. Fd were added at 0.8 nM in 150 µL of PBS. Scale bars indicate 20 µm. Fluorescence is as follows: DAPI (blue), anti-HER2 (red), anti-EGFR (green). Top row (L to R): bright field image, green (**A**) or red (**B**) channel only, blue channel only; bottom row (L to R): all fluorescence channels, merge.

Figure S10

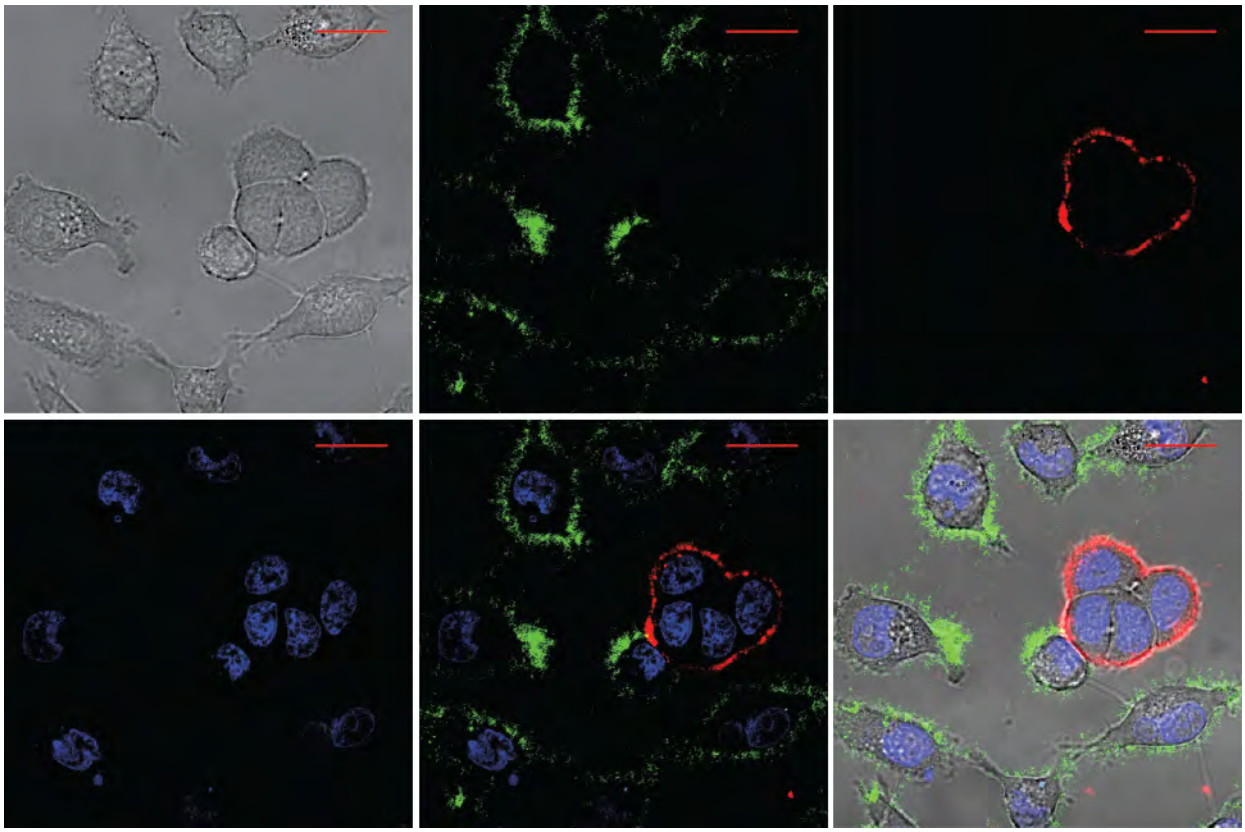

Figure S10. Live cell confocal microscopy images of MDA-MB-231 and MCF7 clone 18 cells treated with anti-HER2 and anti-EGFR fd. Fd were added at 0.8 nM in 150 µL of PBS. Scale bars indicate 20 µm. Fluorescence is as follows: DAPI (blue), anti-HER2 (red), anti-EGFR (green). Top row (L to R): bright field image, green channel only, red channel only; bottom row (L to R): blue channel only, all fluorescence channels, merge.

Figure S11

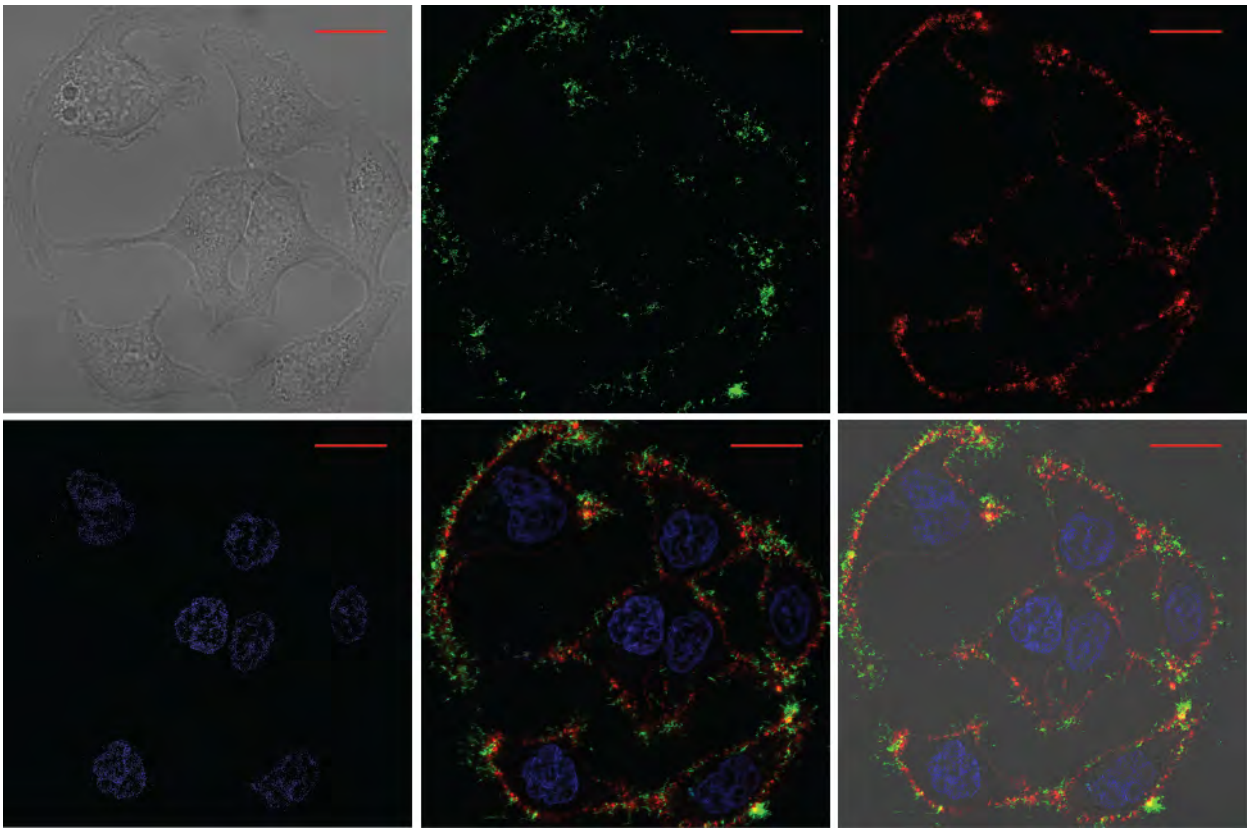

Figure S11. Live cell confocal microscopy images of HCC1954 cells treated with anti-HER2 and anti-EGFR phage. Phage were added at 0.8 nM in 150 µL of PBS. Scale bars indicate 20 µm. Fluorescence is as follows: DAPI (blue), anti-HER2 (red), anti-EGFR (green). Top row (L to R): bright field image, green channel only, red channel only; bottom row (L to R): blue channel only, all fluorescence channels, merge.

Figure S12

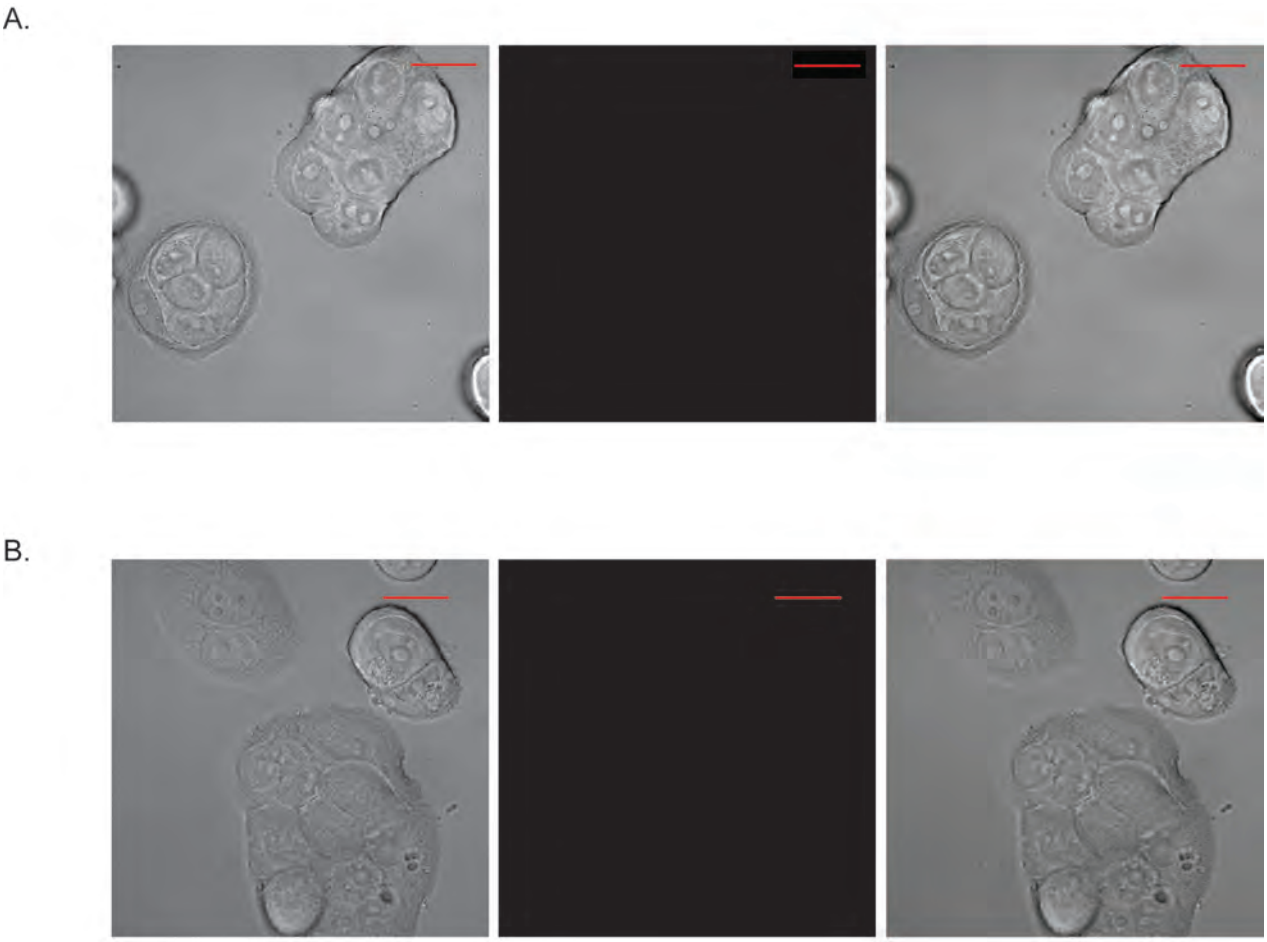

Figure S12. Live cell confocal microscopy images of SUM52PE cells treated with anti-HER2 (**A**) and anti-EGFR phage (**B**). Phage were added at 0.8 nM in 150 µL of PBS. Scale bars indicate 20 µm. Fluorescence is as follows: anti-HER2 (red), anti-EGFR (green). (L to R): bright field image, red channel only (**A**) or green channel only (**B**), merge. Due to cellular toxicity, nuclear staining was not used with these cells.

Figure S13

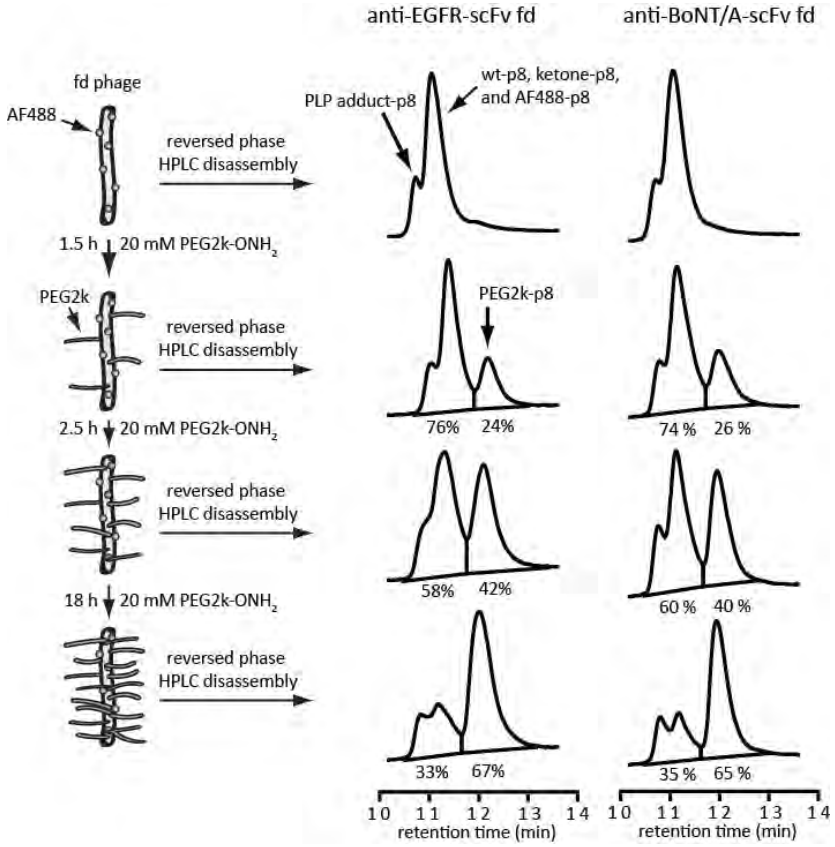

Figure S13. PEG2k modification of fd**.** After transamination using PLP and modification with AF488-ONH_2, the fd were reacted with 20 mM PEG2k-ONH_2 for 1.5, 4, and 22 h. During reversed phase chromatography, the fd disassembled into coat proteins and DNA. The absorbance at 280 nm is shown; p8 was the only coat protein observed. The first peak to elute corresponds to the PLP adduct of p8 (see Figure S2). The second peak is composed of wt-p8, ketone-p8, and AF488-p8 (absorbance at 488 nm is observed), and the last peak to elute (PEG-treated samples only) is PEG2k-p8.

Figure S14

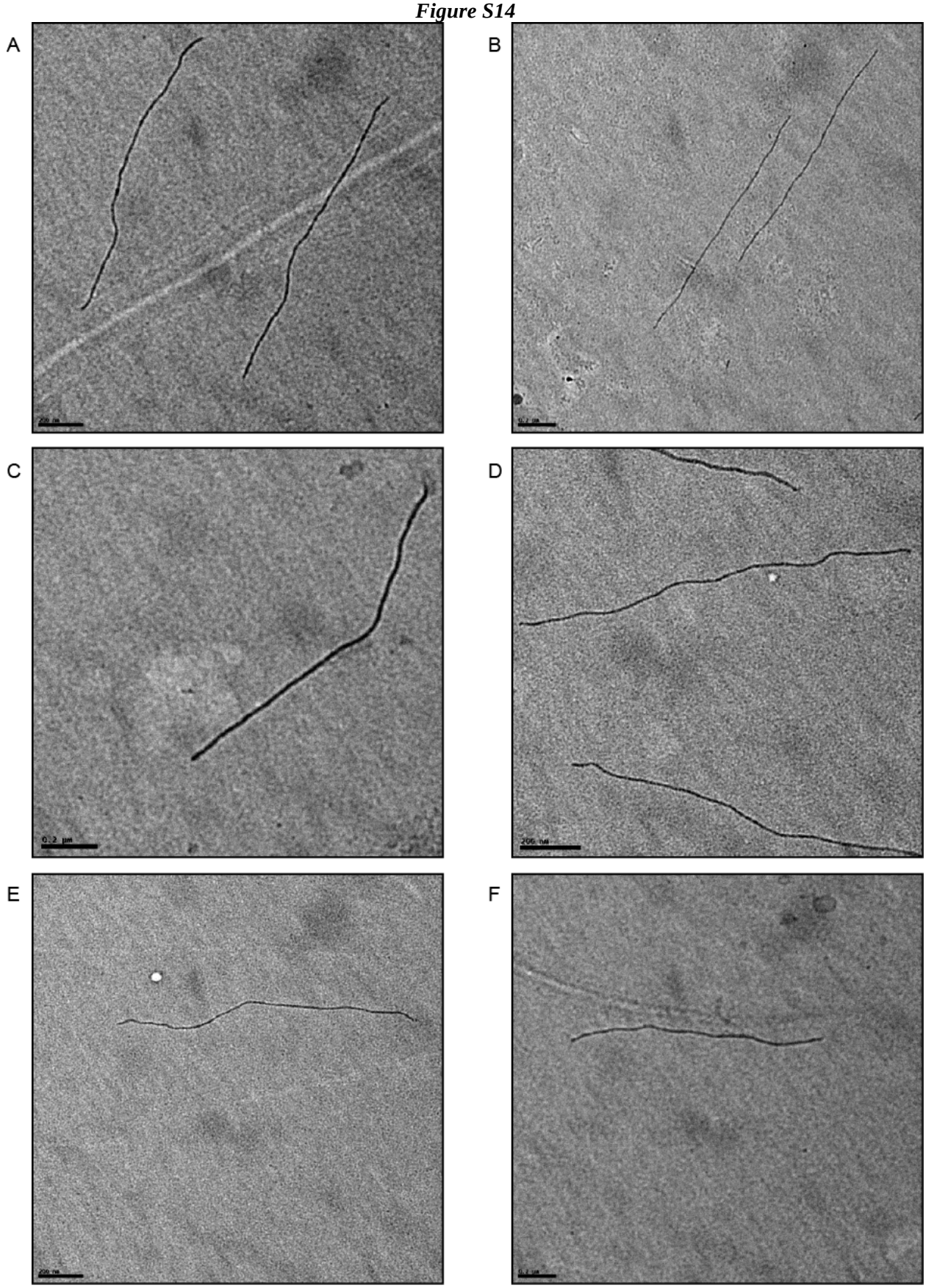

Figure S14. Transmission electron microscope (TEM) images of fd bearing anti-EGFR-scFv molecules**.** (**A**) Wt-fd. (**B**) Fd following PLP-mediated transamination. (**C**) Fd with 2% of the p8 proteins fluorescently labeled with AF488-ONH_2, **(D)** 2% AF488 and 24% PEG2k, (**E**) 2% AF488 and 42% PEG2k, and (**F**) 2% AF488 and 67% PEG2k. All scale bars represent 200 nm.

Figure S15

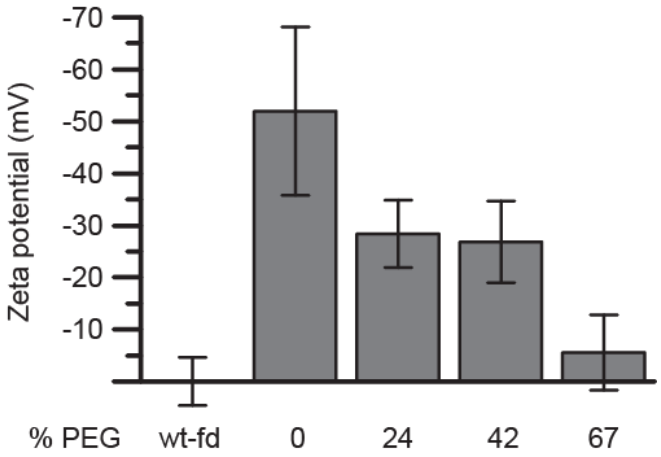

Figure S15. Zeta potential measurements of anti-EGFR fd as a function of the percent of p8 proteins labeled with PEG2k**.** These fd phage have not been modified with AF488.

Figure S16

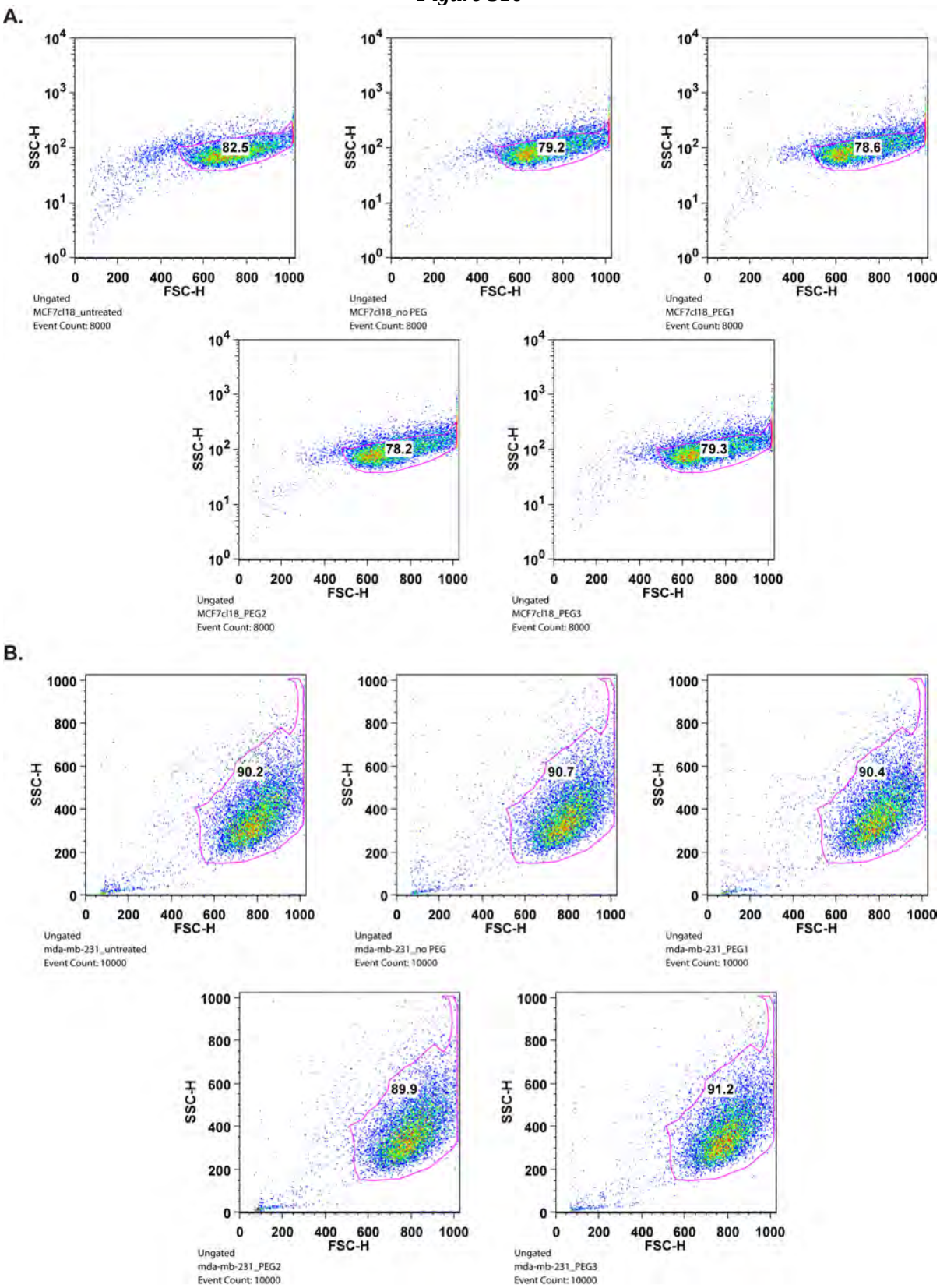

Figure S16. Forward and side scatter plots for flow cytometry with MCF-7 clone 18 (**A**) and MDA-MB-231 (**B**) cells. Plots are shown for untreated, no-PEG (0% modified), PEG1 (15% modified), PEG2 (48% modified), and PEG3 (74% modified) anti-EGFR treated cells. The gating of the majority population was used for histogram generation (Figure 4 in main text) as indicated by the pink outline. The number inside of the plot reflects percentage of cells within each gate.

Figure S17

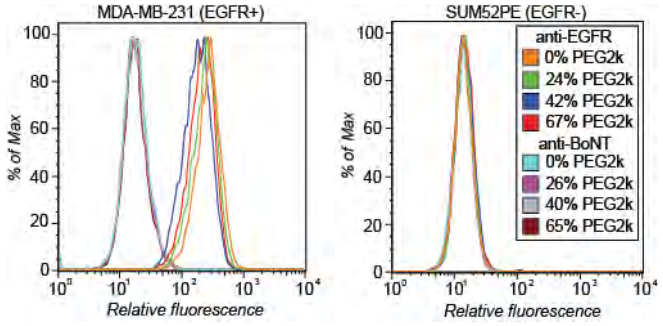

Figure S17. Histograms of MDA-MB-231 (left) and SUM52PE (right) cell-binding by anti-EGFR and anti-BoNT fd with various percentages of p8 proteins labeled with PEG2k.

Figure S18

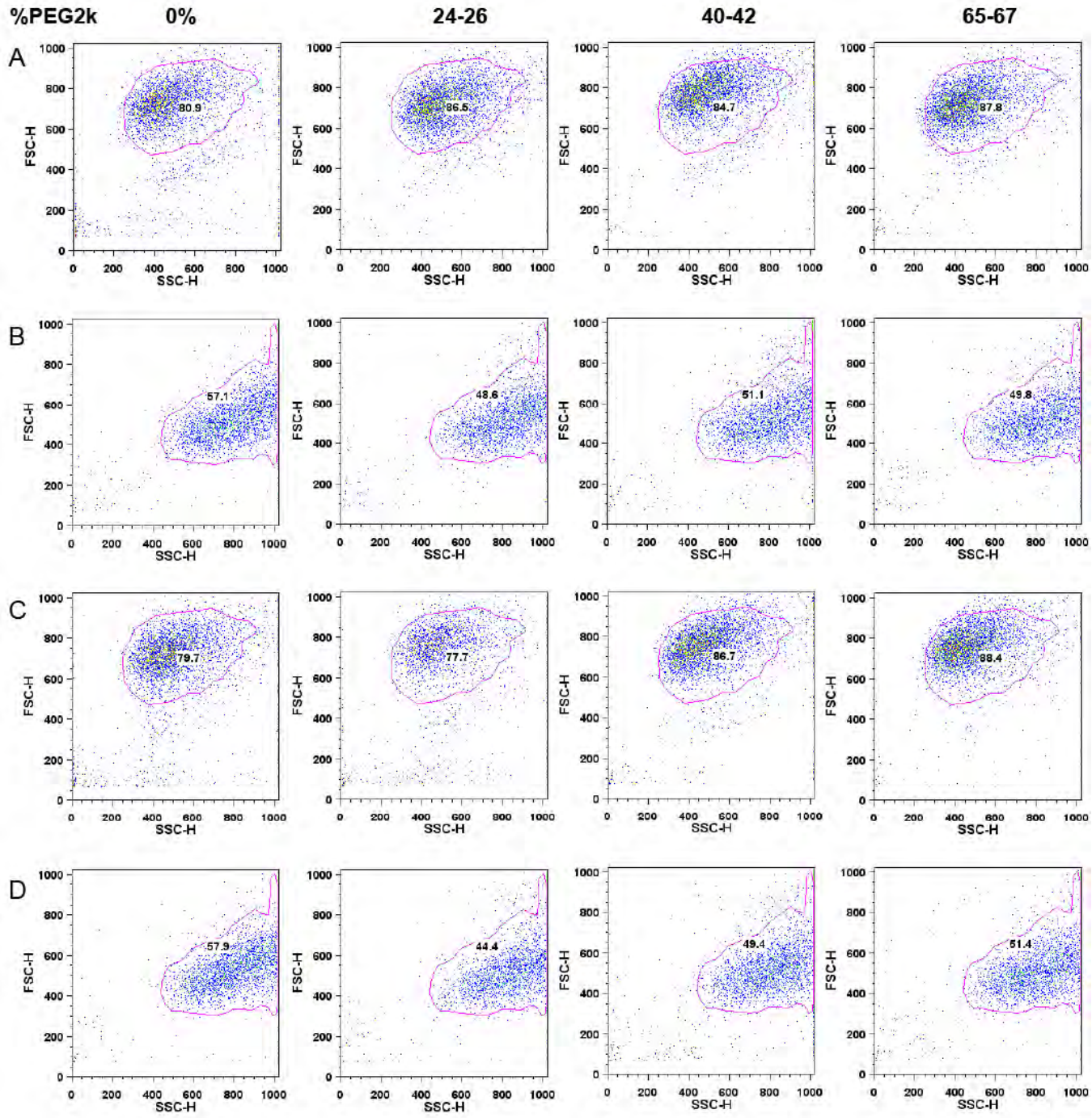

Figure S18. Forward and side scatter plots for flow cytometry with PEG-modified phage. Columns (L to R) indicate p8 proteins modified with various percentages of PEG2k. Plots are shown for (**A**) anti-EGFR fd treated MDA-MB-231 cells, (**B**) anti-EGFR fd treated SUM52PE cells, (**C**) anti-BoNT fd treated MDA-MB-231 cells, and (**D**) anti-BoNT fd treated SUM52PE cells. Gating used for histogram generation (Figure S17) is indicated by the pink outline. The number inside of the plot reflects percentage of cells within each gate.

molecular pharmaceutics

Article

pubs.acs.org/molecularpharmaceutics

PET Imaging and Biodistribution of Chemically Modified Bacteriophage MS2

Michelle E. Farkas,[†] Ioana L. Aanei,[†] Christopher R. Behrens,[†] Gary J. Tong,[†] Stephanie T. Murphy,[‡] James P. O'Neil,[§] and Matthew B. Francis*[,†,∥]

[†]Department of Chemistry, University of California, Berkeley, California 94720-1460, United States

[‡]Department of Radiology and Biomedical Imaging, University of California, San Francisco, California 94107, United States

[§]Life Science Division, Lawrence Berkeley National Laboratory, Berkeley, California 94720, United States

[∥]Materials Sciences Division, Lawrence Berkeley National Laboratory, Berkeley, California 94720-1460, United States

Supporting Information

ABSTRACT: The fields of nanotechnology and medicine have merged in the development of new imaging and drug delivery agents based on nanoparticle platforms. As one example, a mutant of bacteriophage MS2 can be differentially modified on the exterior and interior surfaces for the concurrent display of targeting functionalities and payloads, respectively. In order to realize their potential for use in *in vivo* applications, the biodistribution and circulation properties of this class of agents must first be investigated. A means of modulating and potentially improving the characteristics of nanoparticle agents is the appendage of PEG chains. Both MS2 and MS2-PEG capsids possessing interior DOTA chelators were labeled with ^{64}Cu and injected intravenously into mice possessing tumor xenografts. Dynamic imaging of the agents was performed using PET-CT on a single animal per sample, and the biodistribution at the terminal time point (24 h) was assessed by gamma counting of the organs *ex vivo* for 3 animals per agent. Compared to other viral capsids of similar size, the MS2 agents showed longer circulation times. Both MS2 and MS2-PEG bacteriophage behaved similarly, although the latter agent showed significantly less uptake in the spleen. This effect may be attributed to the ability of the PEG chains to mask the capsid charge. Although the tumor uptake of the agents may result from the enhanced permeation and retention (EPR) effect, selective tumor imaging may be achieved in the future by using exterior targeting groups.

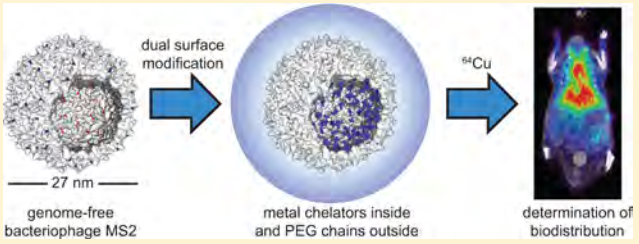

KEYWORDS: *drug delivery, modified viruses, nanoparticles, PEGylation, protein modification, PET imaging*

INTRODUCTION

Viral nanoparticles have received a significant amount of attention in the development of next-generation imaging and drug delivery agents. Relative to traditional carriers, they offer a greater capacity for loading imaging or drug moieties, and through chemical or genetic modifications they can be targeted to deliver their payloads to specific tissues or cell types. When derived from plants and bacteria, these entities are considered to be biocompatible and safe because humans and animals are not the natural viral hosts.[1,2] Although a number of studies involving viral nanoparticles have been conducted *in vitro*, highlighting the potential uses of these agents, relatively few have evaluated their *in vivo* characteristics. Among the icosahedral particles studied *in vivo* are the cowpea chlorotic mottle virus (CCMV),[3] bacteriophage Qβ,[4] and cowpea mosaic virus (CPMV).[5,6] In addition, nonplant/bacterial viruses have also been studied, including the hemagglutinating virus of Japan envelopes (HVJ-Es).[7] CCMV and Qβ are both 28 nm in diameter, while CPMV is 31 nm and HVJ-Es is 300 nm. Although each particle was studied using different experimental conditions, all were found to localize in the liver, all but HVJ-Es in the kidneys, and all but Qβ in the spleen. CCMV and CPMV were rapidly cleared from circulation, and Qβ was cleared within 5 h. HVJ-Es was difficult to assess since the study was performed using the short-lived isotope ^{18}F. In parallel with CCMV, a small heat shock protein (HSP) cage originally isolated from the hyperthermophilic archaeon *Methanococcus jannaschii* was studied under the same conditions.[3] This smaller, 12 nm protein behaved similarly to CCMV.

Work in the our own lab has established methods by which the RNA genome of the MS2 bacteriophage can be removed and the empty capsids recovered.[8] The 27 nm capsid is self-assembled from 180 protein subunits, and possesses 32 1.8 nm pores that allow access to the interior. It is easily handled and can be produced using *Escherichia coli* broth cultures.[9−11] We have previously shown that the interior and exterior surfaces of MS2 can be differentially modified using various strategies.[12]

Special Issue: Viral Nanoparticles in Drug Delivery and Imaging

Received: July 10, 2012
Revised: November 27, 2012
Accepted: December 5, 2012
Published: December 5, 2012

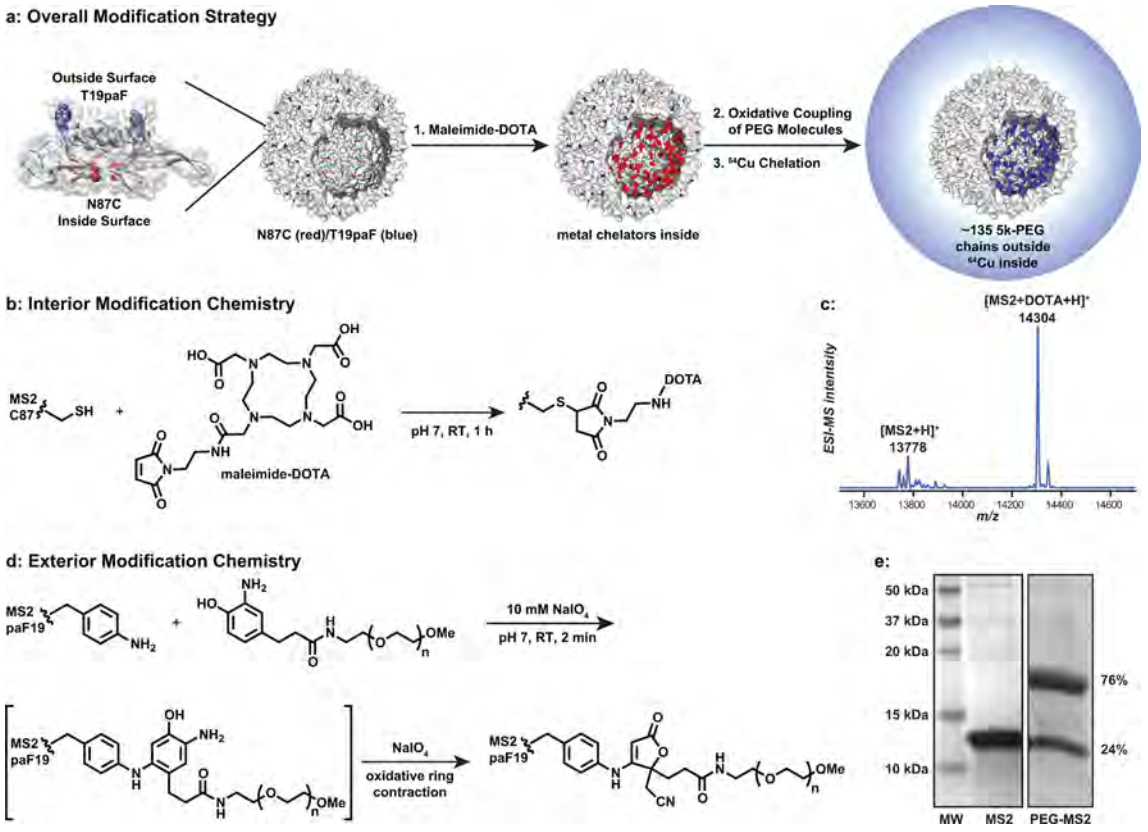

Figure 1. Dual surface modification strategy for genome-free viral capsids. (a) Each MS2 coat protein monomer has a *p*-aminophenylalanine mutation (T19paF) facing the exterior surface and a cysteine mutation (N87C) that faces the interior surface. This provides 180 copies of each modification site in the assembled structures. (b) For radiolabeling, maleimide-DOTA was attached to the interior cysteines to allow ^{64}Cu binding. (c) Analysis of the subsequently disassembled coat proteins by ESI-MS indicated a high level of conversion. (d) In some samples, 5 kDa PEG chains were attached using a rapid oxidative coupling reaction. (e) SDS−PAGE, followed by Coomassie staining and densitometry analysis, indicated that 76% of the coat proteins had been modified in 2 min, corresponding to ~135 polymer chains per capsid.

Capsids have been loaded with contrast agents for MRI,[13] radiotracers for PET,[14] hyperpolarized xenon binders,[15] and therapeutic agents.[16,17] They have also been endowed with cell-specific targeting capabilities via the appendage of external receptor-specific moieties, such as aptamers[18] and peptides.[19]

Given the potential of MS2 as a drug delivery and imaging agent, and its success in *in vitro* experiments, the *in vivo* behavior of this scaffold merits investigation. In the current study, we labeled the interior of MS2 capsids with the radionuclide copper-64 (^{64}Cu), as outlined in Figure 1. This has allowed the current preliminary assessment of their biodistribution and tumor uptake in a small group of mice using dynamic PET imaging (n = 1 per agent) and *ex vivo* gamma counting (n = 3 per agent). One set of samples consisted of capsids with unmodified exterior surfaces, while the other displayed polyethylene glycol (PEG) chains that have been shown in other studies to increase the plasma circulation times of proteins, liposomes, and other nanoparticles.[20−22] Our data indicate that a significant portion of both sets of viral capsids remains in the bloodstream even after 24 h of circulation. Although the capsids used here are not being directed to a specific receptor, some tumor uptake was also observed. This was attributed to the enhanced permeation and retention (EPR) effect. The extended circulation times observed bode well for future studies involving targeted capsids for imaging, drug delivery, or a combination of both purposes.

EXPERIMENTAL SECTION

Chemicals. Maleimide-monoamide-DOTA (maleimide-DOTA) was purchased from Macrocyclics (Dallas, TX). EDTA disodium salt and potassium phosphate dibasic were purchased from EMD Chemicals Inc. (Darmstadt, Germany). Copper-64 was purchased from Medical Cyclotron Laboratory, University of Wisconsin. Normal mouse serum and all cell culture reagents were purchased from Molecular Probes/Gibco/Invitrogen Corp (Carlsbad, CA), and water used in biological procedures and chemical reactions was deionized using a NANOpure purification system (Barnstead, USA). Saline (sodium chloride) solution was Injection USP, 0.9% from APP Pharmaceuticals (Schaumburg, IL).

Synthesis. T19paF N87C-MS2 was produced as previously described.[23] To a 100 μM sample of protein (based on capsid monomer) in 10 mM potassium phosphate buffer, pH 7.2, was added 20 equiv of maleimide-DOTA in DMSO. The reaction was allowed to proceed for 1 h at room temperature and was purified using a Nap 10-Sephadex size exclusion column (GE Healthcare) equilibrated with phosphate buffer, pH 6.5. For the preparation of MS2-PEG samples, PEG5k-aminophenol was synthesized and reacted with DOTA-MS2 as previously described.[24] Briefly, to DOTA-MS2 (60 μM) were added 5 equiv of PEG5k-aminophenol and 2.5 mM $NaIO_4$. The reaction was allowed to proceed for 2 min at pH 6.5 and then purified immediately using a Nap 5-Sephadex size exclusion column (GE Healthcare). The extent of PEG

dx.doi.org/10.1021/mp3003754 | *Mol. Pharmaceutics* 2013, 10, 69−76

modification was determined by using optical densitometry of a Coomassie-stained SDS−PAGE gel. The hydrodynamic diameters of the particles were determined using dynamic light scattering (DLS) with a Zetasizer Nano Series (Malvern Instruments Limited) and low volume quartz cuvette. Solutions were 86 μM for MS2 and 65 μM for PEG-MS2 in 20 mM Na_2HPO_4, pH 7.2.

For the labeling of DOTA-MS2 and DOTA-MS2-PEG samples with ^{64}Cu, 1 mL of 0.1 M ammonium citrate buffer, pH 6.2, was added to the copper stock (33.1 mCi, ~300 μL) to generate a final volume of ~1300 μL at pH 5.5 (determined by pH paper). Each reaction tube was then charged with 400 μL of ^{64}Cu solution and 300 μL of the DOTA-MS2 (50 μM in capsid monomer) samples, resulting in a final volume of 700 μL for each. Labeling of DOTA-MS2 for the stability studies described below was performed using smaller reaction volumes, but similar concentrations of protein and ^{64}Cu. The complexation reactions were allowed to proceed for 1.5 h at room temperature, then diluted with 300 μL of saline solution. The resulting samples were then purified using Nap 5 or Nap 10 columns. Samples were subsequently concentrated using 100 kDa or 10 kDa molecular weight cutoff spin concentrators (Millipore). Centrifugation was performed at 5,000 rpm for 5 min per round of concentrating until the desired volume was reached.

Cell Culture and Flow Cytometry. MCF7 clone 18 (MCF7cl18) cells were obtained from the Preclinical Therapeutics Core Facility, UCSF, and grown in Dulbecco's modified Eagle medium (DMEM) containing 10% fetal bovine serum (FBS) at 37 °C in 5% CO_2. For cell-binding experiments, the cells were trypsinized, harvested, and resuspended in 1% FBS in Dulbecco's phosphate buffered saline (DPBS) at a concentration of 5 million cells/mL. The cells were then aliquotted into Eppendorf tubes at 100 μL (500,000 cells) per tube, and kept on ice. A 100 μL portion of 1 μM protein in 1% FBS/DPBS was added, and the resulting solution was incubated for 1 h at 4 °C. After this, each sample was diluted to 1 mL and washed twice. The cells were finally resuspended in 200 μL of 1% FBS/DPBS and analyzed via flow cytometry (FACSCalibur flow cytometer, BD Biosciences).

***In Vitro* ^{64}Cu-DOTA-MS2 Stability Studies.** Labeling of DOTA-MS2 with ^{64}Cu was performed as described above. Concentrated ^{64}Cu-DOTA-MS2 (~300 μCi) was added to PBS, 10% mouse serum in PBS, or 100% mouse serum to a final volume of 200 μL. The samples were then incubated at 37 °C for up to 24 h using a temperature-controlled heat block (VWR). Aliquots were drawn from the samples at 1, 4, 10, and 24 h time points and injected onto a PolySep GFC-P5000 (Phenomenex) size exclusion chromatography column (300 × 7.8 mm, 5 μm particle size, 500 Å pore size; column flow rate 1.5 mL/min in 10 mM KH_2PO_4 containing 1 mM disodium EDTA, pH 7.2.). The HPLC system consisted of a 590 HPLC pump (Waters, Milford, MA), UV detector operating at 280 nm (Linear Systems), model 105S-1 high-sensitivity radiation detector with 1 cm^3 CsI (T1) scintillating crystal coupled to a 1 cm^2 Si PIN photodiode/low-noise preamplifier (Carroll-Ramsey Associates, Berkeley, CA), and fluorescence detector (Spectrasystem FL3000, Thermo Separation Products St. Peters, MO). Chromatography traces were collected using PeakSimple data system and software (SRI Instruments) and analyzed using the Gaussian multipeak fitting feature of OriginPro v. 8.6.0 (Northampton, MA). For the non-denaturing gel illustrating ^{64}Cu-DOTA-MS2 versus free ^{64}Cu, a 1% agarose gel was used and run for 15 min at 120 V. The image was acquired on a storage phosphor screen and visualized using ImageQuant software (GE Healthcare).

Animal Studies. All animal procedures were performed according to a protocol approved by the UCSF Institutional Animal Care and Use Committee (IACUC). Six-week old female nu/nu mice were purchased from Charles River Laboratories. For tumor inoculation, MCF7cl18 cells were implanted in the number 4 mammary fat pad on the left side. β-Estradiol pellets were implanted subcutaneously in the right flank. The imaging and biodistribution experiments were started two weeks following implantation, when the tumors were ~3 mm in diameter. The mice weighed 19−23 g.

PET/CT and Biodistribution Studies. Tumor-bearing nude mice in sets of 3 animals per study group were injected with 250−350 μCi of ^{64}Cu-labeled DOTA-MS2 capsids (with PEG and without PEG) in 100 μL of PBS. As a control experiment, one group was injected with free ^{64}Cu in 150 μL of PBS. One animal from each group was selected for imaging with microPET/CT (Siemens Inveon microPET docked with microCT). Dynamic imaging was performed from the time of injection (t = 0 h) to 1 h, then 20 min static scans were run at the 4 and 8 h points, followed by a 30 min static scan at 24 h. Each PET scan was followed by the acquisition of a CT scan for registration purposes. Images were reconstructed with CT-based attenuation using the manufacturer-provided ordered subsets expectation maximization (OS-EM) algorithm resulting in 128 × 128 × 159 matrices with a voxel size of 0.776 × 0.776 × 0.796 mm^3, decay corrected, and generated using Amide software. The generation of regions of interest (ROIs) and evaluations of activity based on PET data were performed using Invion Research Workplace (IRW) software.

After a postinjection period of 24 h, all mice were euthanized and dissected. Blood, tumor, and major organs were collected and weighed. The radioactivity present in each sample was determined using a gamma counter (Wizard, Perkin-Elmer) by measuring against standards of known activity generated from the respective samples. All values were decay corrected, and the percentage injected dose per gram (% ID/g) was calculated for each tissue from each mouse. Averages and standard deviations were obtained within each group. Biodistribution data were also analyzed using t-tests in order to determine the statistical significance of the results. Using Excel (Microsoft) software, an unpaired t-test with equal variance and a two-tailed P value was performed for each organ from the DOTA-MS2 and DOTA-MS2-PEG data sets, comparing to each other and against the ^{64}Cu data. A result was considered statistically significant if it occurred at the $P < 0.05$ level.

RESULTS

Synthesis. The T19paF-N87C-MS2 mutant of bacteriophage MS2 was used in these studies. It possesses an internal cysteine residue and an external aniline moiety[25,26] for further functionalization with maleimides and aminophenols, respectively (Figure 1a).[23] Modification of the capsids with DOTA was confirmed via ESI-MS (Figure 1c). For some experiments, the DOTA-MS2 capsids were further modified to display PEG5k chains. This was achieved by reacting the aniline groups with 5 equiv of PEG5k-aminophenol under oxidative conditions using 2.5 mM $NaIO_4$ for 2 min. It was determined that 76% of the aniline groups on the capsid surfaces were modified with PEG5k (Figure 1e), corresponding to ~137 PEG5k chains on each (685 kDa total). The hydrodynamic

diameters of the particles were determined to be 25.1 ± 0.3 nm for the non-PEGylated and 37.3 ± 0.2 nm for the PEG-modified samples (Figure S1 in the Supporting Information). Previous studies by our group have shown that the addition of PEG chains can shield the negative zeta potential of MS2.[12] Chelation of ^{64}Cu by DOTA-MS2 and DOTA-MS2-PEG was accomplished with radiochemical yields of 49.4% and 40.1%, respectively (Figure S2 in the Supporting Information). The specific activity of the DOTA-MS2 was calculated to be 9.3 μCi/μg, while that of the DOTA-MS2-PEG was estimated to be 5.6 μCi/μg (polydispersed PEG was used for modification; the molecular weight used in calculations was 5,000 Da). It was also found that only MS2 functionalized with DOTA was capable of retaining the radionuclide (Figure S3 in the Supporting Information).

Confirming That Untargeted MS2-Based Capsids Do Not Bind to Cancer Cells *in Vitro*. The enhanced permeation and retention (EPR) effect is a result of the increased permeability to macromolecules associated with tumor vasculature, combined with the limited amount of lymphatic drainage that this tissue possesses.[27] Although both DOTA-MS2 and DOTA-MS2-PEG are untargeted agents, they are good candidates to probe this effect due to their sizes. In order to investigate whether these MS2 conjugates exhibit EPR based on the physiological setting and characteristics of the tumor, the absence of binding to cultured tumor cells was first demonstrated *in vitro*. These studies employed MCF7cl18 cells, which are an immortalized breast cancer cell line that overexpresses the HER2 receptor. They can both be maintained *in vitro* and used in *in vivo* xenograft tumor models.[28]

Fluorescently labeled surrogates for DOTA-MS2 and DOTA-MS2-PEG were used in flow cytometry assays to determine the degree of binding or nonspecific adhesion of the agents to cells. Instead of using maleimide-DOTA for coupling to the interior cysteine, a maleimide-Oregon Green functionality was installed. Following incubation for 1 h (a time course that has proven successful for targeted MS2-based agents[18]), no binding of either the PEGylated or non-PEGylated capsids was observed (Figure 2 and Figure S4 in the Supporting Information).

***In Vitro* ^{64}Cu-DOTA-MS2 Stability Studies.** To determine the stability of the ^{64}Cu-DOTA-MS2 complexes, studies of the radiolabeled proteins were performed by incubating the samples in various solutions at physiological temperature and visualizing the presence of intact capsids at various time points using HPLC. For these studies, smaller amounts of the DOTA-MS2 (>250 μL, 50 μM) were labeled with ^{64}Cu under conditions analogous to those described above (radiochemical yield 25.2%, specific activity 2.8 μCi/μg). Following labeling, the sample was analyzed via HPLC; only one peak was detected in the radioactivity channel, indicating a very high level of radiochemical purity, >95% (Figure 3a, t = 0). For reference purposes, a standard HPLC sample was also generated where the ^{64}Cu-DOTA-MS2 sample was coinjected with free ^{64}Cu (Figure 3b).

Following radiolabeling of the DOTA-MS2 capsids, the stability of ^{64}Cu-DOTA-MS2 was monitored following incubation at 37 °C under three different conditions: PBS, 10% mouse serum in PBS, and 100% mouse serum. The samples were analyzed at 1, 4, 10, and 24 h via HPLC. Even after prolonged incubation of the ^{64}Cu-DOTA-MS2 with different percentages of mouse serum at 37 °C, no significant release of ^{64}Cu was observed by either HPLC (Figure 3a, Table 1 and Figure S5 in the Supporting Information) or non-denaturing agarose gel electrophoresis (Figure S6 in the Supporting Information).

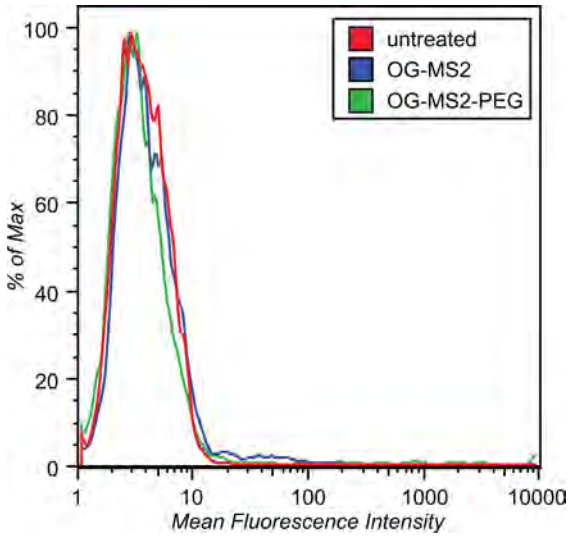

Figure 2. Flow cytometry analysis of MS2 samples shows no binding to MCF7cl18 cells. The fluorescence intensities are shown for cells treated with the Oregon Green (OG)-labeled MS2 and MS2-PEG samples. The fluorescence of an untreated cell population is also shown. The absence of any shift is consistent with a lack of binding to the cell line. Legend: red = untreated cells, blue = OG-MS2-treated cells, green = OG-MS2-PEG treated cells. Supporting Information Figure S4 provides scatter plots indicating the gating that was applied.

PET Imaging of ^{64}Cu-Labeled Agents. In order to monitor the biodistribution of the prepared agents across several time points while limiting the number of animals sacrificed, we used positron emission tomography (PET). Each animal was injected with one of three samples: ^{64}Cu-DOTA-MS2, ^{64}Cu-DOTA-MS2-PEG, or free ^{64}Cu as a control for potentially nonchelated material that may have remained in the protein samples. Dynamic imaging was performed from the time of injection until 1 h post, followed by static imaging at the 4 h, 8 h, and 24 h time points. Both of the MS2 samples (Figure 4 and Figure S7 in the Supporting Information) show significant amounts of signal in the area of the heart through 8 h, indicative of the agent remaining in the circulation. Also observed and anticipated was a signal in the liver, which increased dramatically at early time points, and then more gradually at later times (Figure S8 in the Supporting Information). At 24 h the decay-corrected signal was significantly weaker overall, possibly the result of the agent clearing from the subject.

In contrast, free ^{64}Cu (Figure 5) quickly accumulated in the liver and bladder, showing almost no signal intensity in the area of the heart. It is possible that the signal in the bladder observed in the earlier time points and the lower-abdominals in the later ones for DOTA-MS2-PEG may be attributed to some free copper contamination. Accumulation of signal in the MCF7cl18 xenograft tumors was difficult to ascertain solely based on the images. ROI generation and calculation of signal intensities suggested more retention in the tumor for the proteins than the free ^{64}Cu (Figure S9 in the Supporting Information) and significant tumor-to-muscle ratios (Figure S10 in the Supporting Information). However, we turned to

dx.doi.org/10.1021/mp3003754 | *Mol. Pharmaceutics* 2013, 10, 69−76

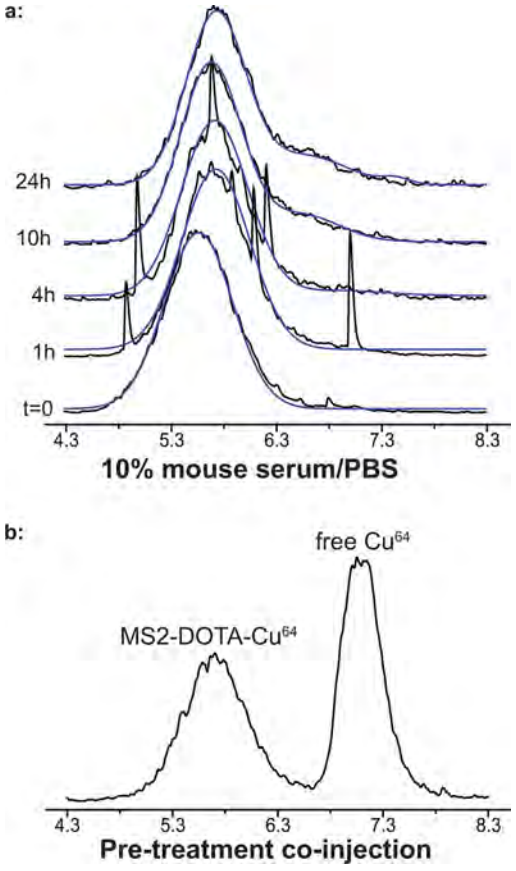

Figure 3. ^{64}Cu-DOTA-MS2 stability studies. (a) ^{64}Cu-DOTA-MS2 was analyzed via HPLC using size-exclusion chromatography following incubation at the indicated time points at 37 °C over 24 h in 10% mouse serum/PBS. Spikes observed are attributed to background noise in the radiation detector. (b) Prior to the start of the study, ^{64}Cu-DOTA-MS2 was coinjected with ^{64}Cu as a standard to confirm adequate peak separation. For all traces, radioactivity detection is shown (black) with accompanying Gaussian correction (blue). 100% PBS and 100% serum treatment conditions and traces illustrating random background noise spikes are included in Supporting Information Figure S5.

Table 1. Percent Intact ^{64}Cu-MS2-DOTA by Treatment[a]

time (h)	PBS	10% serum	100% serum
0	>95	>95	>95
1	>95	>95	84.7
4	94.7	96.0	85.9
10	92.1	84.7	82.1
24	87.3	80.6	80.2

[a]Areas of SEC HPLC peaks corresponding to intact, ^{64}Cu-labeled MS2 capsids represented as percentage of the sum of all peaks in the radioactivity chromatogram. Peaks were fitted with Gaussian functions and integrated using Origin Pro software.

biodistribution studies to characterize this behavior more accurately.

Biodistribution of ^{64}Cu-Labeled Agents. In addition to the single animals used for PET imaging, each agent was administered to two more mice for the purpose of biodistribution analysis. After 24 h from agent administration, all mice (3 per group) were euthanized, and the blood, tumors, and major organs were collected and analyzed in a gamma well counter. Using weights obtained for each organ, the percent injected dose per gram (% ID/g) was determined, along with the statistical correlations for the agent comparisons. (Figure 6, Table 2). Large quantities of all three agents were found in the liver, but only the MS2-based samples showed substantial

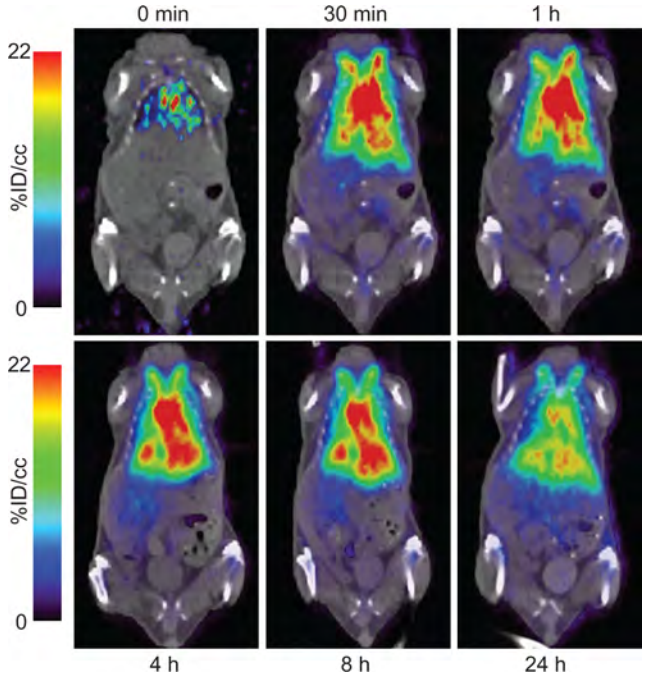

Figure 4. PET-CT images obtained from a mouse injected with ^{64}Cu-labeled DOTA-MS2. A dynamic scan was performed over the first 60 min, followed by scans obtained at 4, 8, and 24 h. All images have been decay-corrected and normalized. The scale is reported as percent injected dose per milliliter (% ID/cc).

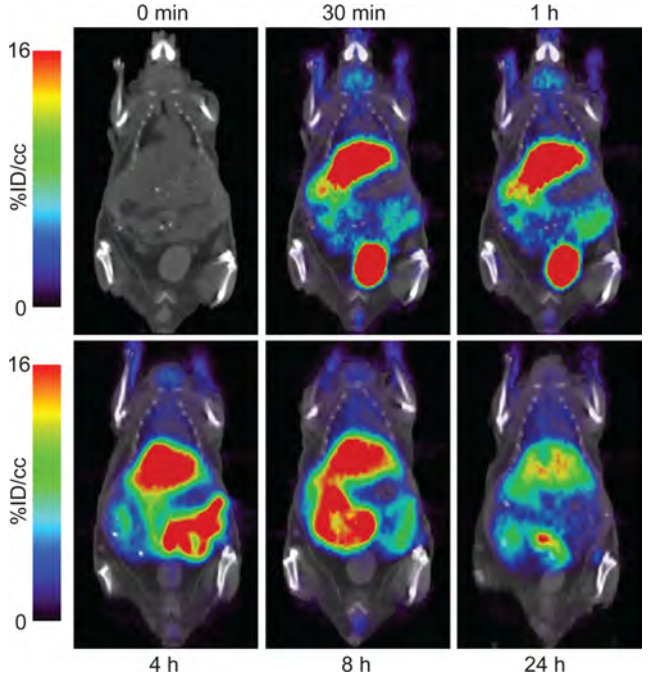

Figure 5. PET-CT images obtained from mouse injected with ^{64}Cu, but no viral capsids. Dynamic scans were performed over the first 60 min, followed by scans obtained at 4, 8, and 24 h. All images have been decay-corrected normalized. The scale is reported as percent injected dose per milliliter (% ID/cc).

dx.doi.org/10.1021/mp3003754 | Mol. Pharmaceutics 2013, 10, 69−76

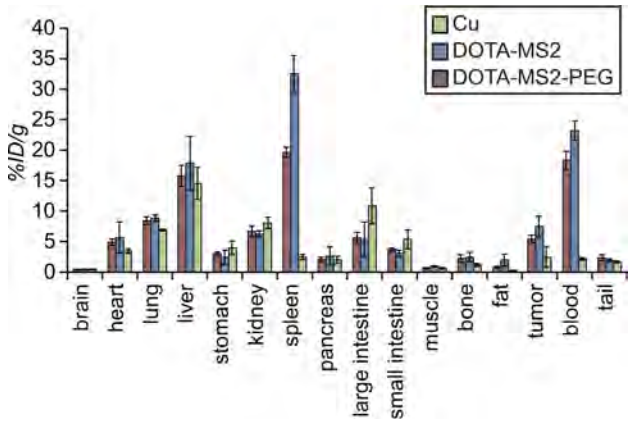

Figure 6. Organ-based biodistribution of free ^{64}Cu, ^{64}Cu-DOTA-MS2, and ^{64}Cu-DOTA-MS2-PEG, as determined by gamma counting. Organs were weighed after excision, and decay corrections were calculated for each individual sample based on individual agent standards. Each agent was administered to 3 animals. The height of each bar represents the average percentage of the injected dose per gram (% ID/g). The error bars indicate the standard deviation of the samples.

Table 2. Biodistribution of ^{64}Cu-Labeled Agents in Mice at 24 h[a]

organ	^{64}Cu only	MS2	MS2-PEG
brain	0.5 ± 0.1	0.4 ± 0.0	0.4 ± 0.0
heart	3.5 ± 0.4$^{\#}$	5.7 ± 2.5	4.9 ± 0.5
lung	6.9 ± 0.1**	8.8 ± 0.5	8.4 ± 0.6
liver	14.5 ± 2.6	17.8 ± 4.4	15.8 ± 1.7
stomach	4.0 ± 1.1	2.4 ± 1.2	3.0 ± 0.3
kidney	8.1 ± 0.9§	6.3 ± 0.5	6.7 ± 0.9
spleen	2.5 ± 0.4‡‡	32.5 ± 3.0‡	19.6 ± 0.8‡
pancreas	2.0 ± 0.6	2.6 ± 1.5	2.0 ± 0.4
large intestine	10.9 ± 2.9$^{\#}$	5.4 ± 2.9	5.6 ± 0.9
small intestine	5.4 ± 1.5	3.1 ± 0.5	3.7 ± 0.3
muscle	0.6 ± 0.1§	1.0 ± 0.1*	0.7 ± 0.1*
bone	1.2 ± 0.2$^{\#}$	2.4 ± 0.8	2.2 ± 0.6
fat	0.3 ± 0.0**	2.0 ± 1.0	0.8 ± 0.2
tumor	2.4 ± 1.7**	7.5 ± 1.7	5.4 ± 0.6
blood	2.2 ± 0.2‡‡	23.1 ± 1.6*	18.3 ± 1.5*
tail	1.7 ± 0.1	2.0 ± 0.2	2.3 ± 0.5

[a]Numbers are reported as the average of the percent injected dose per gram of tissue (% ID/g), plus or minus the standard deviation observed across three subjects. (*) $P < 0.05$ for MS2 samples versus each other. (‡) $P < 0.01$ for MS2 samples versus each other. (**) $P < 0.05$ for each MS2 sample versus ^{64}Cu. (‡‡) $P < 0.01$ for each MS2 sample versus ^{64}Cu. (#) $P < 0.05$ for PEG-MS2 versus ^{64}Cu. (§) $P < 0.05$ for MS2 versus ^{64}Cu.

amounts remaining in the blood, indicating that the agents are indeed still in circulation. A significant amount of these agents was also found in the spleen, but it is noteworthy that the PEG-modified sample showed diminished accumulation compared to uncoated MS2 (approximately 1.6-fold less, $P < 0.01$). At the conclusion of the experiment, it was notable that slightly less of the PEG-modified sample was present in the blood versus the DOTA-MS2 agent. This result will be further examined in subsequent studies, which will also include a more thorough evaluation of biodistribution at additional time points. As anticipated, negligible quantities of the agents were found in the brain. Tumor-to-muscle ratios calculated using the biodistribution data were 7.7 and 7.5 for the DOTA-MS2-PEG and DOTA-MS2 samples, respectively.

DISCUSSION

Due to their inherent capacity to combine multiple types of functionality, nanoparticles are considered to be attractive platforms that may be able to detect and treat tumors and their metastases. They could also be used to monitor treatment and disease progression.[29] Viral nanoparticles normally infecting plants and bacteria are of particular interest because they are considered to be biocompatible, biodegradable, noninfectious, and nonhazardous in humans and other mammals.[2] However in order to facilitate their use, the biopharmaceutical properties of such particles, including the location, time, and duration of action, must be investigated. As we and other groups are interested in developing these scaffolds for further *in vivo* use, the biodistribution properties of bacteriophage MS2 reported herein provide a useful benchmark.

Previously, our group reported PET data using ^{18}F-labeled MS2 capsids in rats acquired using a human scanner.[14] In the current study we elected to use the radionuclide ^{64}Cu, which possesses a half-life of 12.7 h (the half-life of ^{18}F is 109.8 min). This is sufficiently long-lived to evaluate the agents on a scale of hours, rather than minutes.

The processes of opsonization and phagocytosis serve as the main clearance mechanisms for components larger than the renal threshold limit from the blood.[22] Because nanoparticles cannot normally be destroyed by phagocytes, sequestration in the mononuclear phagocyte system (MPS) organs typically occurs, commonly in the liver and spleen.[22,30] Since we expected uncoated MS2 to fall into this category, we also conjugated polymers to the protein in an attempt to circumvent this outcome. PEG chains have been shown to impart nanoparticles with stealth by acting as a steric barrier and interfering in the interactions of the carriers with serum proteins, cells of the immune and reticuloendothelial systems, and with other carriers.[31,32] PEG5k was chosen because research has indicated that a surface PEG chain molecular weight of 2000 or greater is required to achieve MPS-avoidance characteristics, and as the molecular weight is further increased above 2000, the blood circulation half-life of PEGylated particles is also improved.[31]

Based on the data obtained, the circulation and biodistribution properties of both the PEGylated and non-PEGylated DOTA-MS2 carriers are strikingly similar. However, a significant (greater than 1.5-fold) decrease in DOTA-MS2-PEG uptake was observed in the spleen relative to uncoated DOTA-MS2. This is potentially a result of the shielding capabilities of the PEG chains. Previous studies have shown that the attachment of external PEG chains can shield the negative zeta potential of MS2 capsids.[12] Both sets of MS2 capsids were also observed to accumulate in the MCF7cl18 xenograft tumors, despite the fact that neither compound binds to the identical cell line in an *in vitro* flow cytometry assay. This is likely due to the enhanced permeation and retention (EPR) effect.[27] For solid tumors to grow beyond 1−2 mm in diameter, the development of vasculature is required. Compared with smaller sized compounds, nanometer-sized particles are preferentially retained by vascularized tumors following leakage from the bloodstream into the interstitium.[32] Although our long-term plans include the generation of agents targeted to molecular markers on the surface of cancer cells, the targeting of the neovasculature could also be useful, since targeted

dx.doi.org/10.1021/mp3003754 | *Mol. Pharmaceutics* 2013, 10, 69−76

compounds will have to overcome barriers related to diffusion and penetration within the tumor interstitium to reach their markers of interest.

In comparison with other viral capsid-based agents, it was intriguing to observe that 24 h following injection a significant portion of the DOTA-MS2 and DOTA-MS2-PEG agents remained in the bloodstream. As previously mentioned, CCMV, CMPV, and bacteriophage Qβ are all similar in size to MS2, but show substantially different circulation and biodistribution properties. Size may not be the most critical parameter, however, as noted with the differences between the similarly sized T7 and lambda phage particles. When administered intravenously, circulating T7 declines to negligible levels within an hour,[33] while lambda phage particles not only survive longer in circulation but can exhibit circulation time increases of 3 to 4 orders of magnitude upon changing a single coat protein amino acid from a lysine to glutamic acid.[34] This suggests that surface interactions play a major role in determining the plasma clearance of an agent, and even a small change may have a significant effect. The selective attachment of PEG units to CPMV has been described, but *in vivo* studies were limited to assessment of changes in immunogenicity resulting from the modification.[35]

CONCLUSION

We have modified MS2 bacteriophage to carry the copper chelator DOTA, and used this handle to complex ^{64}Cu to both unmodified MS2 capsids and those possessing external PEG chains that have been shown to improve the circulation of other nanoparticles. Both proteins showed similar biodistribution properties *in vivo*, with the exception of a reduced spleen uptake of DOTA-MS2-PEG. Most importantly, significant amounts of the agents remained in circulation 24 h after administration. Some accumulation of the agents in MCF7cl18 tumor xenografts occurred, and was attributed to the EPR effect, together with the extended circulation time of the agents in the bloodstream. The ability of viral capsids to elicit an immune response is a valid concern for these agents. However, drawing upon previous literature examples, it is unlikely that this would be an insurmountable issue.[3,35] Even when an immune response was observed for CPMV particles, it was ablated through the attachment of PEG polymer chains.[35] We are currently evaluating the immunogenicity of MS2 bacteriophage particles. Based on our results, we conclude that MS2 is a promising scaffold for imaging and delivery, whose potential warrants continued investigation.

ASSOCIATED CONTENT

Supporting Information

Figures including ^{64}Cu incorporation gels, flow cytometry scatter plots, additional HPLC traces, PET data for ^{64}Cu-DOTA-MS2-PEG, and PET-determined uptake charts for several tissues. This material is available free of charge via the Internet at http://pubs.acs.org.

AUTHOR INFORMATION

Corresponding Author

*Department of Chemistry, University of California, Berkeley, CA 94720-1460, United States. Phone: 510-643-9915. E-mail: mbfrancis@berkeley.edu. Fax: 510-643-3079.

Notes

The authors declare no competing financial interest.

ACKNOWLEDGMENTS

These studies were generously supported by the DOD Breast Cancer Research Program (BC061995). M.E.F. was supported by DOD BCRP Grant BC100159, and C.R.B. and I.L.A. were supported by the UC Berkeley Chemical Biology Graduate Program (Genentech Fellowship). C.R.B. was supported by DOE California Alliance for Radiotracer Education Grant DESC0002061 and the UC Berkeley Chemical Biology Graduate Program (Training Grant 1 T32 GMO66698). The authors would like to thank Youngho Seo, Ph.D., for helpful discussions, and Byron Hann, M.D., Ph.D., and the UCSF Preclinical Therapeutics Core for assistance with the generation of tumored animals and MCF7cl18 cells. Nick Vandehey is gratefully acknowledged for his assistance with ^{64}Cu handling and for many helpful discussions. Stacy Capehart is thanked for assistance with DLS studies.

ABBREVIATIONS USED

DOTA, 1,4,7,10-tetraazacyclododecane-1,4,7,10-tetraacetic acid; PEG, polyethylene glycol; PEG5k, polyethylene glycol 5000 Da; Da, dalton; EPR, enhanced permeation and retention; CCMV, cowpea chlorotic mottle virus; CPMV, cowpea mosaic virus; HVJ-Es, hemagglutinating virus of Japan envelopes; MRI, magnetic resonance imaging; PET, positron emission tomography; SDS−PAGE, sodium dodecyl sulfate polyacrylamide gel electrophoresis; ESI-MS, electrospray ionization mass spectrometry; DLS, dynamic light scattering; UCSF, University of California, San Francisco; DMEM, Dulbecco's modified Eagle medium; FBS, fetal bovine serum; DPBS, Dulbecco's phosphate buffered saline; IACUC, Institutional Animal Care and Use Committee; ROI, region of interest; IRW, Invion Research Workplace; % ID/g, percent injected dose per gram of tissue

REFERENCES

(1) Steinmetz, N. F. Viral Nanoparticles as Platforms for Next-Generation Therapeutics and Imaging Devices. *Nanomedicine* **2010**, *6*, 634−641.

(2) Yildiz, I.; Shukla, S.; Steinmetz, N. F. Applications of Viral Nanoparticles in Medicine. *Curr. Opin. Biotechnol.* **2011**, *22I*, 901−908.

(3) Kaiser, C. R.; Flenniken, M. L.; Gillitzer, E.; Harmsen, A. L.; Harmsen, A. G.; Jutila, M. A.; Douglas, T.; Young, M. J. Biodistribution Studies of Protein Cage Nanoparticles Demonstrate Broad Tissue Distribution and Rapid Clearance *In Vivo*. *Int. J. Nanomed.* **2007**, *2*, 715−733.

(4) Prasuhn, D. E.; Singh, P.; Strable, E.; Brown, S.; Manchester, M.; Finn, M. G. Plasma Clearance of Bacteriophage Qβ as a Function of Surface Charge. *J. Am. Chem. Soc.* **2008**, *130*, 1328−1334.

(5) Rae, C. S.; Khor, I. W.; Wang, Q.; Destito, G.; Gonzalez, M. J.; Singh, P.; Thomas, D. M.; Estrada, M. N.; Powell, E.; Finn, M. G.; Manchester, M. Systemic Trafficking of Plant Virus Nanoparticles in Mice via the Oral Route. *Virology* **2005**, *343*, 224−235.

(6) Singh, P.; Prasuhn, D.; Yeh, R. M.; Destito, G.; Rae, C. S.; Osborn, K.; Finn, M. G.; Manchester, M. Biodistribution, Toxicity, and Pathology of Cowpea Mosaic Virus Nanoparticles *In Vivo*. *J. Controlled Release* **2007**, *120*, 41−50.

(7) Flexman, J. A.; Cross, D. J.; Lewellen, B. L.; Miyoshi, S.; Kim, Y.; Minoshima, S. Magnetically Targeted Viral Envelopes: A PET Investigation of Initial Biodistribution. *IEEE Trans. Nanobiosci.* **2008**, *7*, 223−232.

(8) Hooker, J. M.; Kovacs, E. W.; Francis, M. B. Interior Surface Modification of Bacteriophage MS2. *J. Am. Chem. Soc.* **2004**, *126*, 3718−3719.

(9) Davis, J. E. Replication of Bacteriophage MS2. *J. Mol. Biol.* **1963**, *6*, 203−208.

(10) Valegard, K.; Liljas, L.; Fridborg, K.; Unge, T. The Three-Dimensional Structure of the Bacterial Virus MS2. *Nature* **1990**, *345*, 36−41.
(11) Cargile, B. J.; McLuckey, S. A.; Stephenson, J. L. Identification of Bacteriophage MS2 Coat Protein from *E. coli*. Lysates via Ion Trap Collisional Activation of Intact Protein. *Anal. Chem.* **2001**, *73*, 1277−1285.
(12) Kovacs, E. W.; Hooker, J. M.; Romanini, D. W.; Holder, P. G.; Berry, K. E.; Francis, M. B. Dual-Surface-Modified Bacteriophage MS2 as an Ideal Scaffold for a Viral Capsid-Based Drug Delivery System. *Bioconjugate Chem.* **2007**, *18*, 1140−1147.
(13) Datta, A.; Hooker, J. M.; Botta, M.; Francis, M. B.; Aime, S.; Raymond, K. N. High Relaxivity Gadolinium Hydroxypyridonate-Viral Capsid Conjugates: Nanosized MRI Contrast Agents. *J. Am. Chem. Soc.* **2008**, *130*, 2546−2552.
(14) Hooker, J. M.; O'Neil, J. P.; Romanini, D. W.; Taylor, S. E.; Francis, M. B. Genome-Free Viral Capsids as Carriers for Positron Emission Tomography Radiolabels. *Mol. Imaging. Biol.* **2008**, *10*, 182−191.
(15) Meldrum, T.; Seim, K. L.; Bajaj, V. S.; Palaniappan, K. K.; Wu, W.; Francis, M. B.; Wemmer, D. E.; Pines, A. A Xenon-Based Molecular Sensor Assembled on an MS2 Viral Capsid Scaffold. *J. Am. Chem. Soc.* **2010**, *132*, 5936−5937.
(16) Wu, W.; Hsiao, S. C.; Carrico, Z. M.; Francis, M. B. Genome-Free Viral Capsids as Multivalent Carriers for Taxol Delivery. *Angew. Chem., Int. Ed.* **2009**, *48*, 9493−9497.
(17) Stephanopoulous, N.; Tong, G. J.; Hsiao, S. C.; Francis, M. B. Dual-Surface Modified Virus Capsids for Targeted Delivery of Photodynamic Agents to Cancer Cells. *ACS Nano* **2010**, *4*, 6014−6020.
(18) Tong, G. J.; Hsiao, S. C.; Carrico, Z. M.; Francis, M. B. Viral Capsid DNA Aptamer Conjugates as Multivalent Cell-Targeting Vehicles. *J. Am. Chem. Soc.* **2009**, *131*, 11174−11178.
(19) Carrico, Z. M.; Romanini, D. W.; Mehl, R. A.; Francis, M. B. Oxidative Coupling of Peptides to a Virus Capsid Containing Unnatural Amino Acids. *Chem. Commun.* **2008**, *10*, 1205−1207.
(20) O'Riordan, C. R.; Lachapelle, A.; Delgado, C.; Parkes, V.; Wadsworth, S. C.; Smith, A. E.; Francis, G. E. PEGylation of Adenovirus with Retention of Infectivity and Protection from Neutralizing Antibody *In Vitro* and *In Vivo*. *Hum. Gene Ther.* **1999**, *10*, 1349−1358.
(21) Caliceti, P.; Veronese, F. M. Pharmacokinetic and Biodistribution Properties of Poly(Ethylene Glycol)-Protein Conjugates. *Adv. Drug Delivery Rev.* **2003**, *55*, 1261−1277.
(22) Owens, D. E.; Peppas, N. A. Opsonization, Biodistribution, and Pharmacokinetics of Polymeric Nanoparticles. *Int. J. Pharm.* **2006**, *307*, 93−102.
(23) Stephanopoulos, N.; Carrico, Z. M.; Francis, M. B. Nanoscale Integration of Sensitizing Chormophores and Porphyrins with Bacteriophage MS2. *Angew. Chem., Int. Ed.* **2009**, *48*, 9498−9502.
(24) Behrens, C. R.; Hooker, J. M.; Obermeyer, A. C.; Romanini, D. W.; Katz, E. M.; Francis, M. B. Rapid Chemoselective Bioconjugation Through the Oxidative Coupling of Anilines and Aminophenols. *J. Am. Chem. Soc.* **2011**, *133*, 16398−16401.
(25) Mehl, R. A.; Anderson, J. C.; Santoro, S. W.; Wang, L.; Martin, A. B.; King, D. S.; Horn, D. M.; Schultz, P. G. Generation of a Bacterium with a 21 Amino Acid Genetic Code. *J. Am. Chem. Soc.* **2003**, *125*, 935−939.
(26) Xie, J.; Schultz, P. G. A Chemical Toolkit for Proteins—An Expanded Genetic Code. *Nat. Rev. Mol. Cell Biol.* **2006**, *7*, 775−782.
(27) Maeda, H.; Wu, J.; Sawa, T.; Matsumura, Y.; Hori, K. Vascular Permeability and the EPR Effect in Macromolecular Therapeutics: A Review. *J. Controlled Release* **2000**, *65*, 271−284.
(28) Hathaway, H. J.; Butler, K. S.; Adolphi, N. L.; Lovato, D. M.; Belfon, R.; Fegan, D.; Monson, T. C.; Trujillo, J. E.; Tessier, T. E.; Bryant, H. C.; Huber, D. L.; Larson, R. S.; Flynn, E. R. Detection of breast cancer cells using targeted magnetic nanoparticles and ultra-sensitive magnetic field sensors. *Breast Cancer Res.* **2011**, *13*, R108.
(29) Wang, M.; Thanou, M. Targeting Nanoparticles to Cancer. *Pharmacol. Res.* **2010**, *62*, 90−99.
(30) Peiser, L.; Mukhopadhyay, S.; Gordon, S. Scavenger Receptors in Innate Immunity. *Curr. Opin. Immunol.* **2002**, *14*, 123−128.
(31) Perracchia, M. T. Stealth Nanoparticles for Intravenous Administration. *STP Pharma Sci.* **2003**, *13*, 155−161.
(32) Sofou, S. Radionuclide Carriers for Targeting of Cancer. *Int. J. Nanomed.* **2008**, *3*, 181−199.
(33) Srivastava, A. S.; Kaido, T.; Carrier, E. Immunological Factors that Affect the In Vivo Fate of T7 Phage in the Mouse. *J. Virol. Methods* **2004**, *115*, 99−104.
(34) Vitiello, C. L.; Merril, C. R.; Adhya, S. An Amino Acid Substitution in a Capsid Protein Enhances Phage Survival in Mouse Circulatory System More Than a 1000-fold. *Virus Res.* **2005**, *114*, 101−103.
(35) Raja, K. S.; Wang, Q.; Gonzalez, M. J.; Manchester, M.; Johnson, J. E.; Finn, M. G. Hybrid Virus-Polymer Materials. 1. Synthesis and Properties of PEG-Decorated Cowpea Mosaic Virus. *Biomacromolecules* **2003**, *4*, 472−476.

PET Imaging and Biodistribution of Chemically Modified Bacteriophage MS2

Michelle E. Farkas,[a] Ioana L. Aanei,[a] Christopher R. Behrens,[a] Gary J. Tong,[a] Stephanie T. Murphy,[b] James P. O'Neil,[c] and Matthew B. Francis[a,d]*

[a]Department of Chemistry, University of California, Berkeley, California 94720-1460. [b]Department of Radiology and Biomedical Imaging, University of California, San Francisco, CA 94107. [c]Department of Molecular Imaging and Neuroscience, Lawrence Berkeley National Laboratory, Berkeley, CA 94720. [d]Materials Sciences Division, Lawrence Berkeley National Laboratories, Berkeley, California 94720-1460.

mbfrancis@berkeley.edu

KEYWORDS: Drug delivery, modified viruses, nanoparticles, PEGylation, protein modification, PET imaging.

Supporting Information and Figures

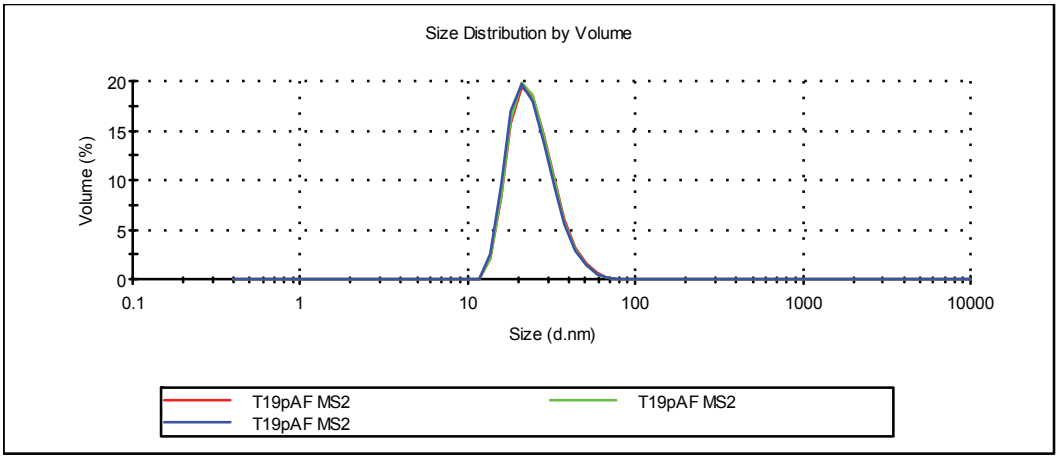

diameter = 25.4, 25.1, 24.8 nm

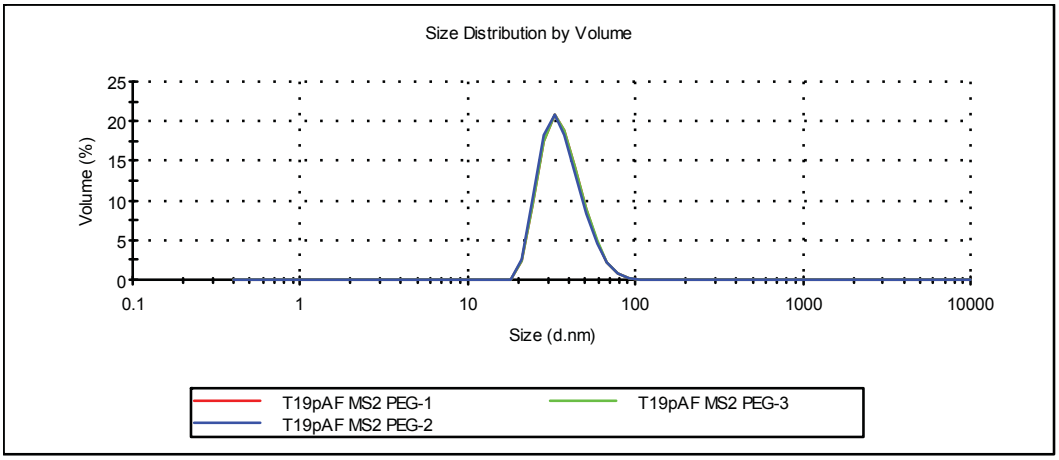

diameter = 37.5, 37.5, 37.1 nm

Figure S1. Hydrodynamic measurements of MS2 (top) and PEG-MS2 (bottom) as determined by DLS via size distribution by volume. Corresponding diameter results are shown to the lower right of each graph. Each sample was repeated n=3.

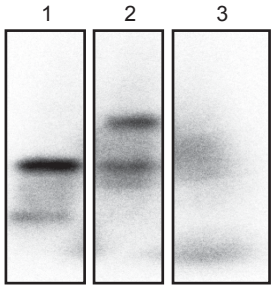

Figure S2. Storage phosphor image of gel following labeling with ^{64}Cu. Lane 1: DOTA-MS2; lane 2:DOTA-MS2-PEG; lane 3: free copper.

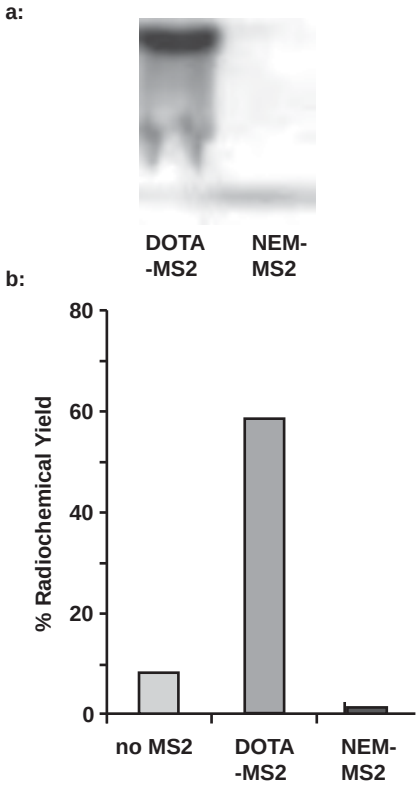

Figure S3. Only DOTA-MS2 is labeled with copper. (a) Autoradiography of DOTA-MS2 and *N*-ethyl maleimide (NEM)-labeled MS2 after exposure to ^{64}Cu. (b) Radiochemical yields of copper labeling, as determined by size-exclusion chromatography. Neither copper without MS2, nor MS2 containing interior NEM resulted in significant yields.

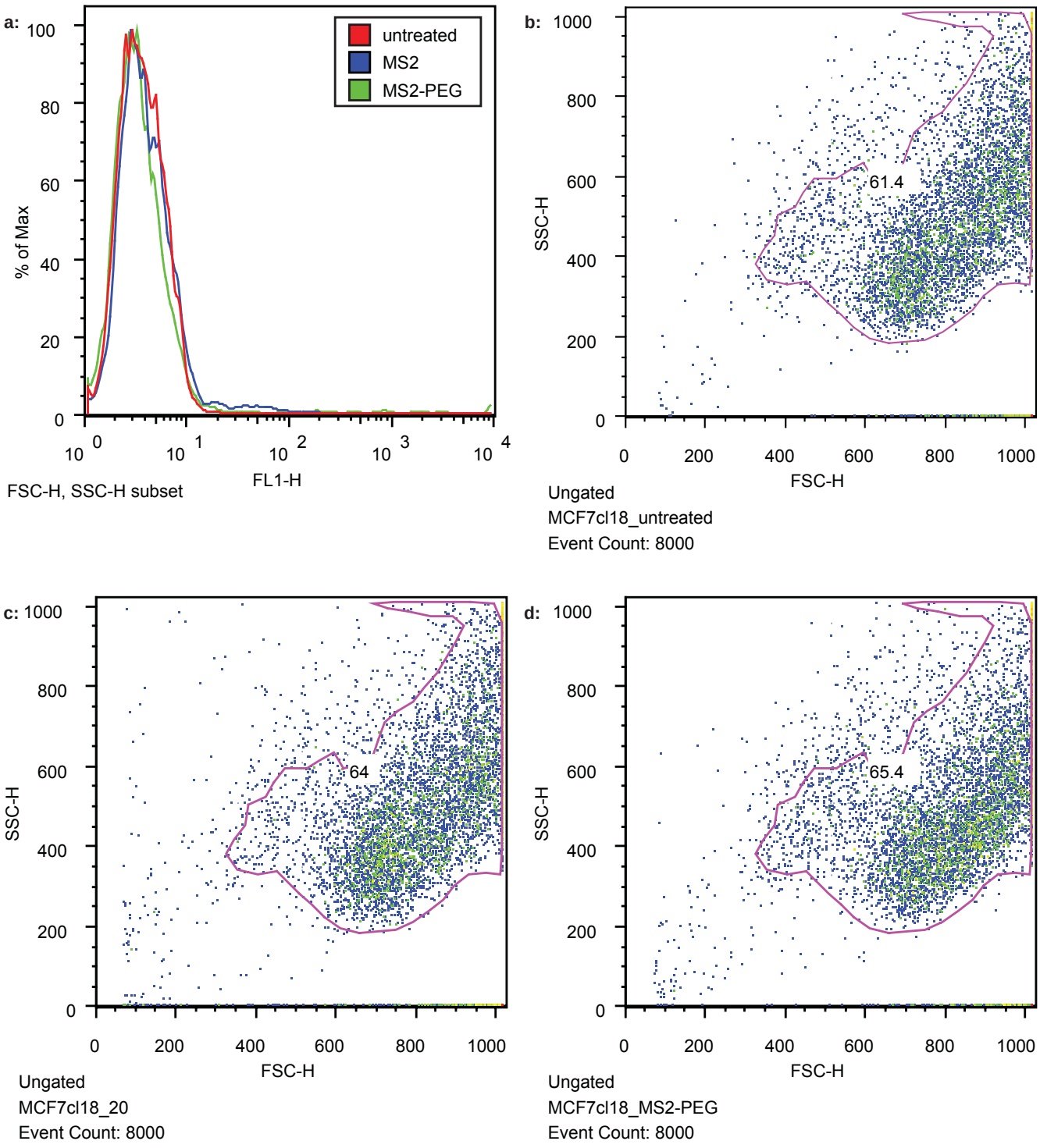

Figure S4. Flow cytometry of MS2 samples shows no binding to MCF7cl18 cells. (a) A histogram is shown for the fluorescence intensity of cells treated with fluorophore-labeled MS2 and MS2-PEG samples, compared to untreated cells. The absence of any shift is consistent with a lack of binding to the cell line. (b-d) Side- and forward-scatter-plots reflect the gating (pink line) that was used to generate the histogram shown in a. The numbers inside of each plot indicate the percentage of the total population of cells within the gate.

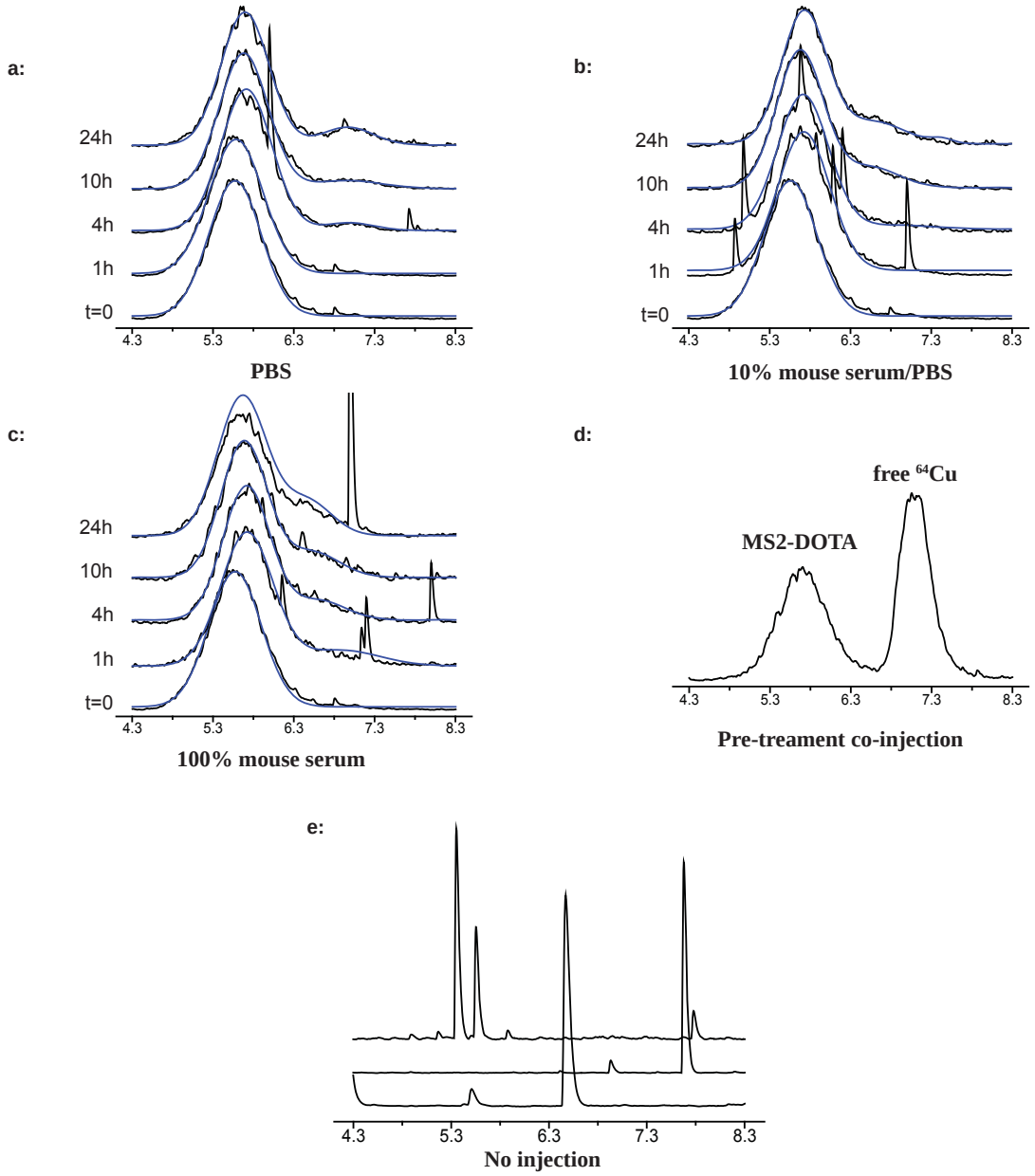

Figure S5. MS2-DOTA-Cu stability studies. MS2-DOTA-Cu was analyzed via HPLC using size-exclusion chromography following incubation at 37 ˚C over the course of 24 hours in (**a**) PBS (**b**) 10% mouse serum/PBS, and (**c**) 100% mouse serum. Prior to the start of the study, MS2-DOTA-Cu was co-injected with ^{64}Cu (**d**) as a standard to evaluate peak separation. For all traces, both radioactivity detection (black) and gaussian correction (blue) are shown. (**e**) HPLC runs with no injection show random background noise spikes in the radioactivity channel

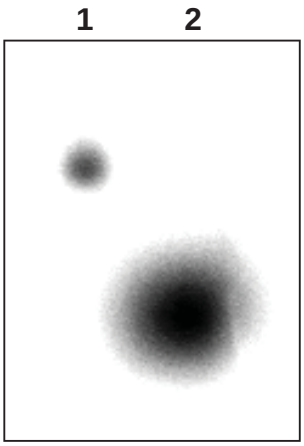

Figure S6. Storage phosphor image of 1% agarose gel comparing ^{64}Cu-labeled MS2-DOTA following 24 hours incubation in PBS at 37 ˚C (lane 1) to free copper (lane 2).

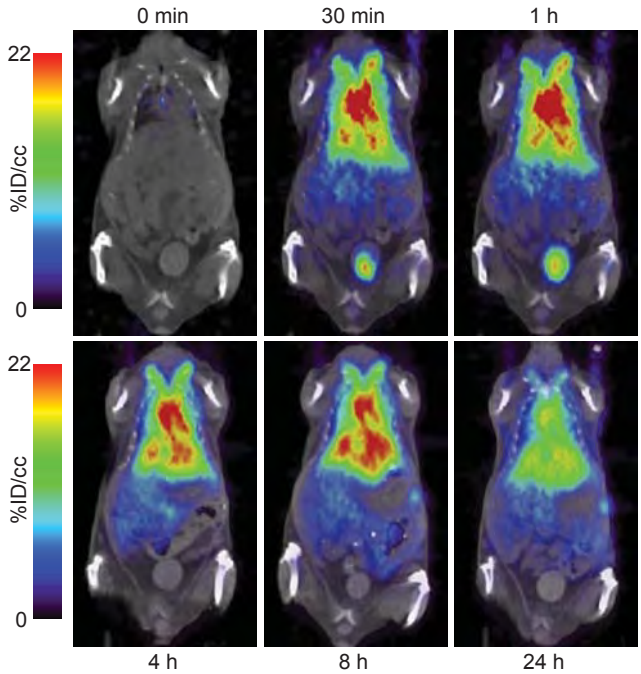

Figure S7. PET-CT images obtained from a mouse injected with ^{64}Cu-labeled DOTA-MS2-PEG. A dynamic scan was performed over the first 60 min, followed by scans obtained at 4, 8, and 24 h. All images have been decay-corrected and normalized. The scale is reported as percent injected dose per milliliter (%ID/cc).

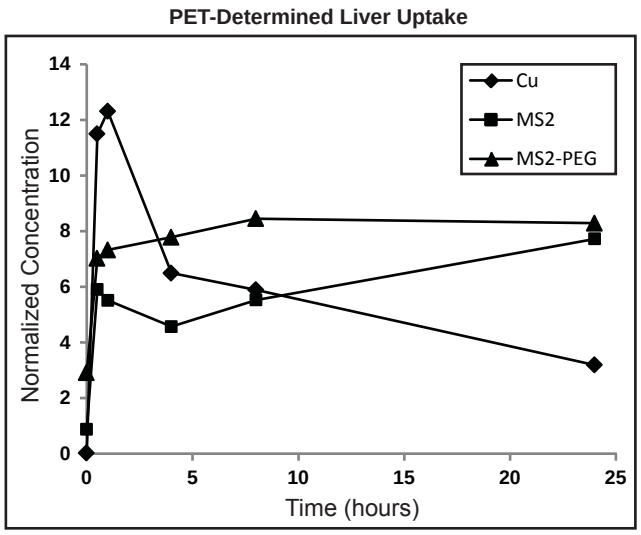

Figure S8. Liver uptake of ^{64}Cu-labeled agents in mice as determined from PET-CT images. Regions of interest (ROIs) were generated in an area of the liver and surrounding the entire mouse (total activity). Concentrations in Bq/mL were determined and decay-corrected. Each data point was normalized versus total activity measured at that time. Legend: diamonds = free ^{64}Cu, squares = MS2, triangles = MS2-PEG.

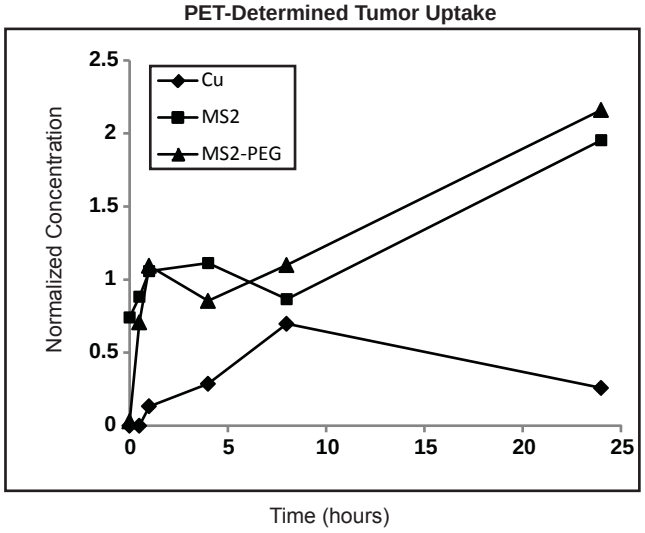

Figure S9. MCF7cl18 xenograft tumor uptake of ^{64}Cu-labeled agents in mice, as determined from PET-CT images. Regions of interest (ROIs) were generated surrounding the tumor, as well as the entire mouse (total activity). Concentrations in Bq/mL were determined and decay-corrected. Each data point was normalized versus total activity measured at that time. Legend: diamonds = free ^{64}Cu, squares = ^{64}Cu-DOTA-MS2, triangles = ^{64}Cu-DOTA-MS2-PEG.

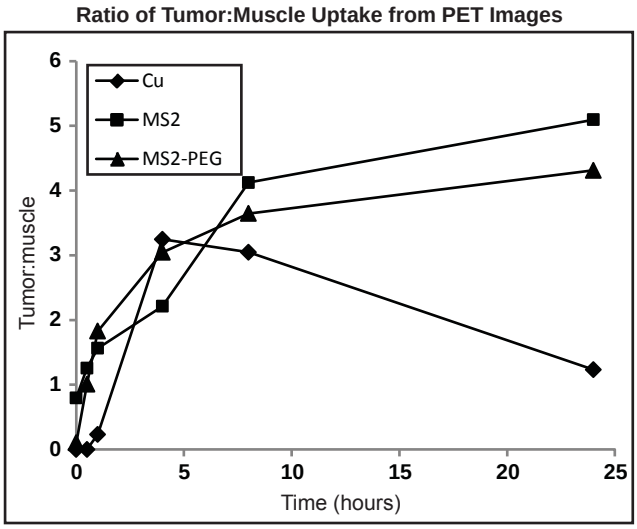

Figure S10. Evaluation of tumor:muscle uptake ratios for MS2-based agents, as determined from PET-CT images. Regions of interest (ROIs) were generated in an area of the leg (muscle) and at the tumor site. Concentrations in Bq/mL were obtained and the ratios determined for each time point. Legend: diamonds = free ^{64}Cu, squares = ^{64}Cu-DOTA-MS2, triangles = ^{64}Cu-DOTA-MS2-PEG.

TOC Graphic

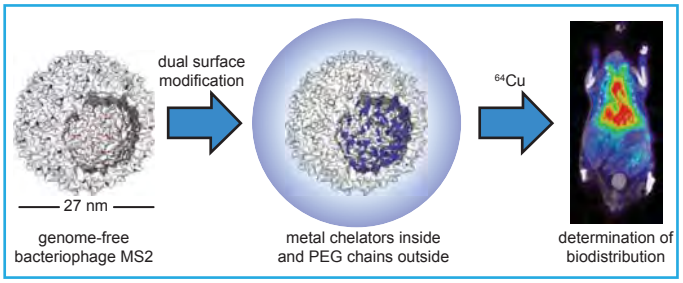
dual surface
modification
64Cu
27 nm
genome-free
bacteriophage MS2
metal chelators inside
and PEG chains outside
determination of
biodistribution